AD 295 853

AFCRL-62-1071

A STUDY OF PROCESSES IN THE IONOSPHERE BY MEANS OF GYRO-INTERACTION EXPERIMENTS CARRIED OUT WITH ROCKETS

Sponsored by

AIR FORCE CAMBRIDGE RESEARCH LABORATORIES
OFFICE OF AEROSPACE RESEARCH

FINAL REPORT

Covering Period
1 June 1959 to 30 April 1962

Contract No. AF19(604)-5565
P 8653
T 865305

August 1962

Prepared for

GEOPHYSICS RESEARCH DIRECTORATE
AIR FORCE CAMBRIDGE RESEARCH LABORATORIES
OFFICE OF AEROSPACE RESEARCH
UNITED STATES AIR FORCE
BEDFORD, MASSACHUSETTS

Antenna Laboratory and Gaseous Electronics Laboratory
Electrical Engineering Research Laboratory
Engineering Experiment Station
University of Illinois
Urbana, Illinois

"This research sponsored by Defense Atomic Support Agency under WEB No. 04.054"

NOTICES

Requests for additional copies by Agencies of the Department of Defense, their contractors, and other Government agencies should be directed to the:

ARMED SERVICES TECHNICAL INFORMATION AGENCY
ARLINGTON HALL STATION
ARLINGTON 12, VIRGINIA

All other persons and organizations should apply to the:

U.S. DEPARTMENT OF COMMERCE
OFFICE OF TECHNICAL SERVICES
WASHINGTON 25, D.C.

AFCRL-62-1071

A STUDY OF PROCESSES IN THE IONOSPHERE BY MEANS OF GYRO-INTERACTION EXPERIMENTS CARRIED OUT WITH ROCKETS

Sponsored by

AIR FORCE CAMBRIDGE RESEARCH LABORATORIES
OFFICE OF AEROSPACE RESEARCH

FINAL REPORT

Covering Period
1 June 1959 to 30 April 1962

Contract No. AF19(604)-5565
P 8653
T 865305

August 1962

Prepared for

GEOPHYSICS RESEARCH DIRECTORATE
AIR FORCE CAMBRIDGE RESEARCH LABORATORIES
OFFICE OF AEROSPACE RESEARCH
UNITED STATES AIR FORCE
BEDFORD, MASSACHUSETTS

Antenna Laboratory and Gaseous Electronics Laboratory
Electrical Engineering Research Laboratory
Engineering Experiment Station
University of Illinois
Urbana, Illinois

"This research sponsored by Defense Atomic Support Agency under WEB No. 04.054"

CONTENTS

CONTENTS (Continued)

ILLUSTRATIONS

ILLUSTRATIONS (Continued)

ILLUSTRATIONS (Continued)

INTRODUCTION

The general purpose of this project is to demonstrate the possibility of controlling some processes in the ionosphere by application of radio energy at the gyrofrequency. Another purpose is to estimate the magnitude of the effects produced, to relate them to the properties of the ionosphere, and thus eventually to devise new methods of probing the ionosphere.

Another prupose of the contract is to perform laboratory experiments on the interaction phenomena in an ionized gas subjected to a steady magnetic field, and to scale the results of these experiments to the actual ionosphere in view of its possible control.

An experiment has been planned and executed which consisted of firing a rocket through the D and lower E regions of the ionosphere. The rocket carried a transmitter which periodically radiated a strong pulse at the gyrofrequency (about 1.4 mc) The temperature of the electrons in the vicinity of the rocket having been raised by this "heating" signal, the properties of the medium (collision frequency, rates of various processes, and the electron density, if the signal were strong enough) would have been modified These modifications were detected by observing amplitude modulation upon a sensing signal propagated through the heated region.

The planning phase of the project began in mid 1959 The analogy between the rocket-borne experiment and the 'Luxembourg effect' was helpful; however, the differences were important and necessitated careful study in several areas. Graphical methods were developed for the computation of refractive index and polarization in a magneto ionic medium[1,2,3]. Maxwell's equations were solved for the case of an infinitesimal dipole antenna in an anisotropic plasma and both radiation patterns and near fields were obtained[4].

Other studies more directly related to the rocket borne experiment have been included in progress reports These include the choice of sensing wave frequency, heating antenna system, and heating signal parameters (such as pulse width, pulse repetition frequency and power level)

Chapter 1 of this report concerns the planning, instrumentation and preliminary analysis of results obtained from the gyroresonance probe carried by Aerobee sounding rocket AA1 193 on 1 May 1962 In addition to the detection

of cross modulation on the sensing wave the experiment included the measurement of the polarization ellipse of the sensing wave, the gyrofrequency radiated power, radiated field intensity, and antenna impedance. Nonlinear effects measured included the excitation light produced near the heating antennas and the difference frequency generated by mixing of the heating and sensing signals in the ionosphere. System performance was monitored along with the aspect of the earth's magnetic field Unfortunately much of this data was not obtained due to the failure of motor drivenswitch. This device served the dual purpose of data sampling commutator and clock, its failure resulted in loss of both synchronization and time sharing modes of data acquisition. However the sensing wave modulation and polarization ellipse as well as gyrofrequency field intensity were obtained intact. The analysis of this data is far from complete and will be included in work done on the next contract. This experiment has provided useful information to guide the instrumentation of future gyroresonance probes. It has also demonstrated the applicability of the electron heating technique in studying the composition of the lower D region by modulation of Faraday rotation.

In conjunction with the planning of the rocket experiment it was necessary to carry out plasma experiments in the laboratory and to relate the results to ionospheric problems Included were studies of the ion sheath, plasma heating, and antenna impedance A theory for the impedance of a short antenna in an anisotropic plasma was developed, verified experimentally, and used to design the heating antenna matching network for the rocket experiment. This work is discussed in Chapter 2.

The results of a laboratory study of the nonlinear interaction of an RF electromagnetic wave and a plasma have been published[5] and are summarized in Chapter 3. The instrumentation of the difference frequency measurement for the rocket experiment was included in the course of this work.

1. GYRORESONANCE PROBE EXPERIMENT - R. R. Hodges

1.1 Introduction

Cross-modulation occurring in the ionosphere was first reported by Tellegen[6] in 1933. This effect is commonly known as the "Luxembourg effect" because it was observed that modulation of the Radio Luxembourg station (250 kc) was impressed upon weaker signals traversing the region of the ionosphere near this station.

The first theoretical explanation of the "Luxembourg effect" was presented in 1934 by Bailey and Martyn[7]. They evaluated the average energy received by electrons between collisions, deduced the increase in collision frequency, and obtained a formula for the cross modulation. Refinements upon this theory have been made and much experimental work has been done. Notably a prediction by Bailey[8] in 1938 that a resonance effect should occur when the disturbance is produced by a signal at the gyrofrequency has been verified[9,10] An additional prediction by Bailey[8] was that a small amount of power (1 watt for example) at gyroresonance and concentrated in a sufficiently narrow beam should produce an observable amount of cross modulation in the ionosphere.

Due to the impracticalities of the required antenna system (one wavelength at the gyrofrequency being about 200 meters), Bailey's latter prediction has not been verified experimentally.

However, by carrying the gyroresonant transmitter into the ionosphere with a rocket the antenna problem is alleviated. All of the radiated gyrofrequency energy is available to heat electrons.

A probe designed to perform such an experiment was carried to an altitude of 94 km by Aerobee sounding rocket AA1 193 on 1 May 1962 The disturbance of the ionosphere was produced by a rocket borne gyrofrequency transmitter. It was detected by a sensing wave radiated from the ground through the ionosphere and received at the rocket The cross modulation was telemetered and recorded.

In addition to the measurement of cross modulation the probe was instrumented to obtain data from which the gyroresonance heating antenna impedance and radiated power could be obtained. The near electric field

produced by the heating signal and the excitation light due to inelastic electron-molecule (or atom) collisions near the heating antennas were also measured.

The measurement of nonlinearities in the ionospheric properties was provided by a receiver tuned to the difference frequency of the sensing and heating signals.

Monitoring of the operation of the system was accomplished by means of a data sampling switch Such things as magnetic aspect and sensing receiver AGC voltage were included

The data sampling function occupied one deck of a two pole switch. The other was used as a clock to provide synchronization of the experiment. This device failed mechanically at burnout. As a result the data was limited to the cross modulation experiment, the heating field intensity, and the sensing receiver AGC voltage. (The latter is the point at which the data sampling switch fortuitously happened to stop.)

The cross modulation data does exhibit the expected results. However the lack of subsidiary measurements limits the accuracy of interpretation of this data.

In subsequent sections of this part of the report the planning of a gyroresonance probe experiment, the instrumentation of an initial experiment, and a preliminary analysis of the results of this experiment are given.

1.2 Properties of the Lower E Region of the Ionosphere

The choice of experimental parameters for the gyroresonance probe was based upon a set of assumptions concerning the properties of the lower E region of the ionosphere. These properties are as follows

(1) The E region is a weakly ionized gas which means that the electron number density, n_e, is much smaller than the number density of molecules, N For example

at 70 km $n_e = 1.5 \times 10^{8}$ m^{-3} while $N = 2.1 \times 10^{21}$ m^{-3}

at 100 km $n_e = 10^{11}$ m^{-3} while $N = 7.8 \times 10^{18}$ m^{-3}

(Electron densities are from Waynick[11] and molecular densities from Minzner, et al.[12])

(2) The gas is electrically neutral on the average, and negative ions are assumed to have an inconsequential density Some fluctuations of net charge may occur over regions of the order of the Debye

length λ_D. This length, given by $6.9\sqrt{T/n}$ cm, can be a few centimeters in the lower E region and becomes much less at higher altitudes. At 100 km the temperature is 200° K[12], the electron thermal velocity is 9.5×10^4 m/sec and λ_D, which can be interpreted as the distance traveled with this velocity during a radian period of the plasma frequency ($\omega_p \cong 2 \times 10^7$), is only 4.8 mm. At 70 km, taking $n_e = 1.5 \times 10^8$ m^{-3}, hence $\omega_p \cong 7 \times 10^5$ and T = 210° K, hence v = 9.8×10^4 m/sec, the Debye length is about 10 cm. Thus the Debye length is small compared to the dimensions of the rocket or the wavelength for the gyrofrequency (approximately 200 meters).

(3) The collisions of electrons occur mainly with neutral molecules. This is a consequence of (1) and (2).

(4) For low enough energies electron-molecule collisions are elastic. Since the molecules are much heavier than the electrons, a collision produces only a small energy transfer and mostly a change in momentum. For a perfectly elastic collision between an electron of mass m and a molecule of mass M the fraction of energy lost per collision is given by

$$G = \frac{2m}{m + M} \cong \frac{2m}{M}$$

The mean molecular weight of air is 28.766 at sea leveal and 28.90 at 100 km[12], therefore taking $M \cong 29$, $G \cong 4 \times 10^{-5}$. When the collisions are not elastic (for higher average electron energies) we shall still assume that the fractional loss of energy per collision is represented by a constant $G \cong 10^{-3}$

(5) The molecules move very slowly compared to the electrons At thermal equilibrium the ratio of the rms velocities is $\sqrt{M/m} \cong 250$. [At 100 km, if T $\cong 200^\circ$ K, $v_e \cong 9.5 \times 10^4$ meters per second, $v_m \cong 380$ meters per second] The velocity of molecules may be neglected in the sense that their distribution and the manner in which it changes with electron temperature are not important They form a background capable of taking energy from the electrons at a certain rate and capable of providing changes of electron momentum at each collision

(6) When an electromagnetic field is applied to the medium it will act mostly on the electrons, changing their momentum The collisions have two effects:

(a) They "thermalize" the kinetic energy of the electrons, i.e. orient the velocities randomly.

(b) By transferring a fraction of the energy to the molecules they prevent the electron energy from increasing indefinitely. Since molecules are much more numerous than electrons they are capable of taking this energy without appreciably changing their statistical properties (for example the molecular temperature or cross section for electron collision) To be sure some molecules will be excited or even ionized by non-elastic collisions but the proportion of those that are affected will remain small. The assumption of $G > 2m/M$ in (4) above takes this into account

(7) The scattering of the electrons by the molecules may have some directive properties. Lacking information on this point we shall assume the scattering to be isotropic. This means it is unnecessary to distinguish between the frequency of collisions and the collision frequency for transfer of momentum.

(8) The effective cross section can be expected to depend on the electron velocity relative to the scatterer In the first approximation it is sometimes assumed to be constant Then the collision frequency ν will be proportional to the square root of electron temperature and to the number density of molecules. When the electron temperature differs from the molecular temperature we shall assume

$$\nu = \nu_o \sqrt{\frac{T_e}{T_o}} = \nu_o \frac{v}{v_o}$$

where ν_o is the value of collision frequency in thermal equilibrium (i e $T_e = T_o$), and v and v_o are rms electron velocities for heated and equilibrium cases respectively

(9) Relevant parameters that are functions of altitude are temperature, electron density and collision frequency These are plotted in Figure 1.1 according to the following sources:

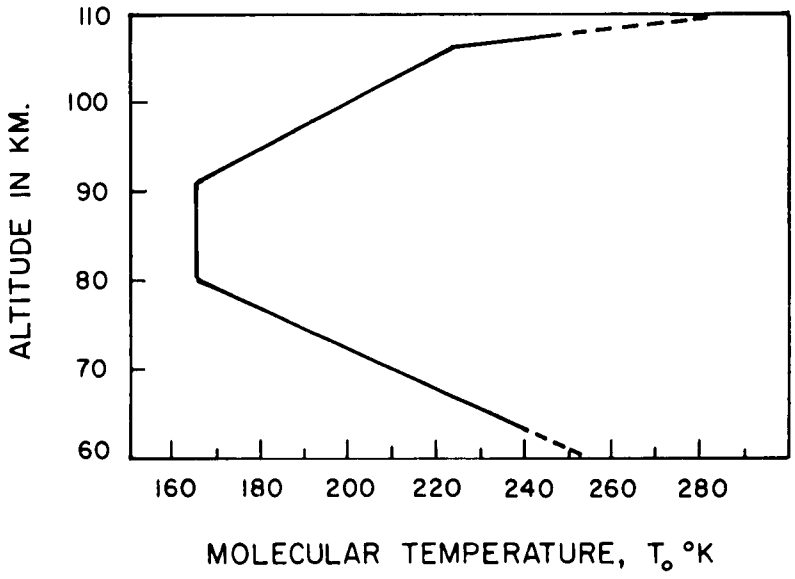

a. Molecular temperature versus altitude (Minzner, et al[12])

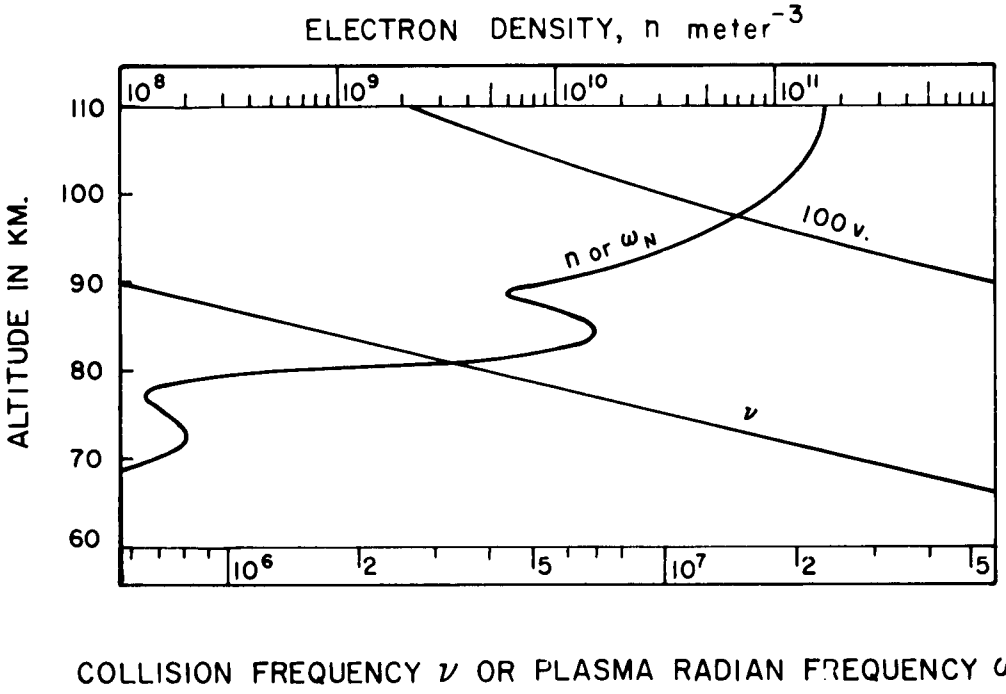

b. Collision frequency (Nicolet[11]), electron number density (Waynick[13]), and deduced plasma frequency as functions of altitude

Figure 1.1. Parameters of the E-layer

(a) Temperature from Minzner, et al.[12]

(b) Electron density (noon average) from Waynick[13] and collision frequency from Nicolet[11].

1.3 Experimental Procedure

The experiment designed to study electron gyroresonance heating within the ionosphere uses a rocket-borne pulsed gyrofrequency transmitter as the source of disturbance of the medium. The detection of electron heating is performed in the same manner as that commonly used in investigating the "Luxembourg effect", i.e. a continuous sensing wave is propagated through the heated region. Cross modulation detected on the sensing wave indicates the extent of the heated region weighted by the degree of heating along the path of the sensing wave.

Figure 1.2 shows a schematic of the cross modulation experiment. The sensing wave propagates from a ground based transmitter to a receiver in the rocket; this insures that it is sufficiently weak so as to have negligible effect upon electron energy. The direction of propagation of the sensing wave and the geomagnetic field are near enough to being parallel to justify use of the quasi-longitudinal approximations for the Appelton-Hartree equations, provided the experiment is performed at Eglin Air Force Base, Florida. Note also that the portion of the heated region through which the sensing wave passes is that heated by a quasi-longitudinal gyrofrequency wave in the first approximation. The output of the sensing receiver is telemetered using a wide bandwidth channel and recorded on magnetic tape at the APGC telemetry facility.

The size of the heated region is limited by the absorption of the gyrofrequency wave as it transfers energy to the electrons. For example the attenuation of a gyrofrequency wave of extraordinary sense of polarization propagating parallel with the magnetic field is approximately 3 db per meter at 85 km and 8 db per meter at 92 km prior to heating. The effect of electron heating is to decrease absorption of this wave which results in a gradual increase of the disturbed region, but not to dimensions greater than the order of one kilometer. This subject is discussed further in Section 1.5.

As a result of the limited region of gyroresonance heating the experiment may be considered to occur in a nearly homogeneous medium. The local values

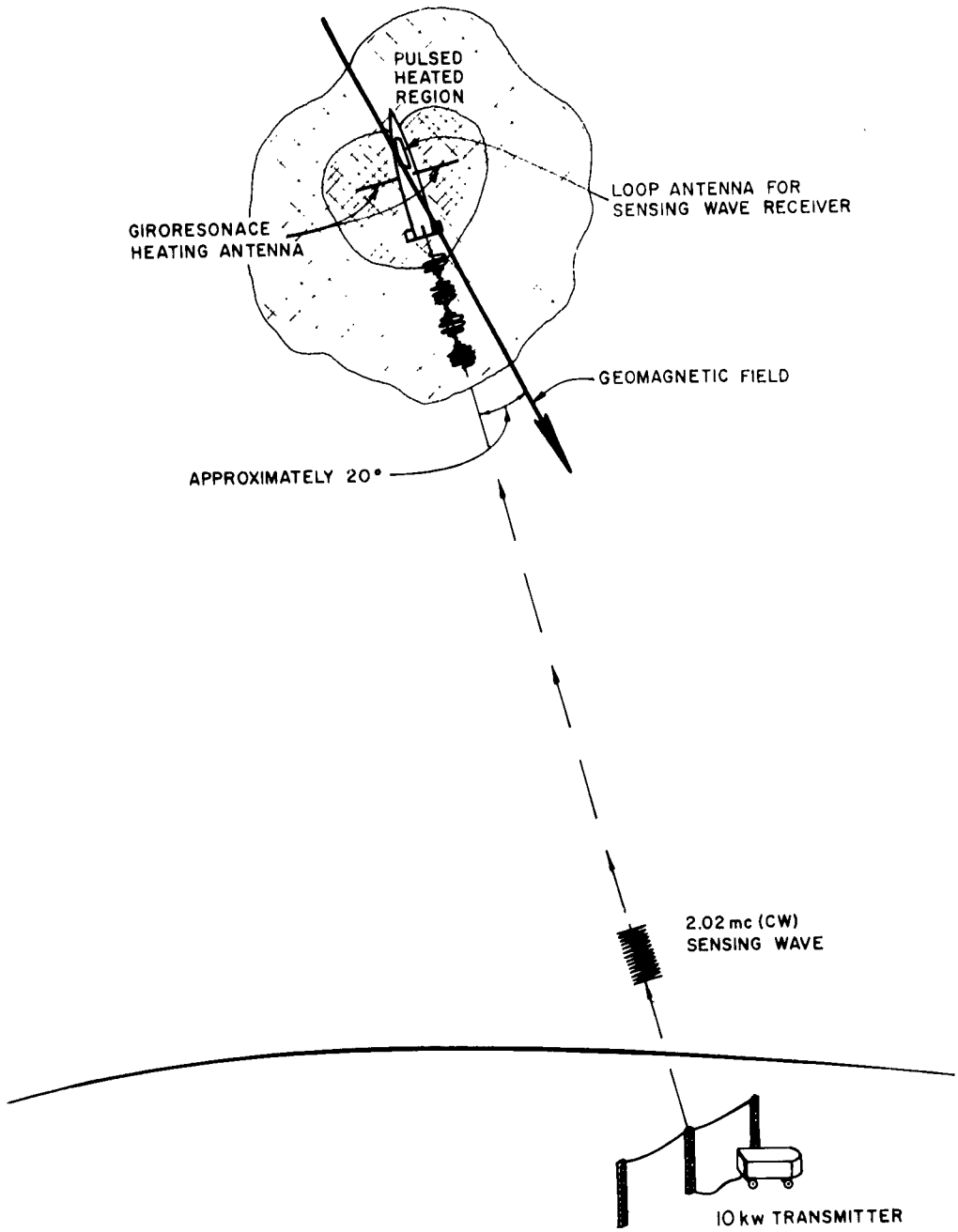

Figure 1.2. Gyroresonance probe experimental schematic

of electron density, collision frequency and molecular temperature, which are functions of altitude, are variable parameters in the experiment. In addition the peak power output of the heating transmitter is continuously varied through three power levels separated by 10 db to provide another parameter.

The altitude range of the experiment is determined primarily by the gyroresonance bandwidth, which is defined as $\nu/2\pi$. Below 76 km there is no resonance. At 88 km the fractional bandwidth is 10%. At 100 km it is 1%. However, the accuracy with which the gyrofrequency as a function of altitude can be predicted is roughly $\pm$ 1% for a dipole approximation of the geomagnetic field. Therefore the rocket flight should be limited to a maximum of 100 km to insure that the heating signal frequency is within the resonance and that the probe remains in the desired part of the ionosphere as long as possible.

The geomagnetic field at Eglin Air Force Base is 0.5276 gauss. Based on the inverse cube law the gyrofrequency at 100 km is 1.41 mc This frequency is within the resonance bandwidth for all lower altitudes.

In the instrumentation of the initial gyroresonance probe several subordinate experiments were performed. Included with the heating transmitter subsystem were the instantaneous measurement of heating antenna impedance, power radiated, and radiated near electric field. These were intended as indicators of design improvements for future experiments as well as data relevant to interpretation of simultaneous cross modulation measurements.

A 10 stage photomultiplier (type 7767) was included to detect excitation light induced by inelastic collisions of heated electrons and molecules (or atoms)

In conjunction with the investigation of non-linearities in plasmas by J. Verdeyen (see Chapter 3) a receiver to detect mixing of the sensing (2.02 mc) and heating (1.41 mc) signals was included The receiver was tuned to the difference frequency (610 kc).

A functional block diagram of the entire gyroresonance probe experiment is shown in Figure 1 3

The block denoted System Operation Monitors includes the sampling of voltages which indicate the status of various components (such as deployment of whip antennas power supply operation sensing receiver AGC, and magnetic aspect).

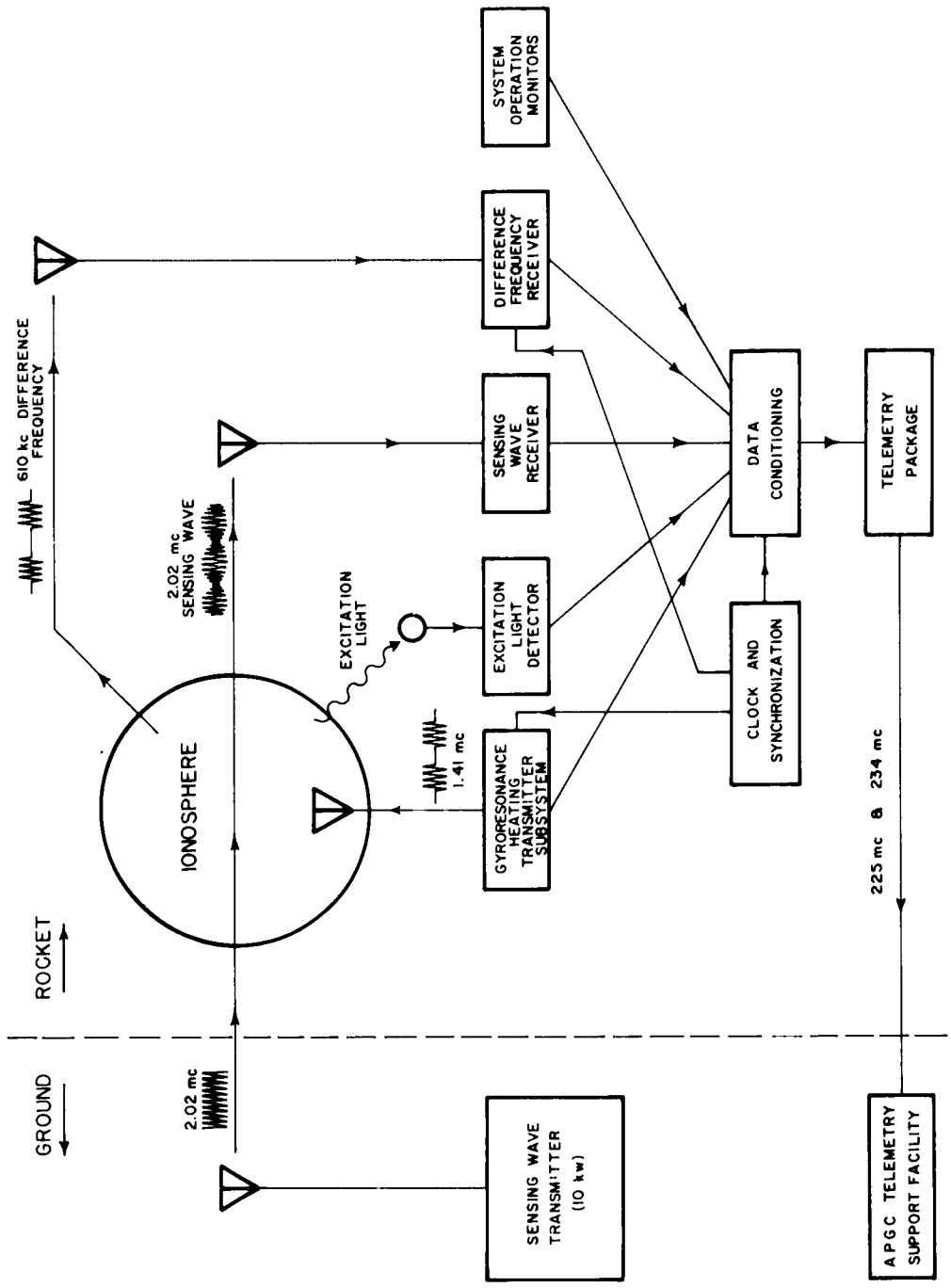

Figure 1.3. Functional block diagram of gyroresonance probe experiment

Telemetry, data conditioning, and synchronization will be discussed later.

1.4 Probe Configuration

The gyroresonance probe instrumentation was installed in a fiberglass-epoxy ogive nose cone and a 15 inch extension section. Telemetry and range safety functions utilized two 10 inch extensions.

Figure 1.4 shows the locations and orientations of the antennas associated with the experiment. Telemetry and beacon antennas are omitted.

The gyroresonance heating antennas consisted of two base loaded fiberglass whips, each 10 feet long. During launch they were folded down along the rocket body and were to be deployed at approximately 70 km.

Loop antennas located within the ogive served the sensing wave and difference frequency receivers. The sensing wave loop antenna and the heating antennas were orthogonally oriented to reduce coupling of the heating signal into the sensing receiver.

The electric field intensity of the heating signal was detected by measuring the RF voltage between two parallel plates located within the nose cone near its upper extremity (approximately 2 meters from the heating antennas).

Excitation light was detected by means of a photomultiplier tube at one end of a 10 inch long collimating pipe. The other end terminated in a window at the skin of the rocket. Its axis was oriented to intersect one of the deployed heating antennas at a point 8 feet from the rocket. The 3 db beamwidth was approximately 3°.

The coordinates shown in Figure 1.4 are used to designate the axes of three magnetic aspect sensors. The use of three magnetometers gives directly the magnetic aspect of heating (x) and sensing (y) antennas as well as precession of the z axis.

1.5 Gyroresonant Heating of Electrons within the Ionosphere

A rigorous treatment of the problem of electron gyroresonance heating within the ionosphere would involve finding the self-consistant radiation pattern of the heating antenna and the electron distribution function by simultaneous solution of Maxwell's equations and the Boltzmann equation. The complexities of this problem are greatly reduced if it is simplified

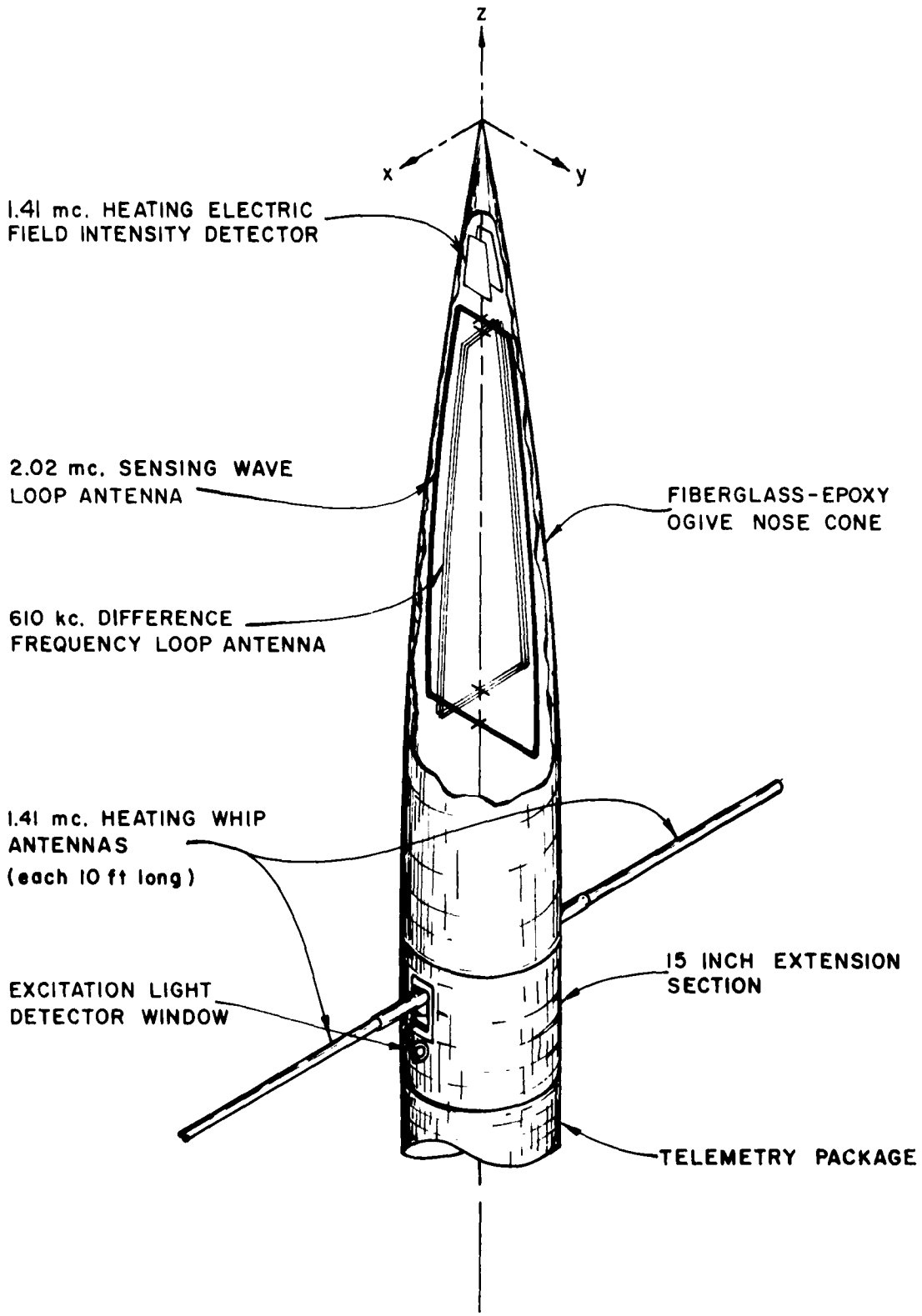

Figure 1.4. Locations and orientation of antennas with respect to the airframe

to one dimension. This will demonstrate the time-distance dependence of electron temperature upon the radiated electric field.

The model chosen to approximate the actual situation of a rocket-borne gyroresonance heating source consists of a plane wave incident upon an infinite homogeneous plasma. The direction of propagation will be taken parallel to that of the applied magnetic field, and it will be assumed that the source produces circularly polarized waves having the sense of the extraordinary characteristic waves.

In the presence of a gyrofrequency electric field of extraordinary sense of polarization the aveage energy gained by an electron between collisions, $\bar{w}$, is equal to the work done on an "average electron" by the field in the same interval of time Based upon the assumptions of the previous section, isotropic collisional scattering implies that the "average electron" has zero momentum immediately following a collision (i.e. its energy is "thermalized" by the collision). For quasi-longitudinal propagation of the gyrofrequency field,

$$\bar{w} = \frac{e^2E^2}{2m} \langle\tau^2\rangle \tag{1.1}$$

where E is the field intensity and $\langle\tau^2\rangle$ is the mean square free time for an electron. Assuming a Poisson distribution of free time, $\langle\tau^2\rangle = 2/\nu^2$ and

$$\bar{w} = \frac{e^2E^2}{m\nu^2} \tag{1.1a}$$

(Derivations of this result may be found in References 1 and 14.)

The average electron energy in the presence of a gyrofrequency field satisfies the equation

$$\frac{dU}{dt} + G\nu(U - U_o) = \bar{w}\nu \tag{1.2}$$

where U = average electron energy ($= 1/2\ m\langle v^2\rangle = 3/2\ kT_e$)

U_o = average molecular energy ($= 3/2\ kT_o$)

Letting v represent rms electron velocity and $\nu = \nu_o\, v/v_o$, the solution of (1.2) (for $t \geq 0$ and $E = 0$ when $t < 0$) is given by

$$\frac{\nu_o G}{2\sqrt{\frac{3kT_o}{m}}} (v'^2 + v''^2)\, t = v' \left(\tanh^{-1} \frac{v}{v'} - \tanh^{-1} \frac{v_o}{v'} \right) - v'' \left(\tan^{-1} \frac{v}{v''} - \tan^{-1} \frac{v_o}{v''} \right) \tag{1.3}$$

where

$$v'^2 = \frac{1}{2} \left[v_o^2 + \sqrt{v_o^4 + \frac{24kT_o}{Gm} \left(\frac{eE}{m\nu_o} \right)^2} \right]$$

$$v''^2 = \frac{1}{2} \left[-v_o^2 + \sqrt{v_o^4 + \frac{24kT_o}{Gm} \left(\frac{eE}{m\nu_o} \right)^2} \right]$$

It is evident that v increases as t increases, which corresponds to increasing electron temperature with time during the gyrofrequency disturbance; thus we call this a heating signal. As $t \longrightarrow \infty$,

$$\tan^{-1} \frac{v}{v''} < \frac{\pi}{2}$$

for all v and therefore

$$\tanh^{-1} \frac{v}{v'} \longrightarrow \infty$$

or v must approach a heated equilibrium value v'. Thus

$$v_o < v < v' \qquad \text{for } t > 0$$

and $v \longrightarrow v'$ as $t \longrightarrow \infty$.

We now make the assumption that electron density remains constant (i.e. neglect effects of heating on diffusion, ionization, attachment and recombination rates). The heating field intensity as a function of time and distance z from the source is

$$E(z,t) = E_o \exp\left[\frac{\omega}{c} \int_0^z \chi(\xi, t)\, d\xi \right] \tag{1.4}$$

where E_o is the field at the source and χ is the absorption index of the medium. In the first approximation χ may be assumed to be that found from the steady state Appelton-Hartree equations:

$$\chi = \mathrm{Im}\sqrt{1 - i\frac{\omega_N^2}{\omega\nu_o}\frac{\nu_o}{\nu}} \qquad (1.5)$$

where ω_N is the plasma frequency. Now from Equation (1.3) and Equation (1.5) we know χ as a function of time only when E is constant. Therefore it is necessary to approximate the solution to Equation (1.4) in the following manner.

It is assumed that the source of the disturbing wave is turned on at $t = 0$, and from then until $t = t_1$, an interval of approximately $1/\nu_o$, it is assumed that $\chi(z,t) = \chi(z,0)$ or in other words does not change in the interval The value of $|E|$ can then be found as a function of z from Equations (1 4) and (1.5) and the increase in electron velocity at various distances from the source (for the time interval from $t = 0$ t_o $t = t_1$) can be found from Equation (1.3). From these data and Equation (1.5) a curve of χ versus z for $t = t_1$ is plotted and the integration of Equation (1.4) performed graphically. This gives $|E(z,t_1)|$ which is held constant for the next interval while the process is repeated Successive repetition gives the approximate solution to Equation (1 4) for later values of time.

Sample calculations of this type have been made for altitudes of 85 km and 92 km, which are in the range of interest for the rocket experiments. The assumed parameters of the ionosphere for these altitudes are tabulated below

Altitude	ω_N	ν_o	T_o °K
85 km	7.0×10^6	1.48×10^6	165.7
92 km	8.4×10^6	4.20×10^5	168.4

The values of ω_N are calculated from data of Waynick[13], those of ν_o are obtained from Nicolet[11], and molecular temperature T_o from Minzner, et al[12].

Figures 1 5 and 1 6 show computed curves of intensity of the disturbing field E and of v/v_o respectively with time as a parameter for $E_o = 10$ volts

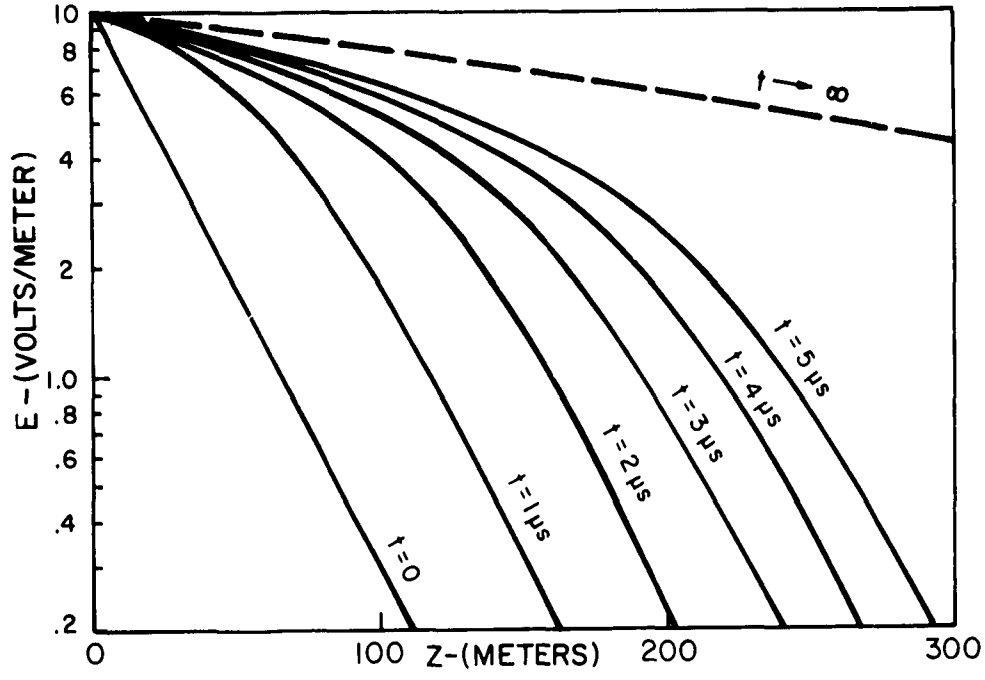

Figure 1.5. Field strength of heating wave as a function of distance from source for various instants of time. Field strength at source E_o = 10 volts/meter; altitude = 85 km

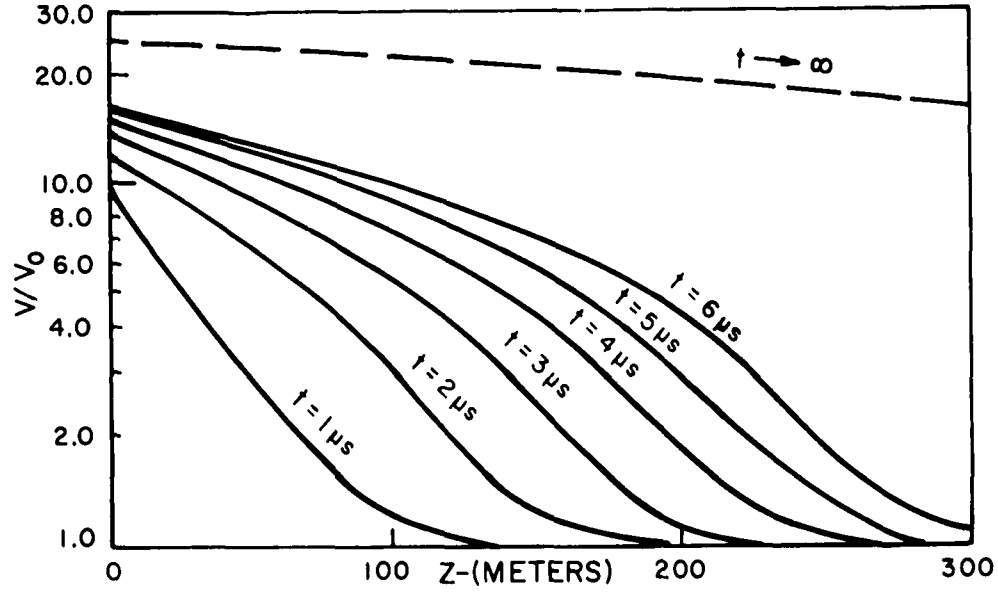

Figure 1.6. Relative electron velocity as a function of distance from source of heating wave for various instants of time. Field strength at source E_o = 10 volts/meter; altitude = 85 km

per meter at 85 km, Figure 1.7 and 1 8 show E and v/v_o respectively for the same time intervals and at the same altitude but for E_o = 1 volt per meter. In Figure 1.9 and 1.10 E and v/v_o are plotted for various times for E_o = 1 volt per meter at an altitude of 92 km.

1.6 Relaxation of Heated Electrons

At the end of a gyroresonant heating pulse it is presumed that the medium has reached a heated equilibrium state. At this time the electron rms velocity is roughly v' given in the preceeding section (where E is the electric field pattern) Equation (1.2) now becomes

$$\frac{dU}{dt} + G\nu(U - U_o) = 0 \tag{1.6}$$

which has the solution (when the substitution $U = 1/2\ mv^2$ is made)

$$\frac{v}{v_o} = \frac{\frac{v}{v_o}\ \mathrm{ctnh}\ \frac{G\nu_o t}{2} + 1}{\frac{v'}{v_o} + \mathrm{ctnh}\ \frac{G\nu_o t}{2}} \tag{1.7}$$

This indicates that $1/G\nu_o$ is the relaxation time constant for the medium.

1.7 The Gyroresonance Heating Signal

The criteria for choosing pulse width, pulse repetition frequency, transmitter power and antenna system for the gyroresonance heating signal are as follows. It is desired that the heating spread over as large a volume as possible In addition the time interval between pulses should be long enough to permit the medium to relax, this insures that the altitude variation of electron density and collision frequency are valid experimental parameters.

The results of Section 1.5 indicate that heating at large distances from a gyrofrequency source occurs much more slowly than near the source. The heating pulse width for the initial experiment was chosen to be 500 microseconds. This was determined mainly from the practical considerations involved in designing equipment.

As pointed out in Section 1.6 the time constant for the decay of electron energy in $1/G\nu_o$ Therefore the pulse repetition frequency should

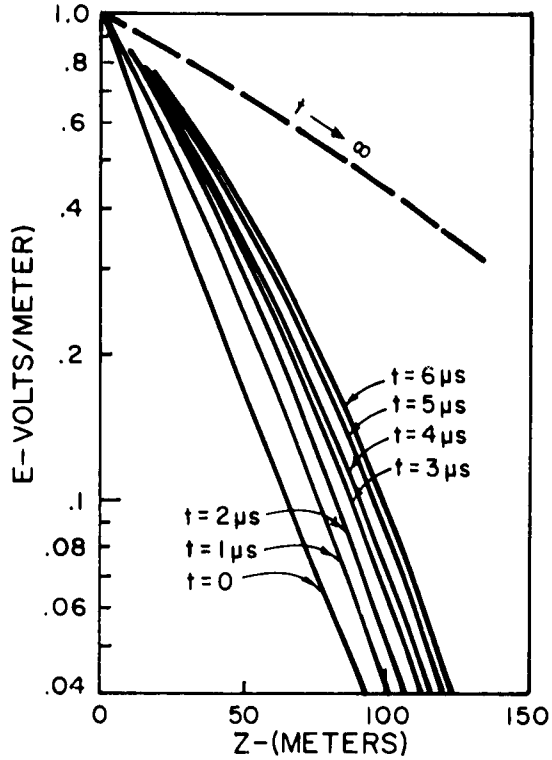

Figure 1.7. Field strength of heating wave as a function of distance from source for various instants of time. Field strength at source E_o = 1 volt/meter; altitude = 85 km

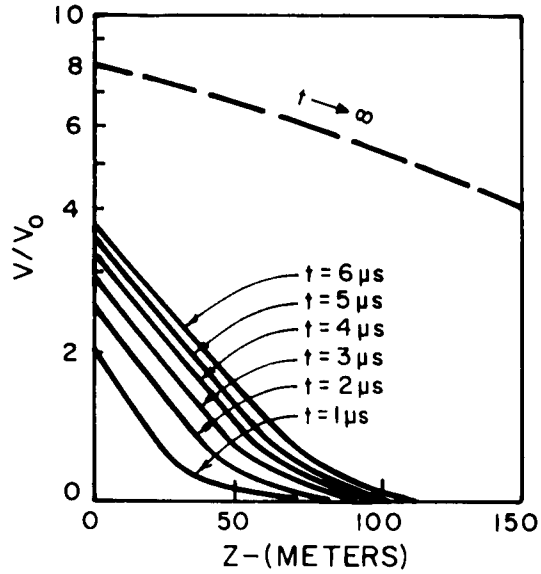

Figure 1.8. Relative electron velocity as a function of distance from source of heating wave for various instants of time. Field strength at source E_o = 1 volt/meter; altitude = 85 km

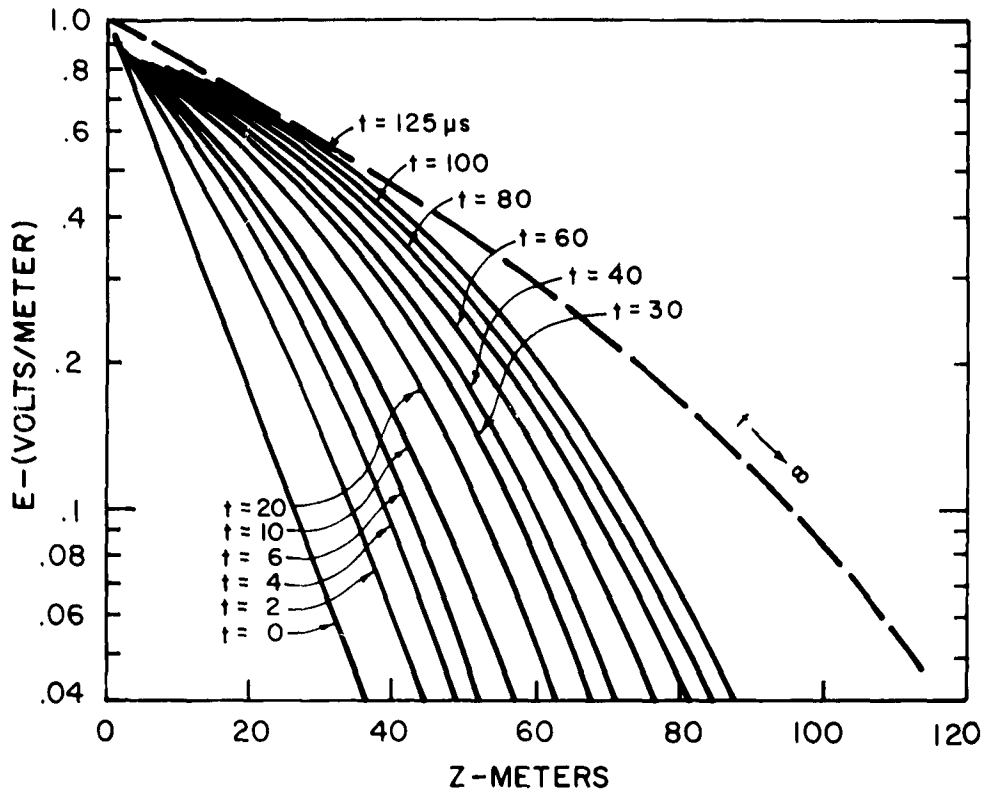

Figure 1.9. Field strength of heating wave as a function of distance from source for various instants of time. Field strength at source E_o = 1 volt/meter; altitude = 92 km

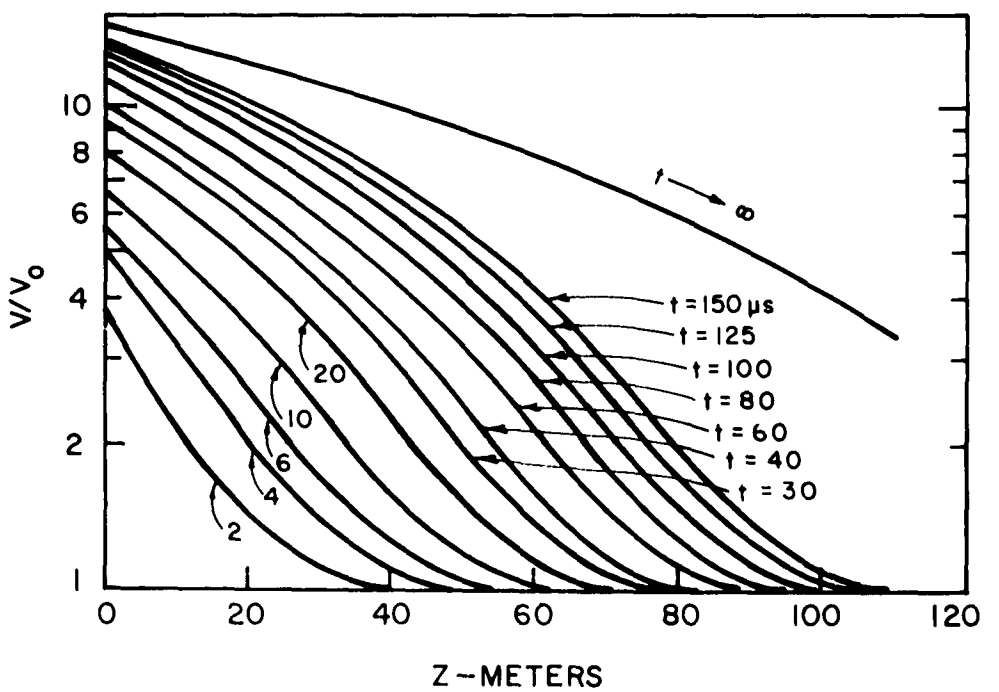

Figure 1.10. Relative electron velocity as a function of distance from source of heating wave for various instants of time. Field strength at source E_o = 1 volt/meter; altitude = 92 km

be less than $G\nu_o$. At 100 km $\nu_o \sim 10^5$, and for $G = 10^{-3}$, we have the result that the repetition frequency should be less than 100 pulses per second. From system synchronization considerations a frequency of 75 pps was chosen with a 45 pps free running capability should the synchronization fail. This also would permit analysis of data from successive pulses as functions of geomagnetic field aspect of the heating antenna based on a rocket rotation rate of 2 rps.

The heating transmitter output power level is an arbitrary parameter in that the antenna radiating efficiency depends upon its impedances which may be expected to be a function of altitude, magnetic aspect and degree of electron heating. Therefore the switching of the output power through several levels seems the prudent approach. For the initial experiment a transmitter with 400 watts peak output power was designed. A step attenuator between the transmitter and the antenna provided power levels of 4, 40 and 400 watts. Each level was maintained for 45 pulses (or .6 sec) which would be sufficient time for one rocket rotation.

The problems involved in designing a heating antenna system do not appear to have corollaries in free space. The medium is anisotropic and during heating inhomogeneous. It is furthermore dependent upon parameters which are functions of altitude. The antenna system design for the initial experiment consisted of a pair of base loaded fiberglass whip antennas each 10 feet long. The impedance of short antennas in an anisotropic medium is discussed in the work of K. Balmain in Chapter 2 of this report, and the heating antenna system is discussed in Quarterly Progress Report No. 10. Briefly the effect of the ionosphere at 90 km is to cause a resistance of the order of 2000 ohms to appear in shunt with the antenna terminals after electron temperature has been increased by a factor of 6. However the effect of increased electron density due to ionization would be to lower this resistance. Therefore a compromise value of 1000 ohms attributable to gyro-resonance heating losses was assumed and the antenna matching network designed accordingly.

A block diagram of the heating transmitter subsystem is shown in Figure 1.11. The synchronization of the various functions is discussed in Section 1.10.

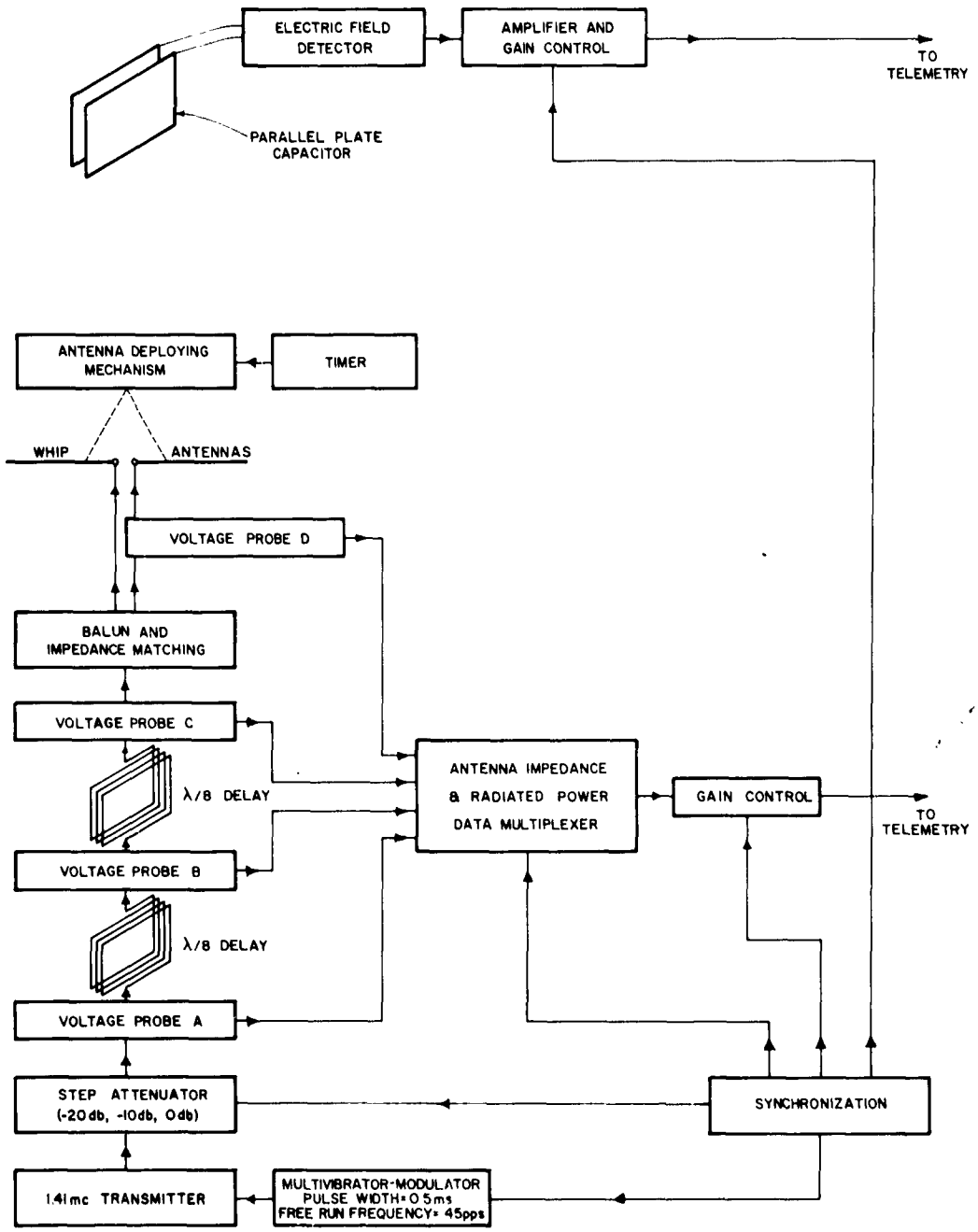

Figure 1.11. Heating transmitter subsystem block diagram

Data from which antenna impedance and radiated power could be computed was obtained by measuring four RF voltages Three (v_A, v_B and v_C) were along a 50 ohm coaxial cable at one eighth wavelength intervals and the fourth (v_D) was the antenna voltage. These probes were sampled successively in such a manner that for each heating pulse a different voltage was measured. A gain control actuated by the position of the step attenuator provided a constant range of data level.

The heating signal electric field data acquisition consisted of the measurement of the RF voltage between two parallel plates near the upper tip of the nose cone. This configuration was chosen because its impedance was affected less than a dipole by variation of the dielectric properties of the medium. Again the gain of the amplifier was adjusted in accordance with step attenuator position.

1.8 Detection of Electron Heating

In "Luxembourg effect" experiments the electron heating is commonly detected by observing the modulation produced on a relatively weak signal traversing the disturbed portion of the ionosphere. The modulation is an integrated effect of the absorption over the entire path and has the form

$$\text{Modulation} = \exp\left[\frac{\omega}{c}\int_a^b (\chi_o(z) - \chi(z,t))\,dz\right] \qquad (1.8)$$

where $\chi_o(z)$ is the undisturbed absorption index and $\chi(z,t)$ the disturbed absorption index.

For a sensing wave of ordinary polarization and propagating parallel with the magnetic field in a homogeneous plasma

$$\chi(z,t) = \mathrm{Im}\sqrt{1 - \frac{X}{1 + Y - i\,Z(z,t)}} \qquad (1.9)$$

where $X = (\omega_N/\omega)^2$

$Y = \omega_c/\omega$ $(= -eB/m\omega)$

$Z(z,t) = [\nu_o/\omega][v(z,t)/v_o]$

The dependence of χ on v/v_o is responsible for the cross modulation as was shown by Bailey and Martyn[9] A plot of $\omega/c\,\chi$ versus v/v_o or T_e at 85 km for a sensing frequency 1 5 times the gyrofrequency is shown in Figure 1 12

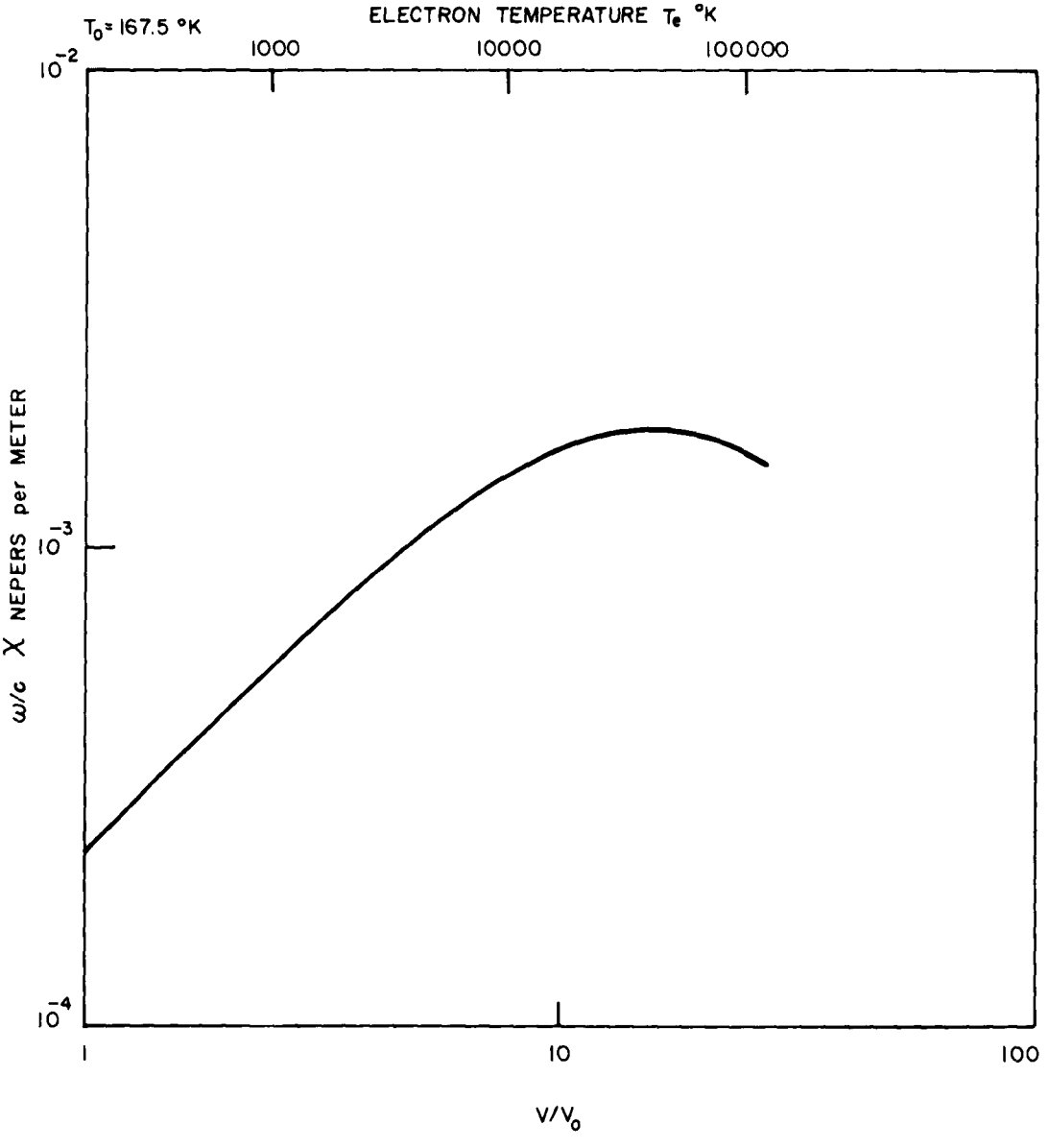

Figure 1.12. $\omega/c\ \chi$ as a function of v/v_o or T_e at 85 km for sensing wave with $\omega = 1.5\ \omega_c$ ($\cong 2.1$ mc)

Note that the absorption coefficient has a maximum value this occurs when $Z/(1 + Y) = 1$. Therefore the maximum absorption at lower altitudes will occur for smaller value of v/v_o and for higher altitudes at greater values of v/v_o.

The sensing wave frequency and time of day for the experiment were decided on the basis of calculations of the attenuation and derivative of attenuation with collision frequency for characteristic waves traveling parallel to the magnetic field This work is reported in Quarterly Progress Report Nos. 5 and 6 and will be briefly summarized here

The night experiment was ruled out because the ordinary wave is not attenuated, nor is it sufficiently affected by changes of collision frequency by a factor of 10.(as would be expected during heating).

The daytime calculations, using the electron density and collision frequency models shown in Figure 1 1b, indicated that the sensing wave should be near 2 mc. A plot of the expected total attenuation for the ordinary wave as a function of altitude is shown in Figure 1 13 The extraordinary wave is attenuated more than 90 db at 80 km

A broadcast transmitter was given to the University of Illinois by the Collins Radio Company for use in these experiments as a sensing wave transmitter. Having been modified, it is now capable of continuous 13 kw output at 2.02 mc (the assigned sensing frequency) and is installed in a semi-trailer

At the rocket it is desirable that the sensing antenna be unaffected by variations of the dielectric properties of the medium. The structure which gives the closest approximation to this requirement is a small loop antenna This is also aerodynamically attractive since it can be mounted within a fiberglass-epoxy ogive One would expect the efficiency of such an antenna to be low. In free space the Q of a lossless circular loop is given by

$$Q_o = \frac{\omega\mu\, b \ln\left(\frac{b}{a}\right)}{31{,}000\left(\frac{\pi b^2}{\lambda^2}\right)^2}$$

where b is the radius of the loop and a the radius of the conductor For 2 mc,

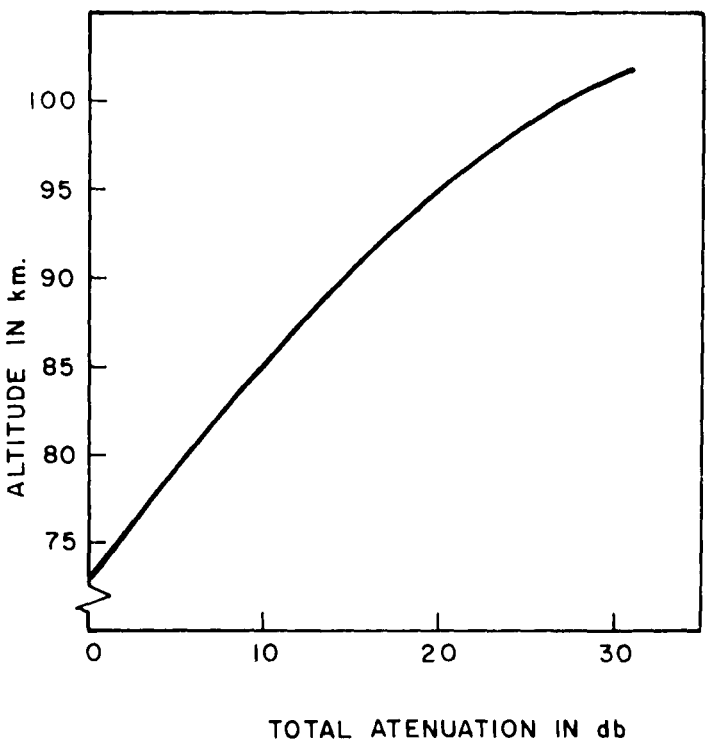

Figure 1.13. Total attenuation of 2 mc. ordinary wave as a function of altitude

letting b = 2 m and a = .003 m it is found that

$$Q_o \simeq 1.4 \times 10^7$$

However, to be able to observe details in the sensing wave modulation during the heating pulse (pulse duration of 500 microseconds) a receiver output bandwidth of DC to 12 5 kc was chosen. (This is compatible with the IRIG standard 70 kc $\pm$ 40% telemetry subcarrier channel) The output frequency range neccessitates an RF input bandwidth of 50 kc or the antenna must have a loaded Q_L at 2 mc of

$$Q_L \simeq 40$$

The resulting antenna efficiency is just $Q_L/Q_o \simeq 3 \times 10^{-6}$.

From Figure 1.13 we see that the ordinary sensing wave is attenuated 27 db in propagating from the ground to 100 km There is also a loss of 3 db in the extraordinary wave and a loss of 3 db due to the linear polarization of the receiving loop antenna. If the sensing transmitter output power were 10 kw the 33 db loss would make it equivalent to a 5 watt transmitter in free space with identically polarized antennas The power density expected at 100 km would be 4×10^{-11} watts per square meter the power delivered to the receiver input is given by

$$P = \frac{Q_L}{Q_o} \times \frac{G\lambda}{4\pi} \times (\text{Power density})$$

$$\simeq 3\ 6 \times 10^{-13} \text{ watts}$$

For a receiver input impedance of 100 ohms the resulting voltage at the receiver input is approximately 6 microvolts This is adequate for detection with a high signal to noise ratio using state of the art techniques. The sensing wave receiver used in the initial gyroresonance experiment was developed for this purpose by Kellogg Division of IT & T

The rocket rotation, sensing receiver output and its AGC voltage are sufficient data from which the polarization ellipse of the sensing wave may be determined as a function of altitude in the D region This gives the ratio of ordinary to extraordinary wave intensity which is indicative of the properties of the lower region of the ionosphere

1.9 Telemetry Data Conditioning

The telemetry channels available for this experiment consisted of a 70 kc ± 40% subcarrier oscillator using 234 mc and 70 kc, 40 kc, and 22 kc (all ± 15%) subcarrier oscillators at 225 mc. These were allocated in the following manner

70 kc ± 40%	sensing receiver output
70 kc ± 15%	heating antenna impedance and radiated power
40 kc ± 15%	heating field intensity and excitation light
22 kc ± 15%	sampled data

The data conditioning for each of these channels will be discussed

(1) 70 kc ± 40% On the basis of computations of cross modulation contained in Quarterly Progress Report No 7, the expected variation of sensing receiver output due to heating is of the order of 40% at 85 km and 10% at 92 km. The sensing receiver output has a frequency response of ± 1 db from DC to 12 kc. The DC component is held at + 10 v (± 1/2 v) by the AGC. (Thus a 1 volt variation corresponds to 10% change in the RF input voltage.) However the 0-5 v limits of the subcarrier necessitated some data conditioning. This was accomplished by biasing the receiver output with a 6.7 volt battery, resulting in a telemetered range of sensing wave amplitude fluctuations of + 17% and -33%

(2) 70 kc ± 15% The heating antenna impedance and radiated power data involved a time sharing scheme for use of the telemetry channel More specifically the measured quantities were the voltages at three points along the transmission line feeding the antenna (separated by eighth wavelengths) and the antenna voltage The changes of altitude and magnetic aspect of the rocket between successive heating pulses is small Therefore during each heating pulse a different voltage (and pulse shape) was measured Four successive pulses would provide sufficient data to compute the variation of antenna impedance and radiated power during the heating provided the other simultaneous measurements (sensing wave, field intensity) should indicate that the four heating pulses produced the same effects

(3) 40 kc ± 15% This channel telemetered the field intensity and excitation light in a time sharing mode. Time sharing was accomplished by a relay which was actuated to provide measurement of field intensity for the first 30 heating pulses and of excitation light for the last 15 heating pulses for each power level. (The heating power level was changed after every 45th pulse.)

(4) 22 kc ± 15% Data which were expected to be very slowly varying were sampled by a 30 position, 5 rps commutator. Position and corresponding data are listed below:

1. +5 v frame sync pulse
2. +5 v frame sync pulse
3. heating transmitter subcommutated data
4. subcommutator position
5. photomultiplier tube high voltage
6. x magnetometer bias voltage
7. y magnetometer bias voltage
8. z magnetometer bias voltage
9. x magnetometer output
10. y magnetometer output
11. z magnetometer output
12. sensing receiver output DC component
13. sensing receiver AGC voltage expanded
14. sensing receiver AGC voltage
15. fuel valve data
16. + 4 05 v calibration battery
17. heating signal step attenuator position
18. heating antenna deployment data
19. heating transmitter peak RF voltage
20. common ground reference
21. heating antenna peak RF voltage
22. sensing receiver output
23. sensing receiver output
24. x magnetometer output
25. y magnetometer output

26. z magnetometer output
27. sensing receiver output DC component
28 sensing receiver AGC voltage expanded
29. sensing receiver AGC voltage
30. difference frequency receiver integrated output

The data on positions 3 and 4 was obtained from a stepping switch within the heating transmitter package. It was advanced one step with each revolution of the data sampling commutator. The measurements made concerned the monitoring of the operation of the heating transmitter. These were

1. +13 v battery (power supplies)
2. +6.5 v battery (filaments)
3. +700 v power supply
4. +300 v power supply
5. oscillator current
6. driver amplifier current

Provision was made to advance this switch and to measure these voltages through the umbilical prior to launch. This was to insure proper operation of the heating transmitter.

1.10 Synchronization

The data acquisition processes which have been described required a source of synchronization for the entire experiment. The data sampling commutator was one deck of a two pole switch. The other was used as a clock, which consisted of a 5 rps 60 position switch.

Among other things, the clock advanced a 12 position stepping motor which drove the heating signal step attenuator. Each revolution of the clock advanced the stepping motor once, every third clock revolution advanced it twice. (Three revolutions of the clock stepped the motor 4 times.) Switches driven by the step attenuator motor provided logic circuits from which other synchronization was derived.

Figure 1.14 shows the time relationships of the synchronized functions of the experiment for one complete cycle of the step attenuator.

The data calibration markers were impressed upon the three continuous data channels at the times shown. Each marker consisted of 3 cycles of a 400 cps square wave. The maximum of this signal was 4.05 volts and the

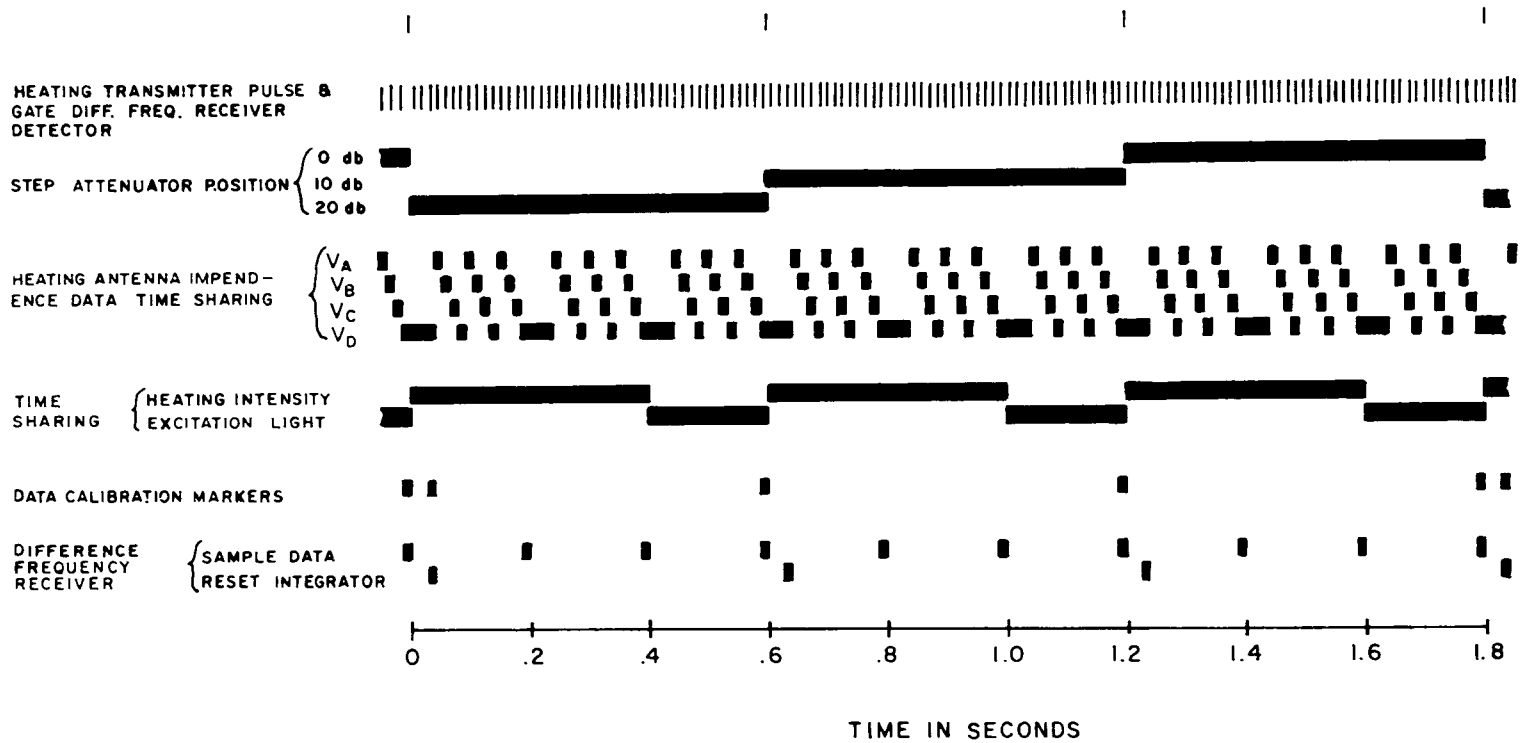

Figure 1.14. Time relationships of the synchronized functions of the experiment

minimum 0 volts These were provided for calibration purposes and as indicators of the heating step attenuator position Note that one marker occurred just prior to each change of attenuation and that a second marker appeared when the -20 db position was reached

1.11 Experimental Results

The initial gyroresonance probe was launched from Eglin Air Force Base at 1318 hours CST on 1 May 1962 The primary objective of the experiment, the detection of gyroresonance heating of electrons in the ionosphere, was successful. However the data sampling switch failed a few milliseconds after burnout when the acceleration reached -1 4 G (from phototheodolite data). The stoppage was sudden indicating a mechanical failure, probably due to foreign matter drifting upward into the gears as the acceleration became less than -1

This failure resulted in the loss of sampled data and of the synchronization functions As a result the following conditions prevailed after burnout and for the remainder of the flight

(1) The heating transmitter operated at 45 pulses per second

(2) The step attenuator remained in the 0 db position

(3) 70 kc ± 40% subcarrier channel functioned normally This channel carried the sensing wave receiver output

(4) 70 kc ± 15% subcarrier channel carried no data The data switch failure occurred during a 4 5 volt reference marker, which then persisted throughout the experiment

(5) 40 kc ± 15% subcarrier channel measured the heating field intensity

(6) 22 kc ± 15% subcarrier channel measured the sensing receiver AGC voltage

A composite of the sensing wave modulation at various altitudes is shown in Figure 1.15 Local equilibrium values of plasma radian frequency, ω_N, and collision frequency, ν_0 (from References 11 and 13 respectively) are given The distance traveled by the rocket between heating pulses Δ is also indicated. Vertical dashed lines represent the onset of heating pulses which had 0 5 millisecond durations The time between pulses was 22 milliseconds and therefore this scale of the data permits study of the sensing wave only during relaxation Each division of the amplitude scale is 1 volt which corresponds

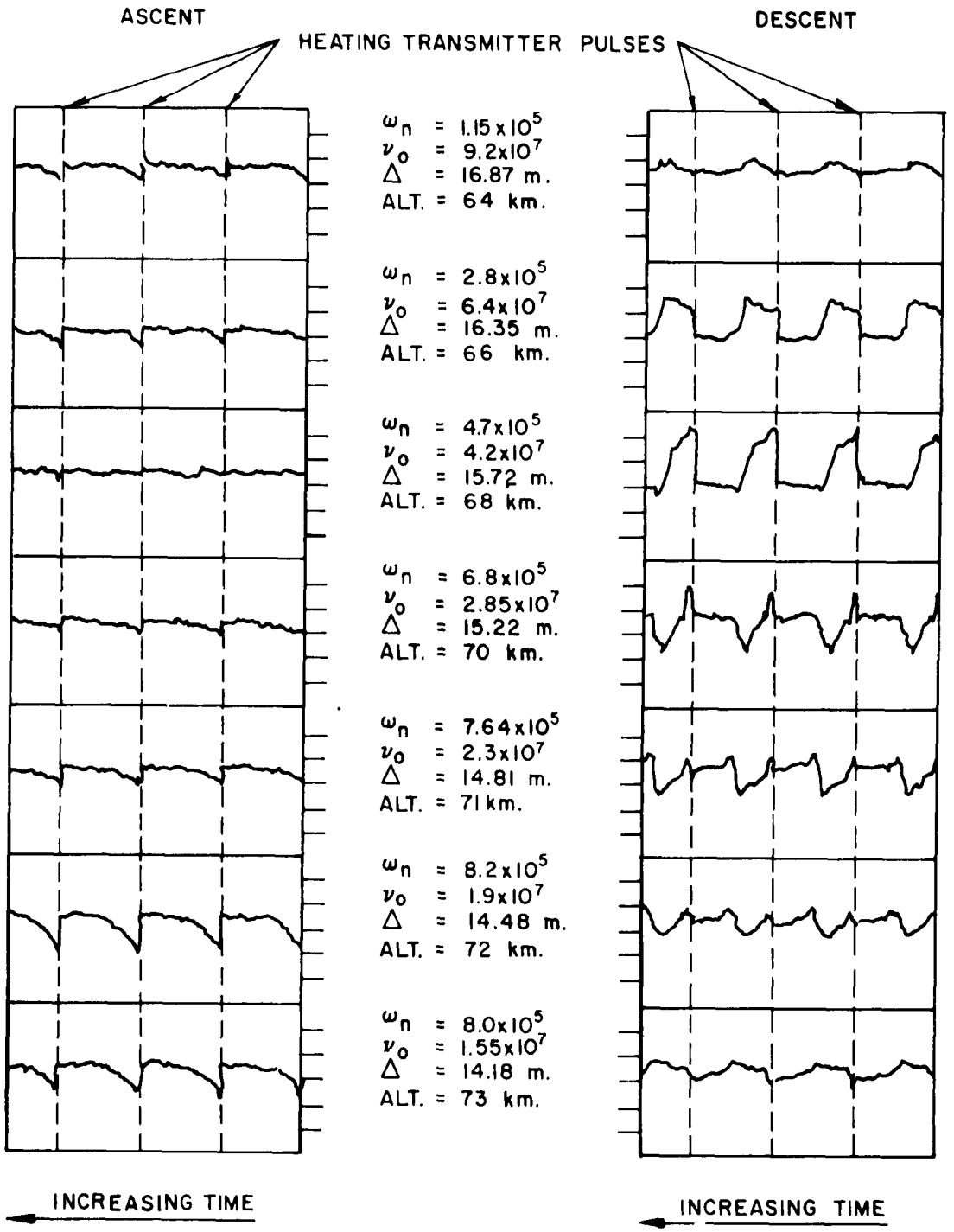

Figure 1.15a. Sensing wave receiver output showing cross-modulation at various altitudes

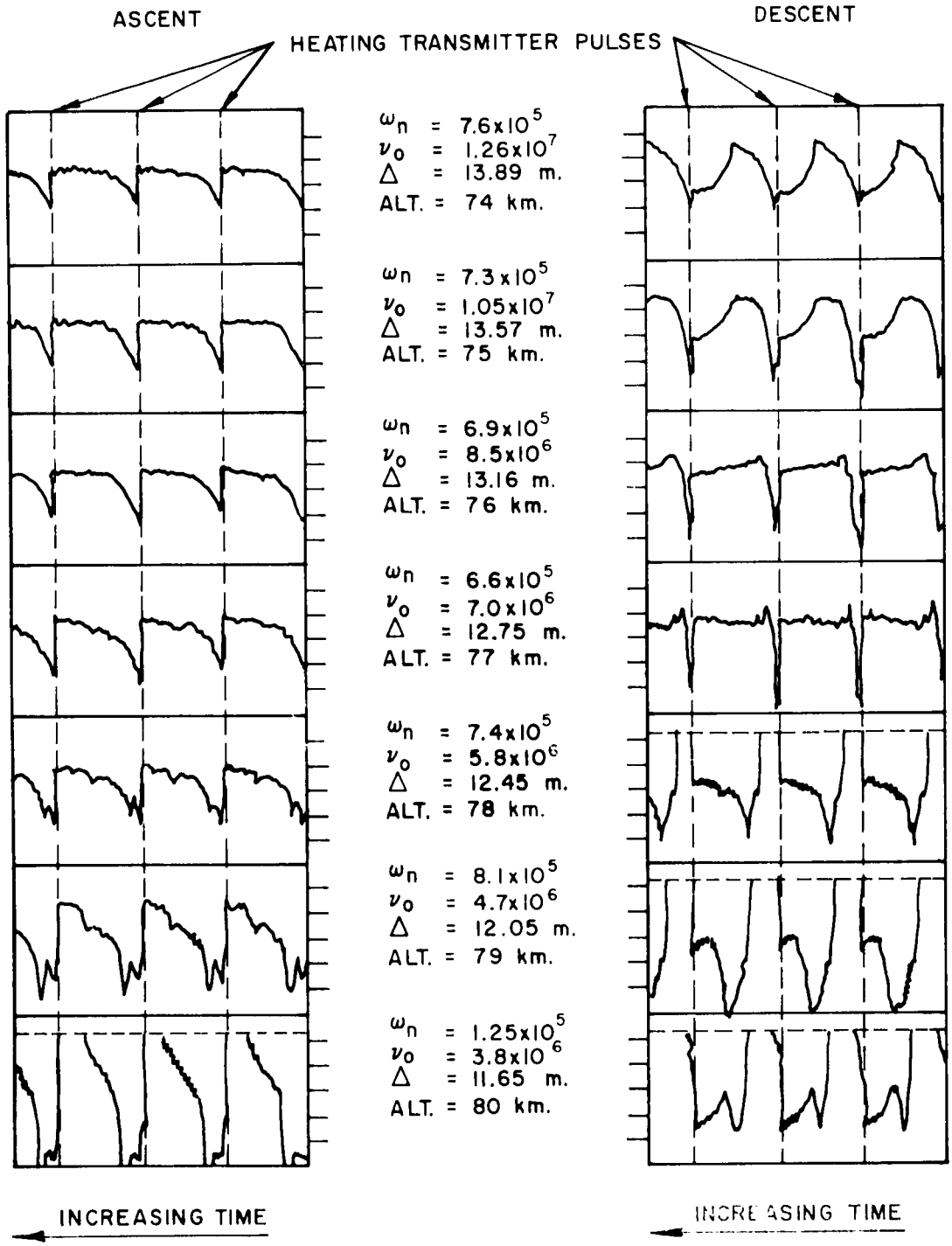

Figure 1.15b. Sensing wave receiver output showing cross-modulation at various altitudes

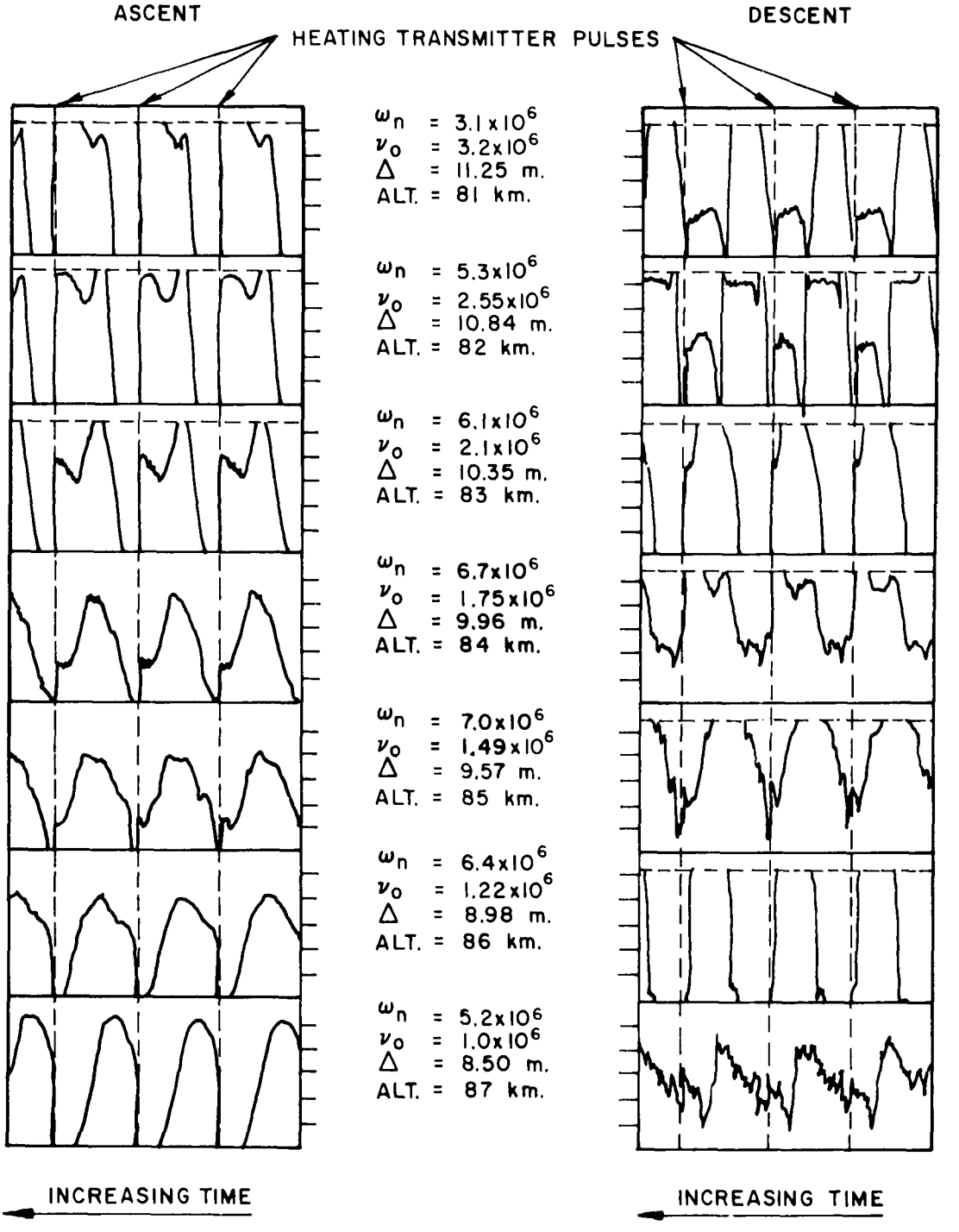

Figure 1.15c. Sensing wave receiver output showing cross-modulation at various altitudes

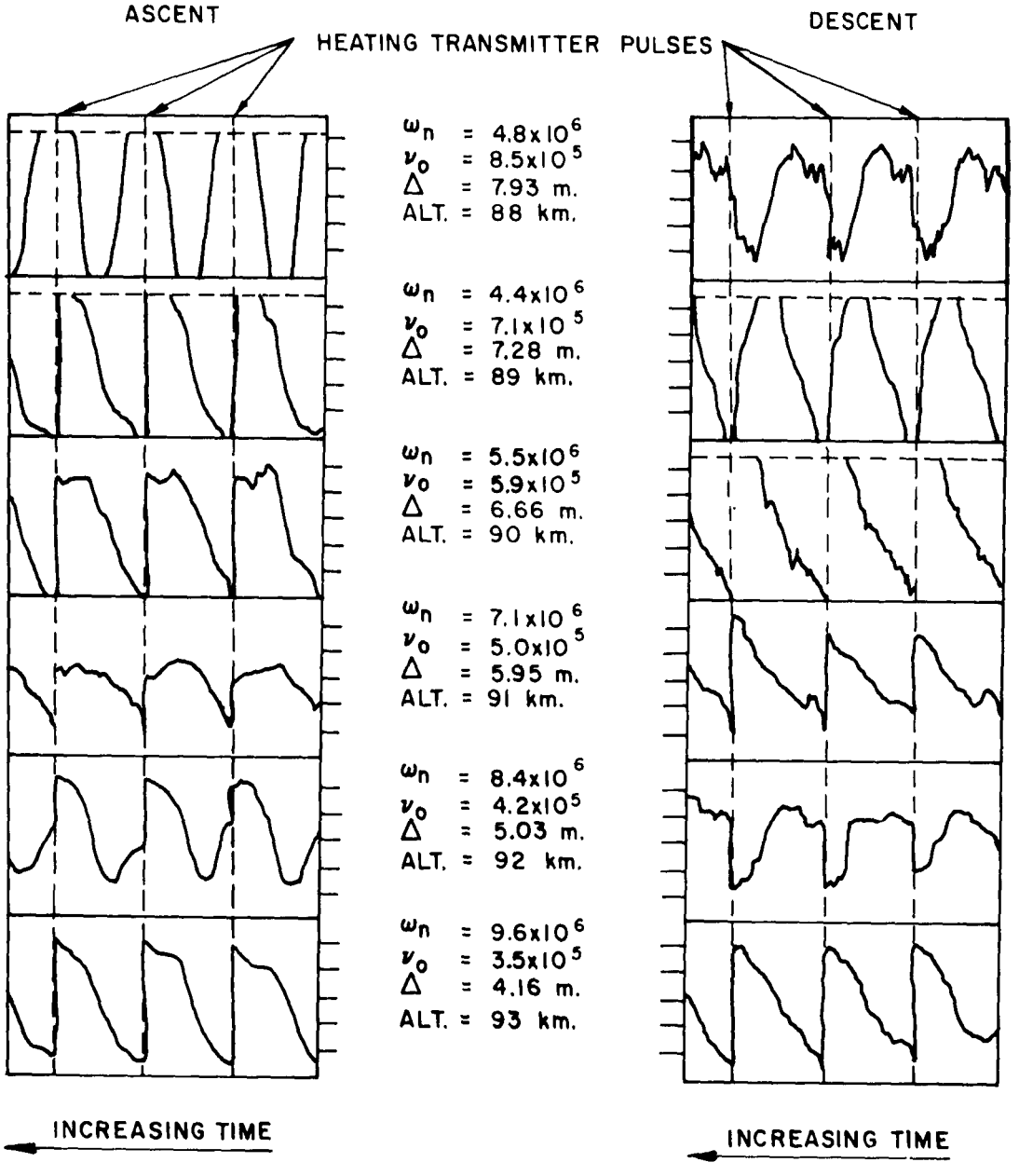

Figure 1.15d. Sensing wave receiver output showing cross-modulation at various altitudes

to 10% variation of the envelope of the input RF from its mean value. The data is biased so that the lower limit of the telemetry channel corresponds to -33% while the upper limit represents +17% deviation of the receiver input.

It is evident from Figure 1.15 that except for very low altitudes the relaxation time of 22 milliseconds was not long enough. Furthermore the character of the disturbances in general is more complicated than would be expected if electron energy decay were the dominant relaxation process involved. This suggests that the heating power was too great, and that some of the cross modulation may have been caused by ionization near the rocket.

There are apparent differences in ascending and descending cross modulation at some altitudes. The heating antennas should have been deployed at T + 76 seconds, corresponding to 62 km. Drag may have delayed this operation, resulting in a different antenna configuration during ascent and descent.

At higher altitudes the differences in sensing wave shapes may have been due to rocket attitude. That is, the heating antenna radiation patterns, and hence the spatial electron energy distribution functions with respect to the sensing wave propagation vector would probably not be the same for ascent and descent. The effect of magnetic aspect upon a gyrofrequency antenna radiation pattern may be found in the work of E. Mattia included in Quarterly Progress Report No. [illegible].

Some interesting results were obtained from the polarization ellipse measurements for the sensing wave, particularly during ascent where the rocket attitude was fairly stable. The rocket rotation rate was roughly one revolution in 8 seconds. Up to 63 km the sensing wave polarization was approximately linear. However, at 67 km it had become almost circular. This indicates that the electron density near 65 km is not negligible, and is substantiated by the fact that cross-modulation began to appear at 62 km. A quantitative analysis of the electron density and collision frequency necessary to produce the observed changes in the axial ratio of the ellipse will be made after further data reduction of the telemetered sensing wave receiver AGC voltage is performed by APGC.

During ascent in the 48 km to 60 km region wherein the rotation of the rocket caused the linear polarizations of the receiving antenna and the sensing wave to pass through a configuration of [illegible]

the antenna polarization pattern) an unusual form of modulation occurred. Figure 1.16 shows the vicinity of the null at 57 km and is typical of all of the nulls in this range of altitudes. (The general shape of the receiver output is due to the AGC which had a time constant of about 0.2 second.) The modulation is characterized by negative going pulses coincident with the heating pulses which become apparent 25^{o} of rotation prior to the null and increase in amplitude as the null is approached. Within one or two degrees of the null the sense of the pulses changes to positive. The modulation becomes negligable 25^{o} past the null. In the remaining 130^{o} between nulls there is no modulation.

This suggests an explanation based upon the modulation of the direction of polarization of the sensing wave, similar to Faraday rotation. For example, if each heating pulse rotated the sensing wave momentarily in a direction opposite to that of the rocket, the receiver input would momentarily decrease prior to the null and increase after. Assuming that the antenna polarization pattern is sinusoidal the percent deviation of the receiver input would be

$$\text{Deviation} \approx 100\% \times \tan\theta \sin\delta_{\phi} \qquad (1.10)$$

where θ is the angle between the null of the receiving antenna and the polarization of the sensing wave, and δ_{ϕ} is the change of angle of the sensing wave polarization due to a heating pulse. Note that a very small value of modulated rotation (δ_{ϕ}) can produce a large and easily detectable deviation near the null ($\theta \approx 0$). The observed data fits equation (1.10) fairly well; and the case shown in Figure 1.16 corresponds to $\delta_{\phi} \approx 1^{o}$

The angle of rotation of the sensing wave at altitude h measured clockwise as viewed from the ground is given by

$$\phi = \frac{w}{2c}\int_{0}^{h} (\mu_{\epsilon} - \mu_{o})\, dz \qquad (1.11)$$

where μ_{ϵ} and μ_{o} are respectively the real parts of the quasi-longitudinal refractive indices of the extraordinary and ordinary characteristic waves.

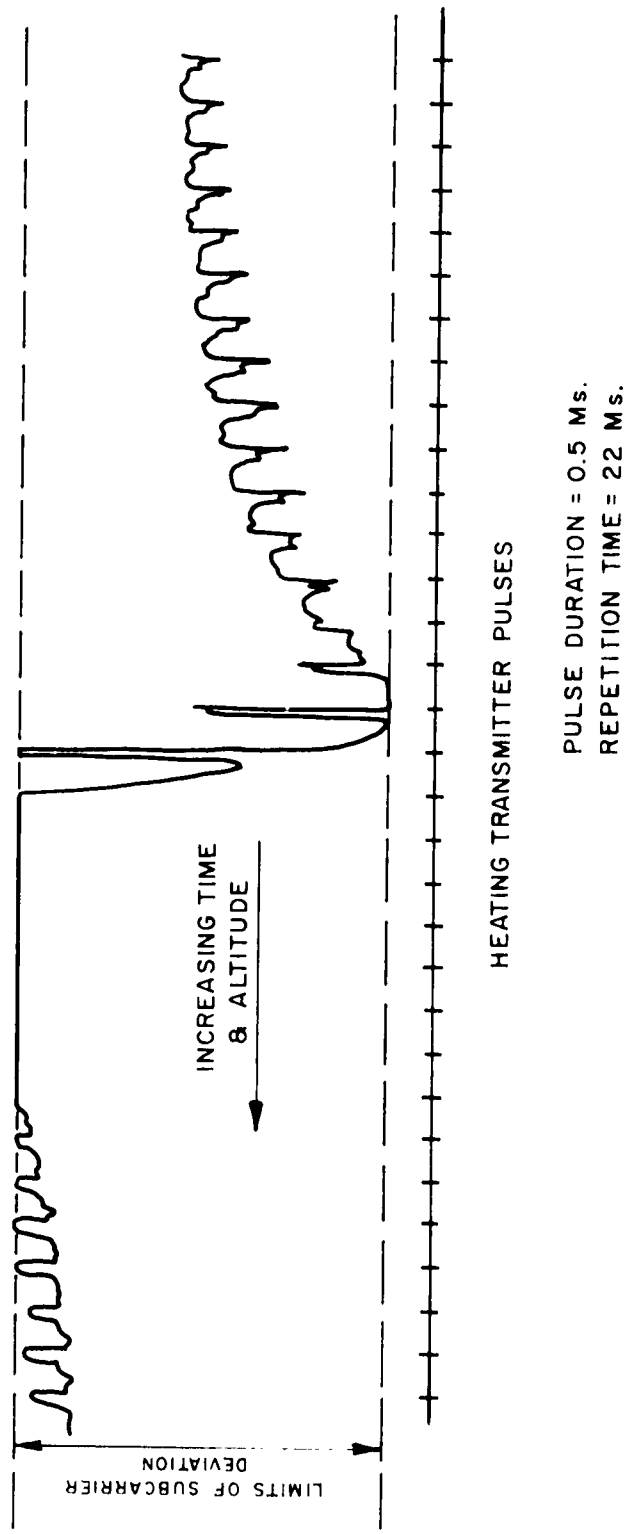

Figure 1.16. Characteristic modulation of the sensing wave near a polarization pattern null. (Altitude = 57 km)

In the altitude range of 48 km to 60 km collision frequency is large while electron density is usually assumed to be small. Under these conditions

$$\mu_\epsilon - \mu_o \simeq \frac{\omega_N^2 \omega_c}{\nu^2 \omega} \qquad (1.12)$$

Magnetic aspect data during the initial part of the flight show that the rocket rotation was clockwise when viewed from the ground. Therefore the polarization rotations caused by the heating pulses were counterclockwise, or momentary decreases in the normal Faraday rotation of the region. From Equation (1.12) this would be expected if ν were increased, due to increased electron energy produced by the heating pulses.

The ionospheric conditions in the 48 km to 60 km region necessary to explain the observed sensing wave rotation, if the above assumptions are correct, are somewhat different from generally assumed properties. For instance, it is necessary that the electron density be from 100 to 400 electrons per cubic centimeter, which is one order of magnitude high. In addition, the fraction of energy lost per collision $\simeq 2 \times 10^{-4}$, which is almost an order of magnitude low. It is also required that $\nu \simeq 2 \times 10^7$ at 60 km and that the radiated heating power be approximately 100 watts. The latter condition is questionable unless the whip antennas were deployed prematurely. The sudden attenuation of the extraordinary component of the sensing wave at 65 km would have required the same order of magnitude of electron density and a collision frequency of less than 10^7. Therefore observations of modulated wave rotation and of extraordinary wave attenuation both lead to the same ionospheric properties near 60 km.

1.12 Conclusions

The preliminary analysis of the telemetered data obtained from the initial gyroresonance probe shows that the prime objectives of the experiment were accomplished. Cross modulation of a sensing wave due to electron heating in the E layer was measured. In addition it was demonstrated that there is an anisotropy in the 45 km to 70 km region of the ionosphere which can be detected by two very sensitive methods: the change of axial ratio of the sensing wave polarization ellipse with altitude, and the modulation of the rotation of the sensing wave with electron heating.

It should be noted that these are new methods for probing the ionosphere and may be extended to other altitude ranges by suitable choice of sensing frequencies. The following experiments are proposed to measure the properties of the 45 to 75 km region

(1) Polarization ellipse measurement This experiment would involve the simultaneous detection of the polarization ellipses of four sensing waves in the 1 8 to 3 mc range This would give overlapping coverage of the 55 to 75 km region and provide both electron density and collision frequency data 'F'G channels C and E would be required for telemetry with two receivers multiplexed on each channel

(2) Modulation of sensing wave rotation In this experiment electron heating would be accomplished by use of a pulsed 2 mc, 400 kw transmitter located on the ground (The 10 kw sensing wave transmitter used with the gyroresonance experiment can be modified for this purpose.) By heating in this manner a uniform 5% modulation of electron temperature, and therefore of wave rotation should be obtained. A sensing wave would be used to detect this rotation just as in the gyroresonance experiment and the receiver output would be telemetered through a 70 kc $\pm$ 40% channel

The study of the results of the first gyroresonance experiment is incomplete, partially because data reduction by AP C has not been finished In addition it is desirable that these results be correlated with those of a second experiment Much has been learned in the process of data analysis which will lead to improvements in the design of the second gyroresonance probe For example it is evident that the radiated heating power should be reduced, and that the time between pulses be increased to permit a more complete relaxation. Also a probe to measure local electron density and collision frequency and their relaxation rates between pulses should be included.

2 THE SHORT DIPOLE ANTENNA AS AN IONOSPHERIC PROBE

K. G. Balmain

2.1 Introduction

2.1.1 Purpose and Description of Research

The purpose of the research covered by this part of the report is to study the characteristics of a short electric dipole antenna mounted on an ionospheric rocket and to provide information helpful in interpreting the results of experiments using such an antenna. Since only the final phase of such a study can be carried out in the ionosphere, it was decided to perform a series of laboratory experiments to measure the impedance of a short probe in an anisotropic plasma.

A program of experimental and theoretical research has been carried out with the result that the near fields and impedance of a short electric dipole in an anisotropic plasma can be predicted with fair accuracy at low signal levels and estimated at high levels. The theoretical work makes use of the quasi-static approach in which it is assumed that the AC electric field near the antenna is much stronger than the AC magnetic field The theory has been checked by laboratory experiments which were carried out in the afterglow plasma of a pulsed DC discharge in helium and neon gases. In the experiments the antenna was a short monopole probe inserted in the anode end of a cylindrical glass discharge tube The plasma was made anisotropic by a DC magnetic field parallel to the monopole axis Measurements of the probe impedance agreed substantially with calculations using the quasi-static theory

The quasi-static theory indicates that a very short antenna is capable of transmitting appreciable power into a lossless anisotropic plasma. In isotropic media the quasi-static theory predicts no power transmission at all because a magnetic field is not induced by an irrotational electric field. In the case of an anisotropic plasma, however, an irrotational electric field does induce a magnetic field and thus electromagnetic phenomena (such as radiation) can occur This effect is the same as that studied by Trivelpiece and Gould[15] who used the term space charge waves to describe it (the authors mentioned used only the source-free equations) The condition for quasi-static power transmission is that the medium must be 'hyperbolic (in the sense that the differential equation used is hyperbolic in form) Under

hyperbolic conditions the input impedance of the short antenna has a resistive component and the near fields are concentrated close to a conical surface with apex at the antenna and axis parallel to the magnetic field. It should be noted that quasi-static theory has been used extensively in the study of ferrites where the analogous propagation modes are referred to as "magneto-static modes" (for instance, see Trivelpiece et al.[16] or Joseph and Schlomann[17]).

The major experimental problem is electron density non-uniformity which influences the antenna impedance considerably. Ambipolar diffusion to the antenna surface makes the plasma non-uniform throughout its volume and, immediately adjacent to the surface, there is formed an ion sheath in which the electron density drops sharply. In the experiments, application of positive DC bias was helpful in minimizing this effect by collapsing the sheath. In accordance with ion sheath theory (Langmuir probe theory) the sheath thickness was increased by RF heating. With the sheath collapsed RF heating produced a measurable change in input impedance when the input power was as low as 10^{-4} watts. Despite the collapse of the ion sheath with bias and the use of low RF input power to avoid heating, the plasma close to the antenna was believed to be non-uniform due to ambipolar diffusion. It is shown analytically that a non-uniform electron density tends to magnify the apparent collision frequency (as measured by a short RF probe)

It should be emphasized that many of the experimental problems encountered were not anticipated and consequently the apparatus had to be modified several times. The vacuum system was rebuilt to make pumping and gas-changing easier and to reduce contamination. The electrode design was modified to permit DC biasing of the antenna probe with respect to the plasma and to make the pulsed discharge more dependable. In addition, the discharge tube was made smaller in terms of wavelengths when it was decided to limit the research to short antennas.

2.1.2 Historical Survey

Rocket-mounted probes have been widely used to measure electron density in the ionosphere. These probe experiments can be classified according to the type of applied voltage suggested classifications are DC experiments (Langmuir probe), low-level RF experiments (which do not perturb the plasma) and high-level RF experiments (which do perturb the plasma locally) A

number of DC experiments have been carried out by a group at the University of Michigan[19-22] whose work centers around a dumbbell-shaped electrostatic probe. Low-level RF impedance measurements have been analyzed by Jackson and Kane[23-25] and by Pfister, Ulwick and Vancour[26] who considered the case of a short dipole in an isotropic plasma. In addition the many impedance experiments by the University of Utah deserve special mention (see, for instance, Haycock and Baker[18]). A high-level RF approach called the "Resonance Probe" method has been described by Takayama and others[27,28] who make use of an anomaly in the DC current to an RF probe. This anomaly occurs when the frequency of the applied signal passes through plasma resonance and thus it permits the electron density to be determined.

The theory of antenna impedance in plasma media is not highly developed. Some work in isotropic media has been done by King and others[29,30] at Harvard. Katzin and Katzin[31] have derived impedance expressions for a dipole of arbitrary length in an anisotropic plasma but their assumption of a sinusoidal current distribution would be applicable only to short antennas. A quasi-static approach has been described by Kononov et al[32] who considered only an infinitesimal dipole. However their theory appears to contain an error which prevents them from observing the resistive part of the antenna impedance mentioned earlier. Other investigators[15,16,33,17] have used quasi-static theory in their studies of propagation in small, anisotropic structures (both plasma and ferrite) but have considered only the source-free solutions. In general one may say that the impedance theory of antennas in anisotropic plasma is in need of further development and that laboratory experiments to measure impedance are almost non-existant.

2.1.3 Summary of Report

In this report the physical factors affecting the impedance of an antenna are discussed with special attention to the problems peculiar to rocket and laboratory experiments. The quasi-static theory of antenna impedance for anisotropic media is developed and its implications discussed The laboratory experimental apparatus is described along with a number of experimental results. The effect of a non-uniform electron density is estimated. The quasi-static theory is applied to the gyro-interaction problem where it is used to estimate the impedance of the rocket antenna and its field intensity

as measured by a monitor in the nose cone. Finally, several suggestions for continued research are put forward

An appendix contains a general impedance theorem derived by Professor G. A. Deschamps This theorem relates the impedance of an antenna in a uniform, isotropic, conducting medium to the impedance of the same antenna in free space.

2.2 Physical Factors affecting Impedance

2.2.1 Introduction

The fundamental difficulty in predicting the impedance of an antenna in a plasma is that the antenna disturbs the surrounding medium Ions and electrons diffuse to the surface of the antenna rendering the medium inhomogeneous and producing a positive space-charge sheath (the ion sheath) adjacent to the antenna. An RF signal applied to the antenna excites the medium non-linearly and heats it non-uniformly. In the ionosphere the magnetic field of the earth, photo-emission and rocket velocity further modify the antenna environment. Since these factors could be important, they will be reviewed in some detail. This chapter is largely a survey of published work together with some observations made in this laboratory

2.2.2 The Ion Sheath

When a surface is introduced into a plasma, the electrons and ions (thermally agitated) diffuse to the surface where they recombine Since the electrons diffuse more rapidly than the ions, the surface acquires a negative charge high enough to establish a state of equilibrium between the electron and ion currents These currents are equal if the surface is an insulator or a "floating" conductor Thus there is formed a region of positive space charge between the surface and the adjacent plasma (which is electrically neutral). We shall assume the boundary between the plasma and the ion sheath to be fairly well defined and call it the 'sheath edge'

The ion sheath theory of a plane conducting surface will be presented this is usually referred to as the plane Langmuir probe (There are many references to Langmuir probes in the literature[38,39,40,41,19,20,21,22,34-37]) The nomenclature is as follows

N = electron and ion density in plasma

-e = charge of electron

m = mass of electron

M = mass of ion

x = sheath thickness

V = voltage across sheath; normalized voltage = $\nu = eV/kT_e$

$\epsilon_o = 1/36\pi \times 10^9 = 8.85 \times 10^{-12}$ farads/meter

k = Boltzmann's constant

T_i = ion temperature

T_e = electron temperature

D = Debye-Huckel shielding distance

J_i = random ion current density crossing sheath edge

J_e = random electron current density crossing sheath edge

A = area of plane probe

For a Maxwellian velocity distribution, the random current densities are

$$J_e = Ne\left(\frac{kT_e}{2\pi m}\right)^{1/2} \tag{2.1}$$

$$J_i = Ne\left(\frac{kT_i}{2\pi M}\right)^{1/2} \tag{2.2}$$

From the theory of the space-charge-limited plane diode, we have

$$J_i = \frac{4\epsilon_o}{9}\left(\frac{2e}{M}\right)^{1/2}\frac{V^{3/2}}{x^2} \tag{2.3}$$

The ions which cross the sheath edge all reach the probe, the electrons, however, are repelled by the negative probe potential. Thus the currents to the probe surface are

$$I_e = A\,Ne\left(\frac{kT_e}{2\pi m}\right)^{1/2} e^{-eV/kT_e} \tag{2.4}$$

$$I_i = A\,Ne\left(\frac{kT_i}{2\pi M}\right)^{1/2} \tag{2.5}$$

$$I_i = A\,\frac{4\epsilon_o}{9}\left(\frac{2e}{M}\right)^{1/2}\frac{V^{3/2}}{x^2} \tag{2.6}$$

Let us assume that the plasma is isothermal ($T_e = T_i = T$) and introduce the Debye-Huckel shielding distance $D = (\epsilon_o kT/2Ne^2)^{1/2}$ which is the distance beyond which a plasma is effectively shielded from the field of a point charge. Defining $\nu = eV/kT$ and using Equations (2.1) and (2.2), we may write Equations (2.4), (2.5), and (2.6) in a simpler form.

$$I_e = A J_e e^{-\nu} \tag{2.7}$$

$$I_i = A J_i \tag{2.8}$$

$$I_i = A J_i \frac{16\pi}{9} \frac{D^2}{x^2} \nu^{3/2} \tag{2.9}$$

Equating (2.8) and (2.9) we have the sheath thickness for a given sheath voltage:

$$x^2 = \frac{16\pi}{9} D^2 \nu^{3/2} \tag{2.10}$$

If there is no net current from the probe (or if we are considering an insulating surface) we may set $I_e = I_i$, giving

$$\nu = \ln\left(\frac{M}{m}\right)^{1/2} = \frac{1}{2} \ln \frac{M}{m} \tag{2.11}$$

Substituting Equation (2.11) in Equation (2.10) gives the sheath thickness for an insulated probe

$$x = \frac{4}{3}\left(\frac{\pi}{8}\right)^{1/4} D \left(\ln \frac{M}{m}\right)^{3/4} \tag{2.12}$$

The shielding distance is given in the accompanying graph (Figure 2.1) for $T = 290^{\circ}$ K (for which $D = D_o$).

The effect of bias may be estimated by considering Equation (2.10) which can be written

$$x = \frac{4\pi}{3}^{1/4} D \left(\frac{eV}{kT}\right)^{3/4} \tag{2.13}$$

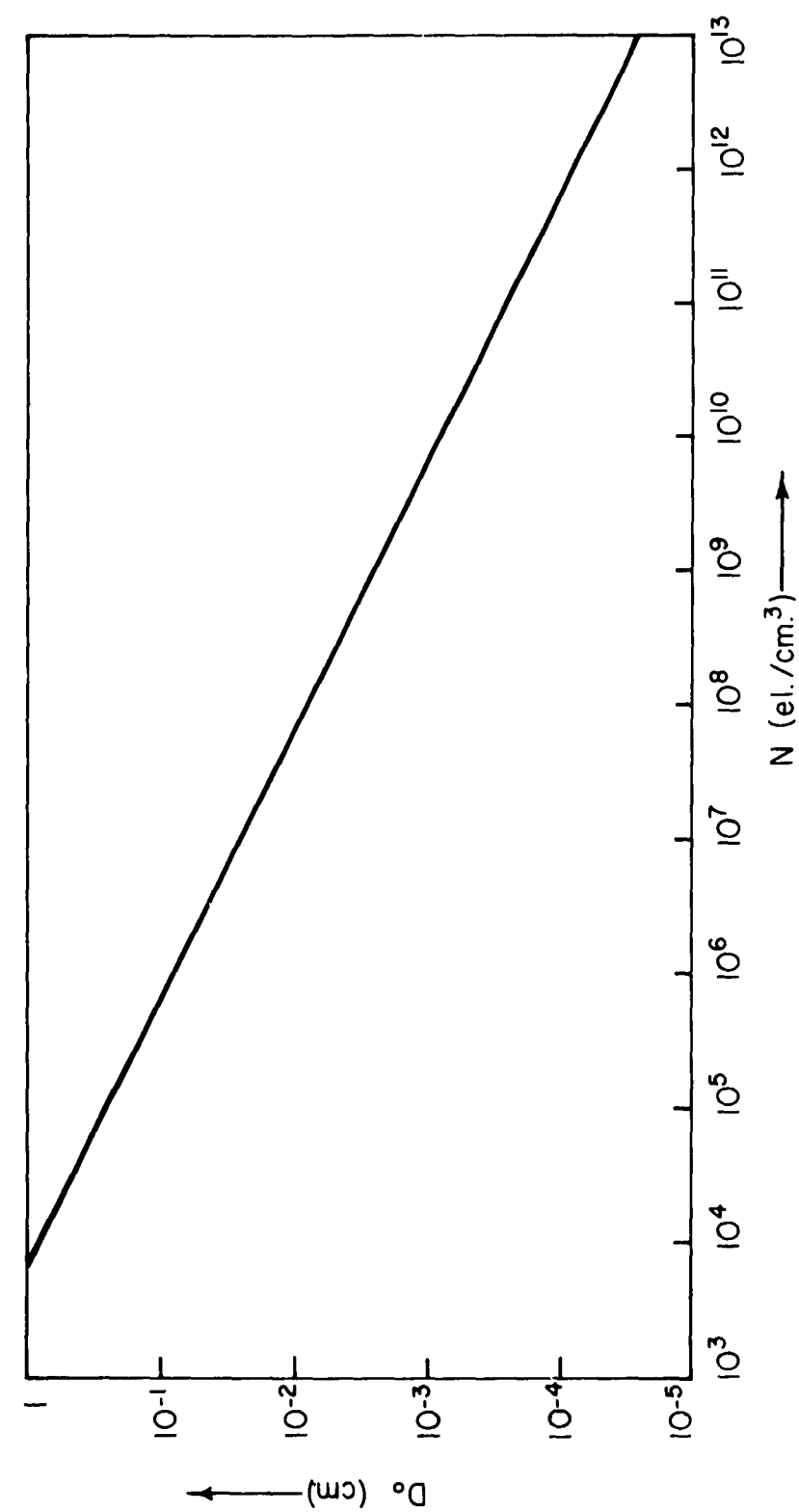

Figure 2.1. Debye-Huckel shielding distance D_o at T = 290^o K

where V is the probe-to-plasma potential If the probe is biased negatively with respect to a large electrode immersed elsewhere in the plasma (see Figure 2.2), V is approximately equal to the bias voltage (the difference being the sheath potential of the large electrode, usually .1 to .2 volts). Thus, for negative bias voltages greater than about one volt, the sheath thickness is proportional to the three-fourths power of the bias voltage.

For an insulated probe, Equation (2 12) states that x is proportional to $T^{1/2}$ as long as $T = T_i = T_e$. The situation is not so simple when an applied RF signal selectively heats the electrons, leaving the ion temperature unchanged. For this case ($T_e \neq T_1$), the expression for sheath thickness can be shown to be

$$x = \frac{4}{3}\left(\frac{\pi}{8}\right)^{1/4}\left(\frac{\epsilon_o k}{2Ne^2}\right)^{1/2}\frac{T_e^{3/4}}{T_1^{1/4}}\left(\ln\frac{T_e}{T_1}\frac{M}{m}\right)^{3/4} \qquad (2.14)$$

which indicates that x is approximately proportional to $T_e^{3/4}$. However, Schulz and Brown[42] argue that J_1 is proportional to $T_e^{1/2}$ rather than to $T_i^{1/2}$. If this were the case, x would be proportional to $T_e^{1/2}$. In any case, heating (selective or not) tends to enlarge the sheath This was borne out by early laboratory experiments here which showed that RF heating and increased negative bias produced the same type of change in probe impedance.

One may obtain an estimate of sheath thicknesses to be found in practice by considering the case $T = 290^{o}$ K for which $V = 40$ V The shielding distance for this case is D_o and is given in the accompanying graph. Equation (2.12) becomes

$$x = 1\ 056\ D_o\left(\ln\frac{M}{m}\right)^{3/4} \qquad (2\ 15)$$

For the case of ionized helium, this becomes

$$x = 6.75\ D_o \qquad (2\ 16)$$

and the sheath voltage V = 149 volts Similarly the effect of bias may be estimated by re-writing Equation (2 13) as

$$x = 28\ 2\ D_o\ V^{3/4} \qquad (2\ 16a)$$

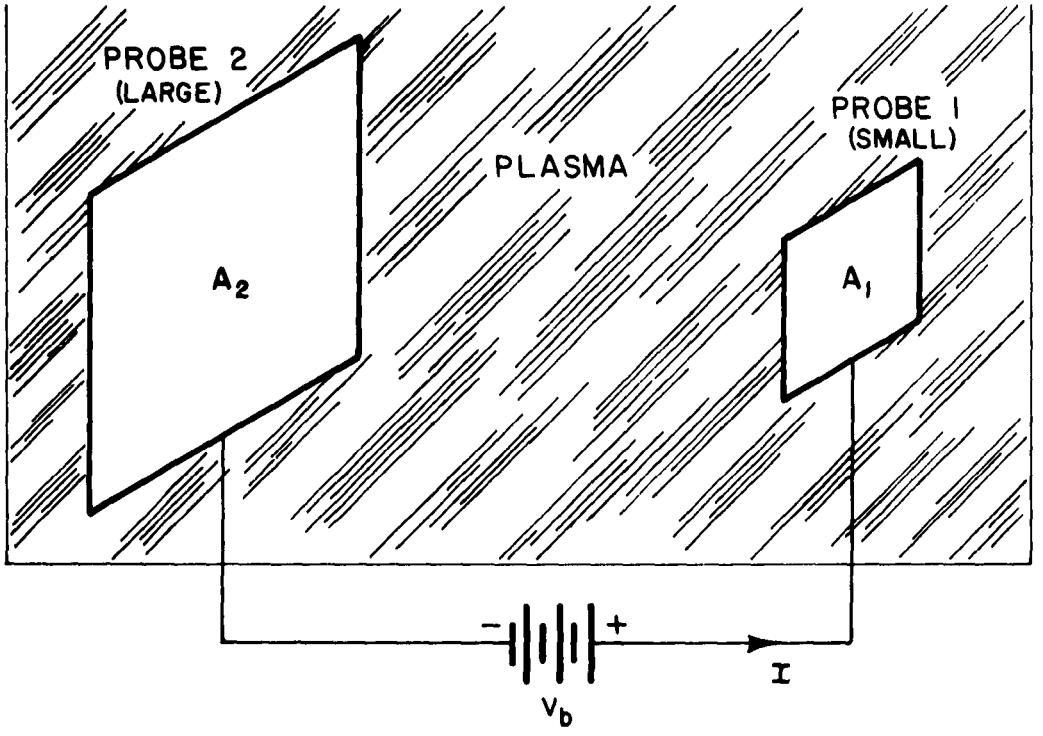

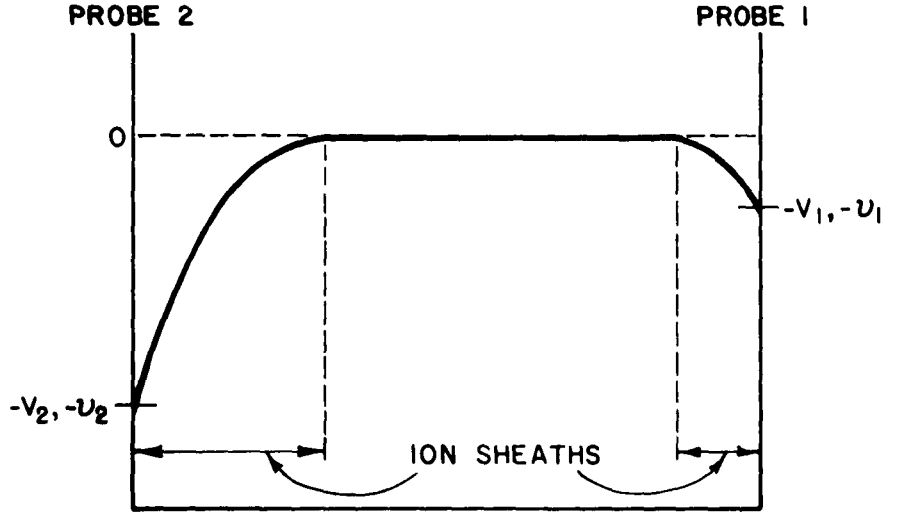

Figure 2.2. Biasing of one electrode with respect to a larger electrode

Since the theory of antennas in plasma assumes a uniform medium, the use of positive bias to collapse the sheath should be considered The probe or antenna must be biased with respect to a reference electrode with area large enough to permit sheath collapse The required area ratio may be estimated as follows (refer to Figure 2 2).

$$I = I_{e_1} - I_{i_1} = I_{i_2} - I_{e_2} \tag{2 17}$$

$$A_1(J_e e^{-\nu_1} - J_i) = A_2(J_i - J_e e^{-\nu_2}) \tag{2 18}$$

$$e^{-\nu_2} = \frac{J_i}{J_e} - \frac{A_1}{A_2}\left(e^{-\nu_1} - \frac{J_i}{J_e}\right) \tag{2.19}$$

If the sheath over A_1 is to be collapsed, $\nu_1 = 0$ Also $J_i/J_e = (m/M)^{1/2}$ which in general is small compared to unity Thus Equation (2 19) may be approximated by

$$e^{-\nu_2} = \left(\frac{m}{M}\right)^{1/2} - \frac{A_1}{A_2} \tag{2 20}$$

For this equation to have a solution it is required that

$$\frac{A_2}{A_1} > \left(\frac{M}{m}\right)^{1/2} \tag{2 21}$$

For example consider Helium for which

$$\frac{A_2}{A_1} > 85\ 7$$

Evidently the area of the reference electrode should be much greater than the area of the biased probe. If a rocket antenna is to be biased with respect to the rocket body, it is important that no insulating cover be placed around the antenna and that a sufficient area of the rocket body be left unpainted.

The potential distribution in a plane sheath has also been calculated[40]. Let ν be the normalized probe potential and η the normalized potential at any point z in the sheath (with z = 0 taken to be the probe surface). Then the potential distribution is

$$\eta = 4 \tanh^{-1} \left[e^{-z/D} \tanh \frac{\nu}{4} \right] \qquad (2.22)$$

The exponential term dominates in the above expression and emphasizes the importance of the shielding distance D

So far only the plane ion sheath has been considered but similar analyses exist for cylindrical and spherical sheaths. The basic equations are summarized in Table I. Simplified ion current formulas are given for the "sheath-area-limited" case (when all the ions entering the sheath are collected by the probe) and for the "orbital-motion-limited" case (when the space-charge in the sheath does not influence the probe current) In general, graphical methods must be used to solve the equations[19,22].

2.2.3 Factors affecting the Rocket Antenna

The ion sheath already discussed is modified by rocket velocity, photo-emission, and the earth's magnetic field These effects all tend to make the sheath around a cylindrical antenna asymmetrical. The magnitudes of the effects are difficult to compute precisely but can be estimated An excellent review on this subject has been prepared by Zachary[45].

Let us compare the gyro-interaction rocket velocity v with the rms electron and ion velocities (v_e and v_1) in the E layer

$$v_e \approx 1\ 2 \times 10^5 \text{ m/sec}$$

$$v_1 \approx 0\ 6 \times 10^3 \text{ m/sec} \qquad \text{at 85 km}$$

$$v \approx 0\ 6 \times 10^3 \text{ m sec}$$

Since $v \approx v_1 \ll v_e$ it appears that the rocket velocity would modify the sheath structure somewhat For most practical purposes, however, it is believed that rocket velocity effects are negligible

The magnitude of the photo-emission effect is by no means settled Boggess[22] estimates that the photo-emission current density in the E-layer

TABLE I

Summary of Ion Sheath Equations

	Plane	Cylinder	Sphere
I_i (general)	$I_i = AJ_i$	$I_i = AJ_i \left[\gamma \operatorname{erf} \left(\frac{\nu}{\gamma^2-1} \right)^{1/2} + e^{\nu} \left\{ 1 - \operatorname{erf} \left(\frac{\nu^2}{\gamma^2-1} \right)^{1/2} \right\} \right]$	$I_i = AJ_i \left[\gamma^2 - (\gamma^2-1)\, e^{-\frac{\nu}{\gamma^2-1}} \right]$
I_i (sheath-area-limited)		$I_i = AJ_i\, \gamma$ $\quad \frac{T}{Nr^2} \leq 10^{-5}$	$I_i = AJ_i\, \gamma^2$ $\quad \frac{T}{Nr^2} \leq 5 \times 10^{-6}$
I_i (orbital motion limited)		$I_i = AJ_i (1 + \nu)^{1/2}$ $\quad \frac{T}{Nr^2} \geq 10^{-3}$	$I_i = AJ_i (1+\nu)$ $\quad \frac{T}{Nr^2} \geq 10^{-3}$
I_i (space-charge limited diode)	$I_i = A \frac{4\epsilon_o}{9} \left(\frac{2e}{M} \right)^{1/2} \frac{V^{3/2}}{x^2}$ $= AJ_i \frac{16\sqrt{\pi}}{9} \frac{D^2}{x^2} \nu^{3/2}$	$I_i = A \frac{4\epsilon_o}{9} \left(\frac{2e}{M} \right)^{1/2} \frac{1}{r^2} \frac{V^{3/2}}{\rho^2}$ $= AJ_i \frac{16\sqrt{\pi}}{9} \frac{D^2}{r^2} \frac{\nu^{3/2}}{\rho^2}$	$I_i = A \frac{4\epsilon_o}{9} \left(\frac{2e}{M} \right)^{1/2} \frac{1}{r^2} \frac{V^{3/2}}{a^2}$ $= AJ_i \frac{16\sqrt{\pi}}{9} \frac{D^2}{r^2} \frac{\nu^{3/2}}{a^2}$
I_e	$I_e = AJ_e\, e^{-\nu}$	$I_e = AJ_e\, e^{-\nu}$	$I_e = AJ_e\, e^{-\nu}$
Nomenclature		$A = 2\pi rl$ $\quad l$ = probe length	$A = 4\pi r^2$
		$\gamma = \frac{a}{r} = \frac{\text{sheath radius}}{\text{probe radius}}$	$\gamma = \frac{a}{r} = \frac{\text{sheath radius}}{\text{probe radius}}$
	$\nu = \frac{eV}{kT}$	$T = T_e = T_i$	$D = \left(\frac{\epsilon_o\, kT}{2Ne^2} \right)^{1/2}$
	$J_i = Ne \left(\frac{kT}{2\pi M} \right)^{1/2}$	$J_e = Ne \left(\frac{kT}{2\pi m} \right)^{1/2}$	

ρ^2 = geometrical factor - Refer to Spangenburg, p. 178[44], Cobine, p. 126[43]

a^2 = geometrical factor - Refer to U. of Michigan, Rpt. GS-1, p. 18[22]

is of the same order of magnitude as the random thermal electron current density and thus photo-emission could have a considerable effect on the sheath. However, Zachary[45] reports later research leading to the conclusion that the photo-emission effect is negligible up to an altitude of 1000 km.

Hok et al.[19] express the opinion that the earth's magnetic field might affect Langmuir probe measurements of electron density but not measurements of ion density. This means that there will be a magnetic field effect as long as there is appreciable electron collection by the probe (as in the case of an insulated probe). In the gyro-interaction experiment the antenna will always be nearly perpendicular to the magnetic field and thus any sheath effect should be nearly constant as the rocket spins.

In conclusion, the rocket effects mentioned above are not expected to have a great influence on the antenna ion sheath and hence on its impedance. Nevertheless in interpreting the rocket flight records it will be necessary to watch for anomalous results which can be correlated with velocity, solar aspect and magnetic field. When the gyro-interaction heating antenna is operating at a high RF level the plasma will be strongly disturbed and the effects discussed should be reduced.

2.2.4 Factors affecting Impedance Measurement in the Laboratory

In the afterglow of a pulsed DC discharge the time sequence of events is very important and may be outlined as follows:

1. The DC pulse terminates
2. The ions quickly reach thermal equilibrium with the gas molecules (near room temperature)
3. The electrons more slowly reach thermal equilibrium with the gas molecules, mainly through a process of diffusion to the container walls.
4. If the electron and ion densities are high enough the dominant plasma decay process becomes volume recombination. Since this process does not involve the container walls, the spatial distribution of charged particles tends to become more uniform (the diffusion process of step 3 has left the distribution highly non-uniform)
5. With the charged particle density much decreased, diffusion again predominates and the plasma density distribution becomes more non-uniform.

The time required for the attainment of electron thermal equilibrium (periods 3) is of major importance and has been studied by Dougal and Goldstein[46].

For helium and neon this time constant (t_e) is given as follows (for gas pressure p between .5 and 5.0 mm):

Helium $t_e \leq 8.4/p + 27$ μs for p = 1 mm, $t_e \leq 36$ μs (2.23)

Neon: $t_e \leq 150/p + 90$ μs for p = 5 mm, $t_e \leq 120$ μs (2.24)

Thus in time, t_e, after the discharge pulse termination the electrons should be near room temperature. However, the persistence of metastable excited states may extend this time somewhat.

When recombination dominates (period 4) the plasma is most nearly uniform and good experimental results are most likely to be obtained. Nevertheless, some ambipolar diffusion will still be present so that a completely uniform plasma is impossible to obtain. Helium and neon are suitable for this type of experiment because their collision cross sections are well known and nearly constant. However, neon is to be preferred because of its higher recombination coefficient, lower diffusion coefficient, and lower collision probability (which permits operation at higher pressures, thus reducing contamination problems). To summarize, at 300° K and 1 mm pressure we have (in cgs units)

	Collision Probability P_c	Recombination Coefficient α	Ambipolar Diffusion Coefficient D_a
Helium	19	1.7×10^{-8}	540
Neon	3.3	2.1×10^{-7}	115

where α and D_a are as given by Goldstein[47] and P_c as given by Brown[48] A DC magnetic field reduces transverse diffusion but does not affect longitudinal diffusion. Thus when the magnetic field is parallel to a cylindrical dipole, diffusion to its surface would be reduced and the plasma consequently would become more uniform

During the course of the experimental work it was found that the RF probe surface became contaminated, probably because the probe is part of the DC discharge anode A yellowish waxy deposit formed on the probe surface, giving it an insulating coat which disturbed the impedance measurement and

made sheath collapse impossible. The deposit probably consists of oxides, sputtering products from the cathode, and hydrocarbons from a small amount of vacuum grease used to seal the RF probe mount. The only known cure for this condition is frequent cleaning of the RF probe.

It is essential in impedance measurements to understand the loss processes and include as many as possible in the theory. It is easy to include any loss process which may be represented by an equivalent collision frequency ν. Electron-molecule and electron-ion collisions are most important in this work and we may write $\nu = \nu_{em} + \nu_{ei}$. The appropriate formula areas follows (given, for instance, by Dougal and Goldstein[46] and discussed by Pfister[49]):

$$\nu_{em} = \frac{4}{3} \bar{v} P_c p_o \qquad \text{(MKS units)}$$

$$\nu_{ei} = \frac{3.62 \times 10^6 N_i}{T_e^{3/2}} \ln \left[\frac{3.30 \times 10^6 T_e^{3/2}}{N_i^{1/2}} \right]$$

where $\bar{v} = \sqrt{8kT_e/\pi m}$ = average velocity of electrons with Maxwellian distribution

$p_o = 273/T\ p$ = pressure reduced to 0^o C

N_i = ion density

These results are presented graphically in Figure 2.3 (a and b). The graph shows that electron-ion collisions must be taken into account in the work covered by this report since the electron density may go as high as 10^{12} per cc. For a convenient reference, a graph of plasma frequency as a function of electron density has been included (Figure 2.4); in MKS units, the relation is $f_N^2 = 80.5\ N$.

There are other loss processes, however, which are non-collisional in nature and thus their effects can only be estimated. Tonks[50] has observed that non-uniformity broadens any plasma resonance effect thus indicating apparent high losses. In addition the non-uniform plasma in a metal-covered glass tube can support surface wave modes which carry away energy, again indicating apparent high loss. The problem of non-uniformity of the electron density is considered further in Section 2.5 in an attempt to interpret the experimental results.

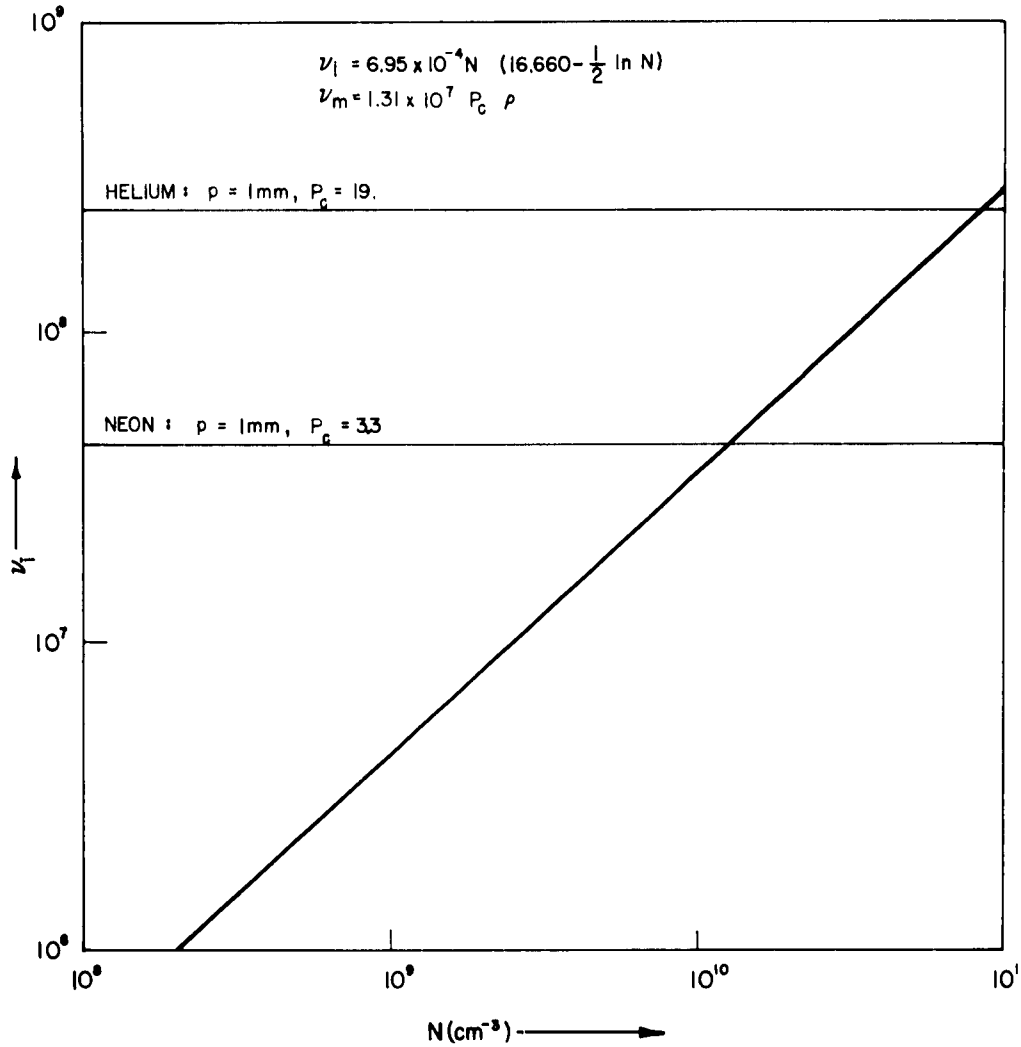

Figure 2.3a. Electron-ion collision frequency at 300^{o} K

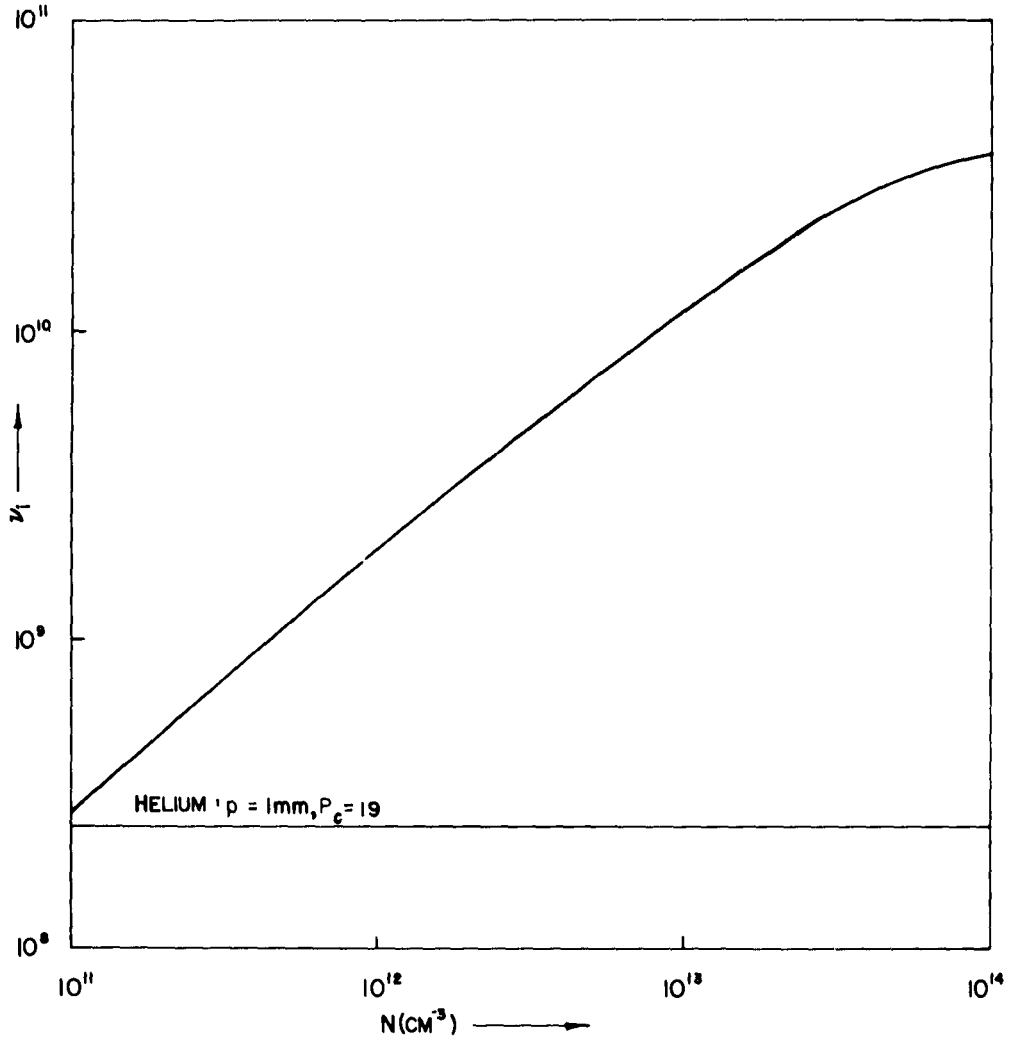

Figure 2.3b. Electron-ion collision frequency at 300^{O} K

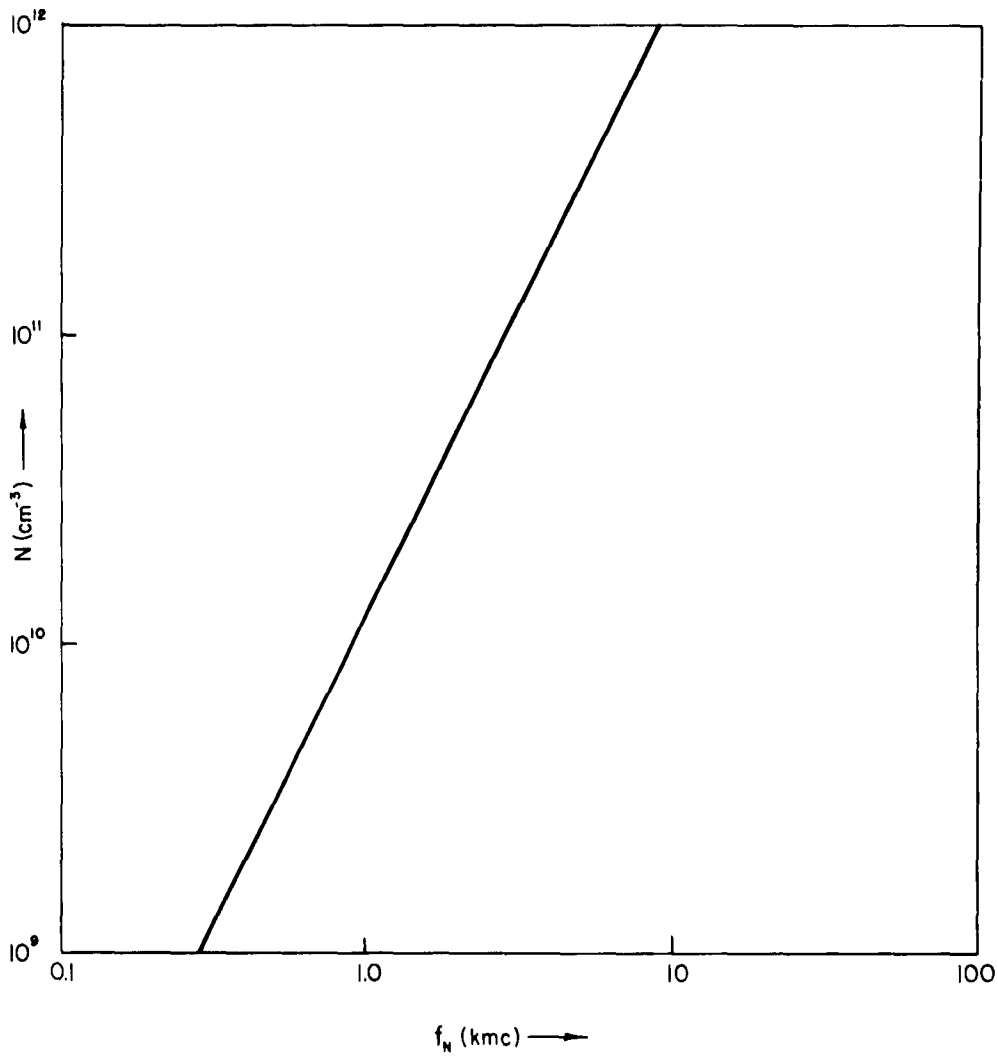

Figure 2.4. Electron density versus plasma frequency

2.3 The Quasi-Static Theory for Near Fields and Impedance

2.3.1 The Necessary Assumptions

In the theory to follow it is assumed that the plasma medium around the antenna is linear and uniform, two requirements often difficult to satisfy in practice. The linearity requirement is easy to satisfy provided that the RF input voltage can be made less than the average thermal energy of an electron (.04 volt at 300° K)[27]; this is out of the question for a practical transmitting antenna but can be satisfied for the case of a receiving antenna or an RF-energized plasma probe. A high RF level not only renders the medium non-linear but also raises the electron temperature non-uniformly. In a theoretical analysis these effects can be approximated very roughly by increasing the assumed losses in the medium. A non-uniform electron density arises from diffusion to the antenna surface (or any other nearby surface) and is very difficult to deal with. The ion sheath resulting from diffusion close to the surface often can be collapsed with positive bias, however this tends to raise the electron temperature Ambipolar diffusion cannot be controlled in the ionosphere but in the laboratory the type of gas and the pressure can be selected to minimize it. To conclude, linearity and heating are not problems at low RF levels, but a non-uniform electron density cannot be eliminated, only minimized

2.3.2 The Quasi-Static Theory

The problem of calculating the near field of a dipole antenna (and thus its impedance) is not easy when the antenna length and the properties of the medium are arbitrary. The problem can be simplified greatly if the antenna is much shorter than a wavelength. this permits the assumption that the current varies linearly along each half of the antenna, vanishing at the ends. Furthermore, in an isotropic medium the magnetic field is negligible compared to the electric field in the near region of a short dipole. This means that the electric field can be expressed as the gradient of a scalar potential and thus the antenna behaves as if it were a capacitor If this quasi-static theoretical approach were applicable to anisotropic plasmas, the input impedance of a short dipole could be computed readily. However, the fact that the DC magnetic field forces moving electrons into circular orbits suggests that the dominant electric field may induce a magnetic field which

is not negligible, thus invalidating the quasi-static theory.

This problem may be clarified by considering Maxwell's equations

$$\nabla \times \bar{E} = -j\omega \mu_o \bar{H}$$

$$\nabla \times \bar{H} = j\omega \epsilon_o \bar{\bar{K}} \bar{E}$$

where the permittivity tensor is

$$\bar{\bar{K}} = \begin{bmatrix} K' & jK'' & 0 \\ -jK'' & K' & 0 \\ 0 & 0 & K_o \end{bmatrix} ,$$

and where

$$K_o = 1 - \frac{X}{1 - jZ}$$

$$K' = 1 - \frac{X(1-jZ)}{(1-jZ)^2 - Y^2}$$

$$K'' = \frac{XY}{(1-jZ)^2 - Y^2}$$

$$X = \left(\frac{\omega_N}{\omega}\right)^2 \qquad \omega_N^2 = \frac{Ne^2}{m \epsilon_o}$$

$$Y = \frac{\omega_H}{\omega} \qquad \omega_H = \frac{eB_o}{m}$$

$$Z = \frac{\nu}{\omega} \qquad \nu = \text{collision frequency}$$

If it is assumed that $-j\omega \mu_o \bar{H}$ is small enough to be negligible, then $\nabla \times \bar{E} = 0$. Consequently $\bar{E} = -\nabla \psi$, where ψ is a scalar potential. In order to see whether or not an $\bar{E}$ field of this form (irrotational) induces a magnetic field, take the curl of the second Maxwell equation

$$\nabla \times \nabla \times \bar{H} = j\omega \epsilon_o \nabla \times \bar{\bar{K}} \bar{E}$$

$$\nabla\nabla\cdot H - \nabla^2\bar{H} = -j\omega\,\epsilon_o\,\nabla\times\bar{\bar{K}}\,\nabla\psi$$

Since $\nabla\cdot H = 0$, this equation becomes

$$\nabla^2\bar{H} = j\omega\,\epsilon_o\,\nabla\times\bar{\bar{K}}\,\nabla\psi$$

If $\bar{G}$ is defined as $\bar{G} = j\omega\,\epsilon_o\,\nabla\times\bar{\bar{K}}\,\nabla\psi$, this becomes

$$\nabla^2\bar{H} = \bar{G}$$

or, if the vector components (rectangular) are considered separately, $\nabla^2 H_i = G_i$, "i" indicating x, y, or z. Now H_i may be expressed in terms of G_i using Green's theorem (A is arbitrary).

$$\int_v (H_i\,\nabla^2 A - A\,\nabla^2 H_i)\,dv' = \int_s (H_i\,\nabla A - A\,\nabla H_i)\cdot\bar{n}\,da'$$

If the surface s approaches infinity and if the medium is slightly lossy, the right-hand side will approach zero. If A is specified as follows:

$$A = \frac{1}{|\bar{r} - \bar{r}'|} = \frac{1}{R}$$

then

$$\nabla^2 A = -4\pi\,\delta(\bar{r} - \bar{r}')$$

Substitution in Green's threorem gives the components of the induced magnetic field

$$H_1(\bar{r}) = -\frac{1}{4\pi}\int_v \frac{G_1(\bar{r}')}{|\bar{r} - \bar{r}'|}\,dv$$

Since $\bar{G}$ is non-zero in general, there exists an induced magnetic field $\bar{H}$ which must be small if the quasi-static theory is to be valid.

If the medium is isotropic, the tensor $\bar{\bar{K}}$ becomes a scalar and $\bar{G}$ vanishes. In other words, an irrotational electric field in an isotropic medium cannot induce a magnetic field. In an anisotropic plasma $\bar{G}$ may be expressed as follows:

$$\bar{G} = j\omega \epsilon_o \nabla \times \bar{\bar{K}} \nabla \psi$$

$$= j\omega \epsilon_o \nabla \times (\bar{\bar{K}} - \bar{\bar{I}}K_o) \nabla \psi \qquad \text{where } \bar{\bar{I}} \text{ is the unit, diagonal tensor}$$

This can be expanded and simplified with the help of the equation

$$\nabla \cdot \bar{D} = \nabla \cdot \bar{\bar{K}} \bar{E} = -\nabla \cdot \bar{\bar{K}} \nabla \psi = 0$$

or

$$\left(\frac{\partial^2}{\partial x^2} + \frac{\partial^2}{\partial y^2} + \frac{K_o}{K'} \frac{\partial^2}{\partial z^2} \right) \psi = 0$$

Thus the expression for $\bar{G}$ becomes

$$\bar{G} = -\omega \epsilon_o \bar{\bar{\mathcal{K}}} \frac{\partial}{\partial z} \nabla \psi$$

$$= +\omega \epsilon_o \bar{\bar{\mathcal{K}}} \frac{\partial}{\partial z} \bar{E}$$

where

$$\bar{\bar{\mathcal{K}}} = \begin{bmatrix} K'' & j(K' - K_o) & 0 \\ -j(K' - K_o) & K'' & 0 \\ 0 & 0 & K'' \frac{K_o}{K'} \end{bmatrix}$$

The elements of the tensor $\bar{\bar{\mathcal{K}}}$ give an indication of the magnitude of the induced magnetic field $\bar{H}$. For the lossless case:

$$K'' = \frac{XY}{1 - Y^2}$$

$$K'' - K_o = -\frac{XY^2}{1 - Y^2}$$

$$\frac{K_o}{K''} = \frac{(1-Y^2)(1-X)}{1 - (X+Y^2)}$$

It is evident that the assumption of negligible magnetic field would be invalid in the vicinity of $Y^2 = 1$ (gyroresonance) and $X+Y^2=1$ for the lossless case. However, if sufficient damping were present the terms of $\bar{\bar{K}}$ would be bounded. Thus the quasi-static approximation is still valid provided that the frequency is low enough or that the antenna is small enough in terms of wavelengths.

The presence of an induced magnetic field not only restricts the applicability of the quasi-static theory but also suggests that unusual electromagnetic effects may occur in anisotropic media. In particular, a very small antenna could become an effective radiator if the induced magnetic field had a phase and direction such that outward power flow could take place In Poynting's theorem, the outward power flow through the surface s is proportional to P where

$$P \int_s \bar{E} \times \bar{H}^* \cdot \bar{n}\, ds$$

Power flow can take place when $\bar{H}$ has a component perpendicular to $\bar{E}$ An examination of $\bar{\bar{K}}$ shows that $\bar{E}$ induces a perpendicular $\bar{H}$ through the off-diagonal terms $\pm j(K''-K_o)$ Thus the magnetic field is 90^o out of phase with the electric field as long as the electric field has no spatial phase variation (since $\bar{H}$ is obtained from a volume integration of $\bar{E}$ over all space). However, if there is spatial phase variation in the electric field, the magnetic field can have an in-phase component so that outward power flow is possible. In 2.3.3 it will be shown that an electric field with spatially varying phase is produced by a short antenna when the differential equation for the field is hyperbolic in the space co-ordinates (cf the field formulas on page 70)

The expression for power flow P can be put into quasi-static form by substituting $\bar{E} = -\nabla\Psi$ and $\nabla \times H = j\omega D$ Thus

$$P = -j\omega \int_S \psi \, \bar{D}^* \cdot \bar{n} \, ds$$

The above expression for P is quite useful; for instance its analogous form for the magneto-static problem gives a result identical to that obtained by Trivelpiece et al[16] in their Equation (A.10).

2.3.3 The Differential Equation for the Field of a Short Dipole

If it is assumed that $\bar{H} = 0$, then $\bar{E}$ may be expressed in terms of a scalar potential.

$$\bar{E} = -\nabla \psi \tag{2.25}$$

If q is the charge density in the medium then $\nabla \cdot \bar{D} = q$ where $\bar{D} = \bar{\bar{\epsilon}} \, \bar{E} = \epsilon_o \bar{\bar{K}} \bar{E}$. This can be written as

$$\nabla \cdot \bar{\bar{K}} \nabla \psi = -\frac{q}{\epsilon_o} \tag{2.26}$$

which is a general expression of the required differential equation. Note that it reduces to Poisson's equation when $\bar{K}$ becomes a scalar. In the expansion of the differential equation the off-diagonal terms of $\bar{\bar{K}}$ cancel (due to skew symmetry) and the equation becomes a modified Poisson's equation of the form

$$\psi_{xx} + \psi_{yy} + \frac{1}{a^2} \psi_{zz} = -b \, q \tag{2.27}$$

where $1/a^2 = K_o/K'$, $b = 1/\epsilon_o K'$ and the subscripts indicate partial differentiation.

The value of $a = \sqrt{K'/K_o}$ is important since it is a measure of the degree of anisotropy of the medium. It is necessary to define a principal value of "a" to facilitate the inverse Fourier transform to be taken later; the principal value is defined such that the argument of "a" is between $-\pi/2$ and $+\pi/2$. Since any plasma medium is lossy, this guarantees that "a" always has a positive real part. If it is desired to consider a "lossless" plasma it is necessary in general to postulate a small loss and let it approach zero in order to select the proper value of "a".

Although a lossless medium cannot be realized in practice, the concept of such a medium is definitely an aid to understanding. For a lossless anisotropic

plasma K_o and K' are both real but may be positive or negative. In contrast for a uniaxial crystal the values of K_o and K' would always be positive and therefore a^2 would always be positive. In the gyrotropic plasma when a^2 is negative the modified Poisson's equation becomes hyperbolic whereas normally (a^2 positive) it is elliptic. This has been observed in the case of ferrite media by Damon and Eshbach[33] who considered only the source-free differential equation. However the real significance of the elliptic-hyperbolic classification becomes apparent only when a source term, (-bq), is included. The source is a type of discontinuity and discontinuities "propagate" (i.e. cannot vanish) on the characteristic surfaces of a differential equation. The characteristic surface of an elliptic equation is complex and thus has no physical significance. On the other hand the characteristic surface of a hyperbolic equation is real and of considerable significance.

Consider a point charge in a "hyperbolic" medium (for the properties of the medium determine the differential equation classification). A charge which goes to infinity at a point will produce a field which goes to infinity everywhere on the characteristic surface passing through that point. Thus the conditions under which the differential equation is hyperbolic are of major importance in determining the nature of the fields. These conditions are presented graphically in Figure 2.5. Note in Figure 2.5 that the "operating point" on the chart moves horizontally with a change in electron density (as in a decaying plasma), vertically with a change in magnetic field, and along a straight line through the origin with a change in frequency.

The equation for the characteristic surface may be obtained easily (see Sneddon[51], for instance). If the modified Poisson's equation in cylindrical coordinates is

$$\psi_{\rho\rho} + \frac{1}{\rho}\psi_{\rho} + \frac{1}{a^2}\psi_{zz} = -bq \qquad (2.28)$$

then the equation for the characteristic surface may be obtained as follows (where the dot represents differentiation with respect to some parameter):

$$\dot{z}^2 + \frac{1}{a^2}\dot{\rho}^2 = 0 \qquad (2.29)$$

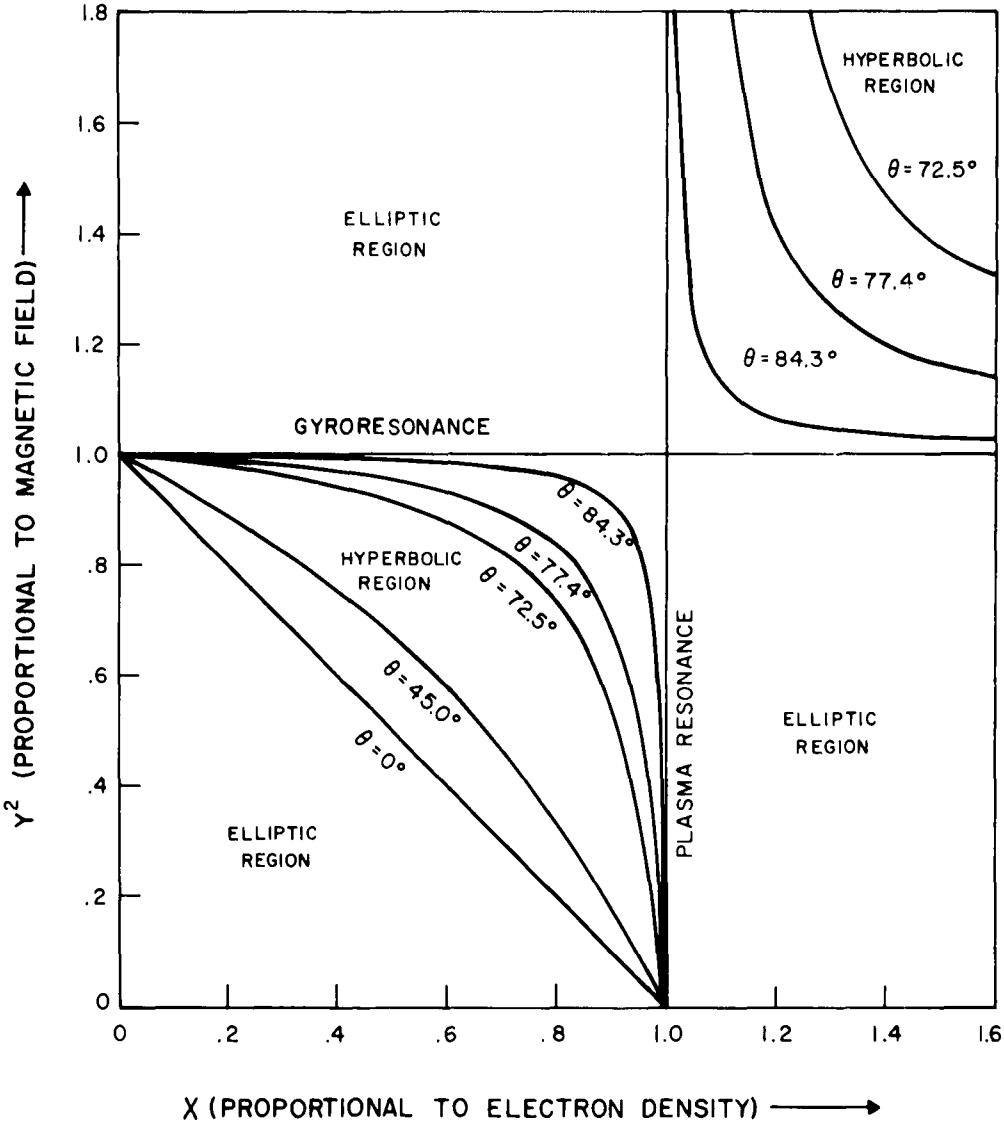

Figure 2.5. The elliptic and hyperbolic regions
Note: θ is the angle (with respect to the Z axis) of the characteristic cone when the differential equation is hyperbolic

$$\dot{z} = \pm j \frac{1}{a} \dot{\rho}$$

$$dz = \pm j \frac{1}{a} d\rho \qquad (2.30)$$

$$z = \pm j \frac{1}{a} \rho + \text{const} \ldots$$

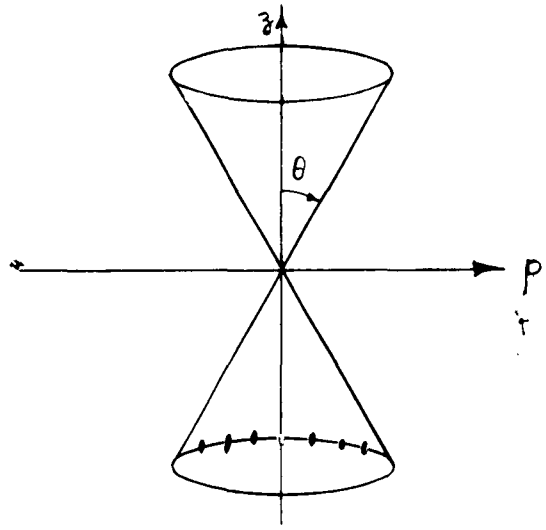

Under lossless hyperbolic conditions "a" is imaginary and the characteristic surfaces are right circular cones with half-angle θ given by

$$\tan \theta = \frac{\rho}{z} = \pm ja = \pm j\sqrt{\frac{K'}{K_o}} = \pm\sqrt{\frac{-K'}{K_o}} \quad \ldots \qquad (2.31)$$

Thus an oscillating point charge in a hyperbolic medium generates fields which become infinite everywhere on the conical surface with apex at the point charge. Thus the most prominent feature of the field can be determined without carrying out a detailed analysis.

It is also worthwhile to see what restrictions the differential equation imposes on a wave-type solution.

If it is assumed that $q = 0$ and that Ψ has the form $e^{j\bar{k}\cdot\bar{r}}$, then the relation

$$k_\rho^2 + \frac{K_o}{K'} k_z^2 = 0 \qquad (2.32)$$

is obtained. This means that $\bar{k}$ can be real if K_o/K' is negative. Thus a

wave solution can exist but the direction of the wave normal $\bar{k}$ is fixed in space. Its angle with respect to the z-axis is ϕ which is given by

$$\tan \phi = \pm \sqrt{-\frac{K_o}{K'}} \tag{2.33}$$

Thus the relation between θ and ϕ is given by

$$\tan \phi = \pm \cot \theta \tag{2.34}$$

where ϕ gives the direction of phase progression and θ gives the direction in which discontinuities propagate.

The detailed analysis of a short dipole is carried out in the following way. First a line current distribution $\bar{J}$ is assumed and using the equation of continuity

$$\nabla \cdot \bar{J} + j\omega q = 0 \quad , \tag{2.35}$$

an equivalent charge distribution q is obtained. Second, the potential ψ is determined using the Fourier transform pair

$$\tilde{f}(\bar{k}) = \iiint_{-\infty}^{\infty} f(\bar{r})\, e^{-j\bar{k}\cdot\bar{r}}\, dr \tag{2.36}$$

$$f(\bar{r}) = \frac{1}{(2\pi)^3} \iiint_{-\infty}^{\infty} \tilde{f}(\bar{k})\, e^{+j\bar{k}\cdot\bar{r}}\, dk \tag{2.37}$$

where $\bar{r} = (x, y, z)$ and $\bar{k} = (k_x, k_y, k_z)$.

Third, the input impedance Z_{in} is calculated approximately by integrating $\bar{E}\cdot\bar{J}$ over the antenna surface. The field $\bar{E}$ is taken to be the field of a line source at the center of the thin, cylindrical dipole, and the current $\bar{J}$ is assumed to be spread over the surface of the dipole. This method of impedance calculation is essentially the same as the "induced EMF method" mentioned often in the literature

2.3.4 The Field and Impedance Formulas

For the sake of brevity, only the results of the analysis will be presented. Refer to Figure 2.6 for a sketch of the coordinates. First, the expressions for the electric field parallel to the dipole will be given. The magnetic field is always parallel to the z axis.

Dipole Parallel to Magnetic Field

$$E_z = \frac{a}{j\omega\, 4\pi\, \epsilon_o K'\, L}\left[(\rho_o^2 + a^2 z_1^2)^{-1/2} + (\rho_o^2 + a^2 z_2^2)^{-1/2} - 2(\rho_o^2 + a^2 z_o^2)^{-1/2} \right] \tag{2.38}$$

where

$$z_1^2 = (z_o - L)^2 \qquad \text{Dipole length} = 2L$$

$$z_2^2 = (z_o + L)^2$$

$$\rho_o^2 = x_o^2 + y_o^2$$

Dipole Perpendicular to Magnetic Field

$$E_x = \frac{a}{j\omega\, 4\pi\, \epsilon_o K'\, L}\left[(\rho_1^2 + a^2 z_o^2)^{-1/2} + (\rho_2^2 + a^2 z_o^2)^{-1/2} - 2(\rho_o^2 + a^2 z_o^2)^{-1/2} \right] \tag{2.39}$$

where

$$\rho_1^2 = (x_o - L)^2 + y_o^2$$

$$\rho_2^2 = (x_o + L)^2 + y_o^2$$

$$\rho_o^2 = x_o^2 + y_o^2$$

Note that E_z and E_x are taken at (x_o, y_o, z_o) which is the point P in Figure 2.6.

In the following formulas for input impedance, it is assumed that the dipole length (2L) is much greater than its diameter (2ρ). When the medium

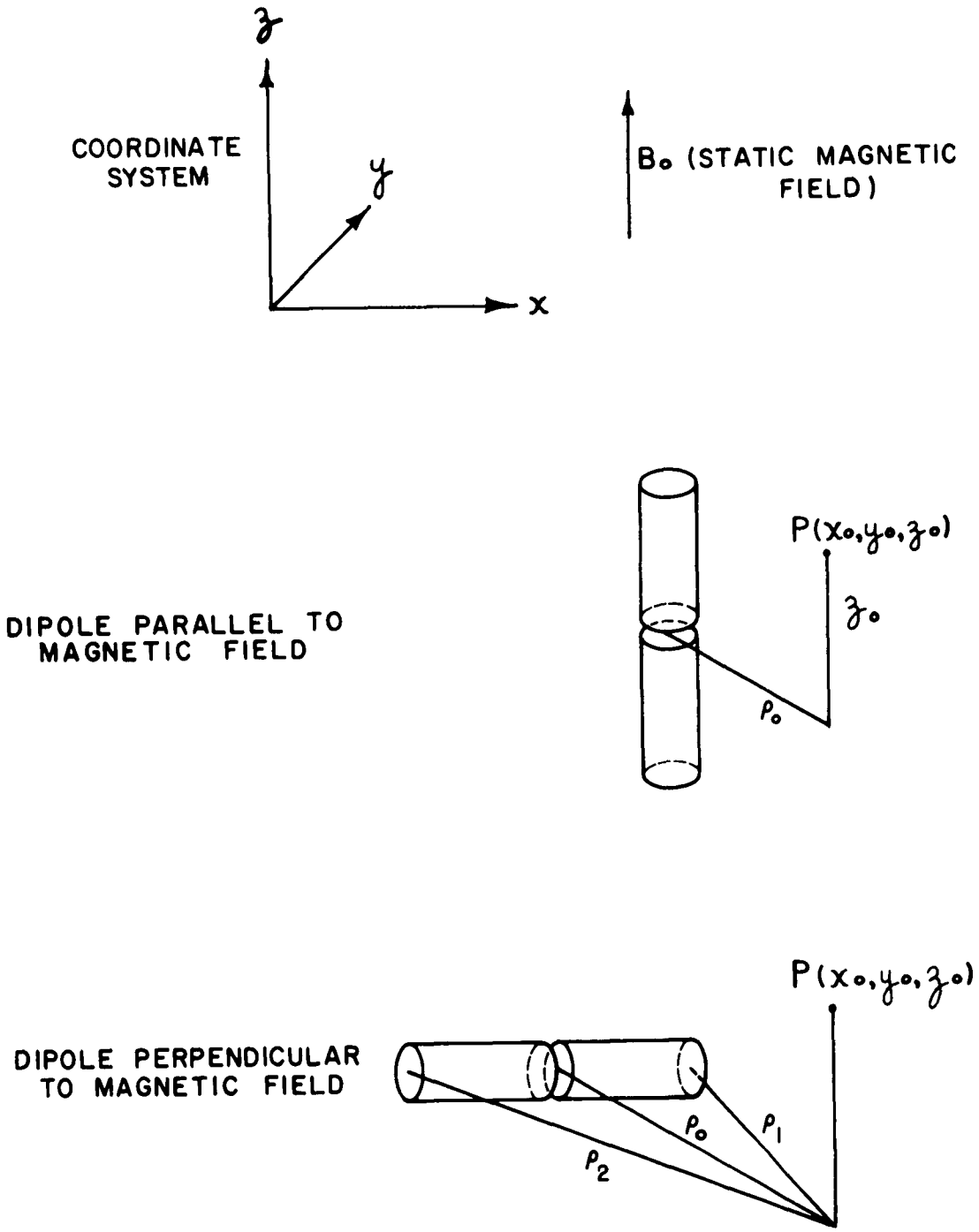

Figure 2.6. The co-ordinate system for the thin, cylindrical dipole
Note: dipole length = 2L, dipole diameter = 2ρ

is isotropic, these results are in agreement with the formulas derived in the appendix.

Dipole Parallel to Magnetic Field

$$Z_{in} = \frac{1}{j\omega \pi \epsilon_o K' L} \left[\ln \frac{L}{\rho} - 1 + \ln a \right] \qquad (2.40)$$

where $L \gg \frac{\rho}{|a|}$

Dipole Perpendicular to Magnetic Field

$$Z_{in} = \frac{a}{j\omega \pi \epsilon_o K' L} \left[\ln \frac{L}{\rho} - 1 - \ln \frac{a+1}{2} \right] \qquad (2.41)$$

where $L \gg |a| \rho$.

An examination of Equations (2.40) and (2.41) shows that K_o and K' play the parts of scale factors. Thus the two formulas can be written as one with direction-dependent scale factors. The impedance formula with normalized frequency, length and radius is

$$Z_{in} = \frac{1}{j\omega_n \pi \epsilon_o L_n} \left[\ln \frac{L_n}{\rho_n} - 1 \right] \qquad (2.42)$$

where $\omega_n = \omega K' \sqrt{K_o}$, $L_n = L\sqrt{K_L}$, $\rho_n = \rho/\sqrt{K_\rho}$. Here, K_L and K_ρ are direction dependent. When the dipole is parallel to the magnetic field, $K_L = K_o$ and $K_\rho = K'$. When the dipole is perpendicular to the magnetic field, $K_L = K'$ and K_ρ is given by

$$\frac{1}{K_\rho} = \frac{1}{2} \left(\frac{1}{\sqrt{K_o}} + \frac{1}{\sqrt{K'}} \right)$$

Equation (2.42) has exactly the same form as Equations (2.40) and (2.41) when the medium is free space. Thus the free space impedance formula may be used if the antenna dimensions and the frequency are suitably scaled. In a similar way electric field Equations (2.38) and (2.39) may be scaled to have the form of fields in free space. In the scaled formulas the electric field components are $\sqrt{K_o}\, E_z$ and $\sqrt{K'}\, E_x$.

2.3.5 Discussion

In the hyperbolic region for the lossless case (a^2 is negative and real), the E field exhibits the conical discontinuities predicted by the study of the characteristic surfaces of the differential equation. When derived for an infinitesimal dipole the field expressions are identical to the near field formulas obtained by Mittra[52]. The expressions are similar to those of Kononov, Rukhadze and Solodukhov[32]; however their work predicts zero field outside the characteristic cone, a result obtained if one does not postulate a slight loss.

The expressions for impedance each have a logarithmic term containing the anisotropy factor "a". In a lossless medium under hyperbolic conditions "a" is imaginary and therefore the logarithmic terms will be complex. This means that the impedance has a real part and therefore energy is transmitted irreversibly into the anisotropic medium. At first glance this result seems very strange especially since only quasi-static, near-field theory was used. However the hyperbolic regions are identical to the quasi-static propagation regions observed by Trivelpiece and Gould[15]. Furthermore, in the hyperbolic regions a magnetic field is induced and electromagnetic power flow can take place (as shown earlier in this chapter). In the following section impedance calculations are displayed graphically and compared with experimental results.

A major source of theoretical inaccuracy may arise from the method of impedance calculation in which the fields at the antenna surface are assumed to be those of a line source of current. In an elliptic medium the fields are continuous and this type of approximate calculation is known to give good results. However, the discontinuous fields in a hyperbolic medium are very much dependent on the nature of the assumed source, and thus the approximate calculation given may be quite inaccurate. A more accurate calculation might result if the antenna were considered to be inside a small close-fitting free space cavity in the anisotropic medium (it is hoped that this calculation will be included in a later report).

2.4 The Laboratory Experiment

2.4.1 The Early Experimental Apparatus

The results from this apparatus (see Figure 2.7) were entirely qualitative but still quite useful. Experimentation indicated the importance of the ion

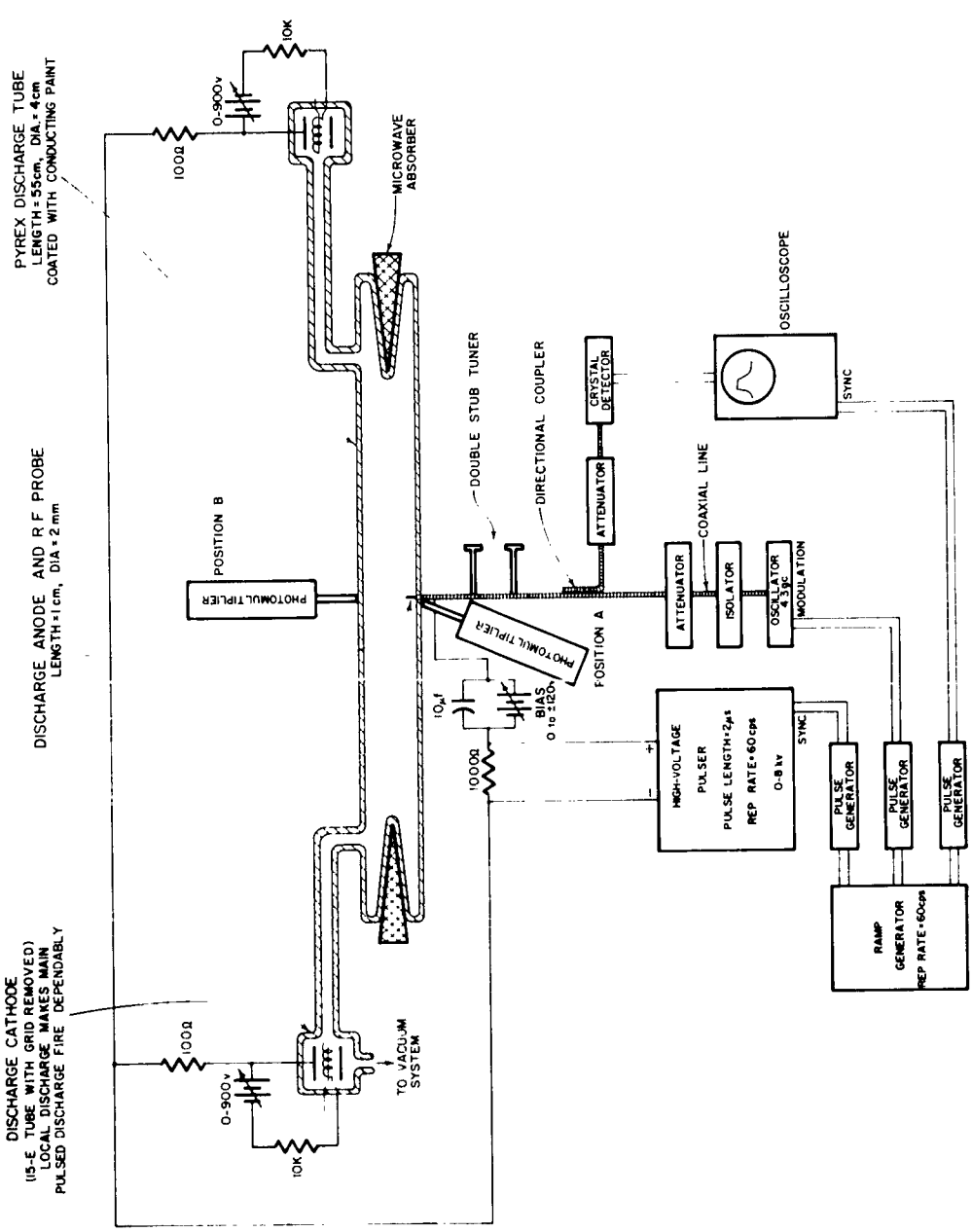

Figure 2.7. Early experimental apparatus

sheath and demonstrated the effects of RF heating of the plasma Experience gained with the discharge tube and the vacuum system aided in the design of improved apparatus suitable for quantitative measurements.

DC bias was applied to the probe using the discharge cathodes as reference electrodes. Negative and positive bias voltages produced the effects on the reflected wave shown in Figure 2.8, with apparent sheath collapse at +9 volts. It is evident that the impedance of the antenna is very much dependent on the size of the ion sheath. Note that Figure 2.8 shows the output from a square-law detector as seen on the oscilloscope and thus the vertical scale is proportional to RF power, not voltage

The effect of RF heating is illustrated in Figure 2.9 No heating was detected below .1 mm but an appreciable effect was observed at 20 mw, the maximum power available. The heating power threshold of .1 mw corresponds to a voltage threshold of .07 volt (with a 50 ohm line). It was expected that the threshold would be about equal to the average energy of an electron at room temperature, about .04 volt. Figure 2.9 shows also that negative bias reduces the effect of heating considerably in comparison with collapsed sheath conditions. In addition, heating always produces the same type of change as negative bias. This suggests that heating produces sheath expansion as predicted by the theory of Section 2.2.2

Quenching of the light output of a plasma takes place when the electrons are selectively heated with an RF voltage[47] A photomultiplier was located in two positions as shown in Figure 2.7 and power input was 20 mw at 4.3 Gc. In position A quenching of the afterglow was detected easily but in position B, quenching could not be detected at all. This indicated that the RF heating was confined to the immediate vicinity of the probe.

Second harmonic output was measured with 20 mw input at 4.3 Gc using a superheterodyne detection system connected to the directional coupler Harmonic output was confined to the first 400 μs of the afterglow and reached a peak about 20 μs after the discharge pulse The peak second harmonic output was 35 db below the fundamental

The pulsed DC discharge was not entirely satisfactory since the discharge density often varied from pulse to pulse as did the balance between the two ends of the discharge tube This was due either to momentary arcs forming

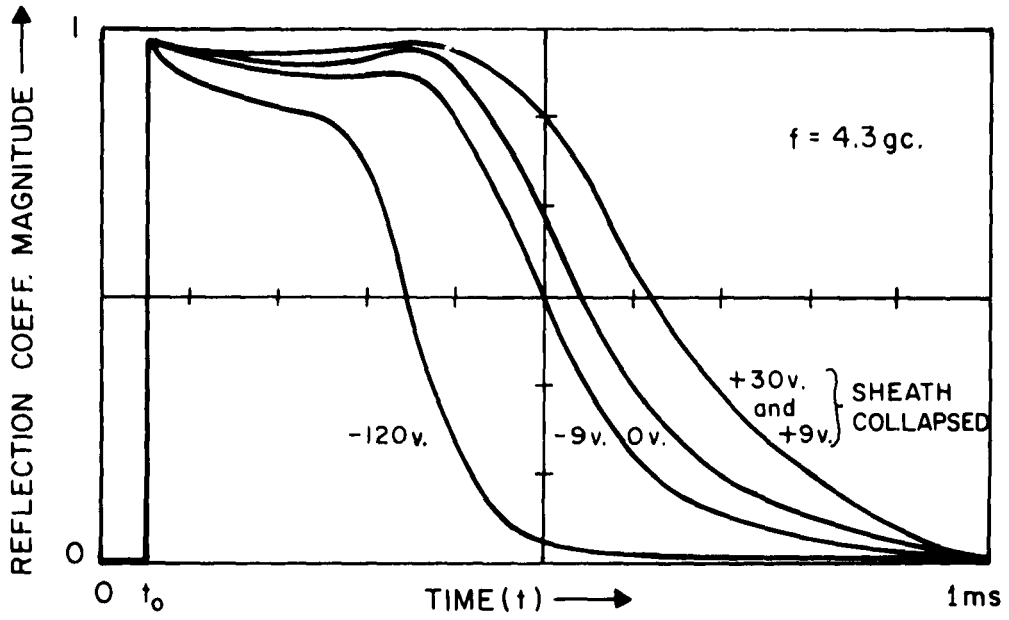

Figure 2.8. Reflected wave magnitude as a function of probe bias. The probe is matched with no plasma ($t < t_o$). $t = t_o$ indicates beginning of discharge

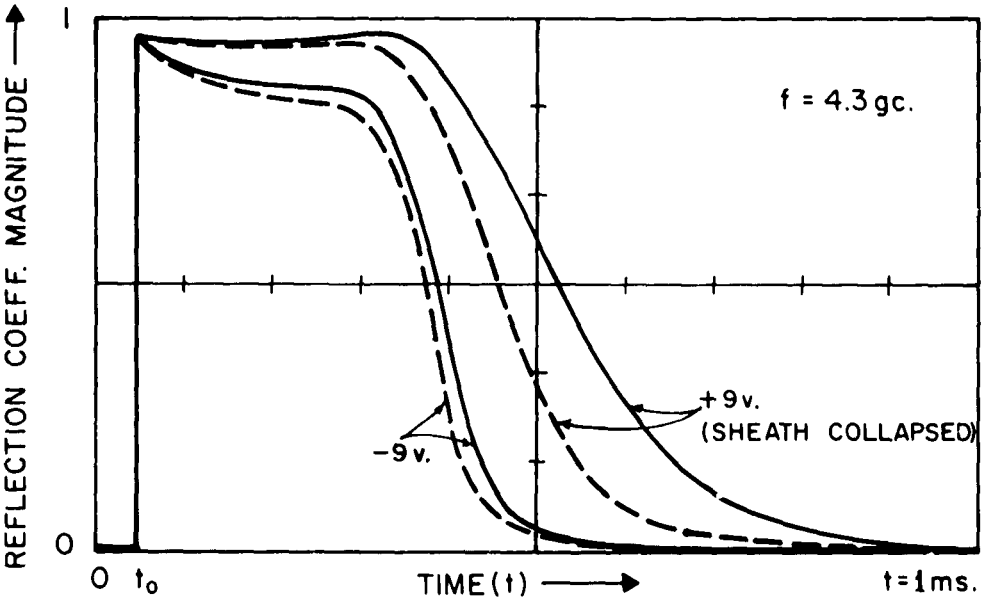

Figure 2.9. The effect of heating as a function of probe bias
——— RF input power = .1 mw
– – – RF input power = 20 mw

at irregularities on the discharge cathodes or to instability in the local discharges (as evidenced by random shifts in the glow structure). Proper operation could be obtained only by careful adjustment of the local discharge voltages and the balancing resistors (shown as 100 ohms in Figure 2.7). As a result of these observations the following recommendations were made:

1. The discharge tube should be single-ended, that is it should have a single discharge cathode.
2. The cylindrical shape of the discharge cathode (15-E triode with grid removed) is satisfactory, but the cylinder should have a much greater volume to ensure dependable starting of the pulsed discharge.
3. The cathode surface should be smooth and its shape regular to discourage arcing.
4. A metallic "ground plane" surrounding the probe should be provided so that a state of sheath collapse could be attained everywhere in the vicinity of the probe. For good bias control of the ion sheath, the following area relationship is necessary (area of cathode) >> (area of "ground plane") >> (area of probe).

These ideas were carried out successfully in the improved apparatus described in the next section.

2.4.2 The Improved Vacuum System and Discharge Tube

The vacuum system used for the quantitative experiments is shown in Figure 2.10. It proved to be quite satisfactory and a gas fill could be left in the system for about two days with no apparent effects of leak contamination. The pump-down period for a pressure of 10^{-6} mm varied from one to four days depending on such factors as the amount of new vacuum grease in the system. In general it was found advisable to outgas the glass discharge tube with a spark coil. The main disadvantages of the system were excessive grease (stopcocks, manometer, O-ring) and slow pumping due to the long, narrow high-vacuum line.

The improved design of the discharge cathode (Figures 2.11 and 2.12) resulted in a very steady, intense discharge with no arcing at all. The discharge had a tendency to concentrate at the tip of the probe but this effect was greatly reduced when the magnetic field was applied. As was mentioned in Section 2.2.4, an insulating deposit forms on the probe and

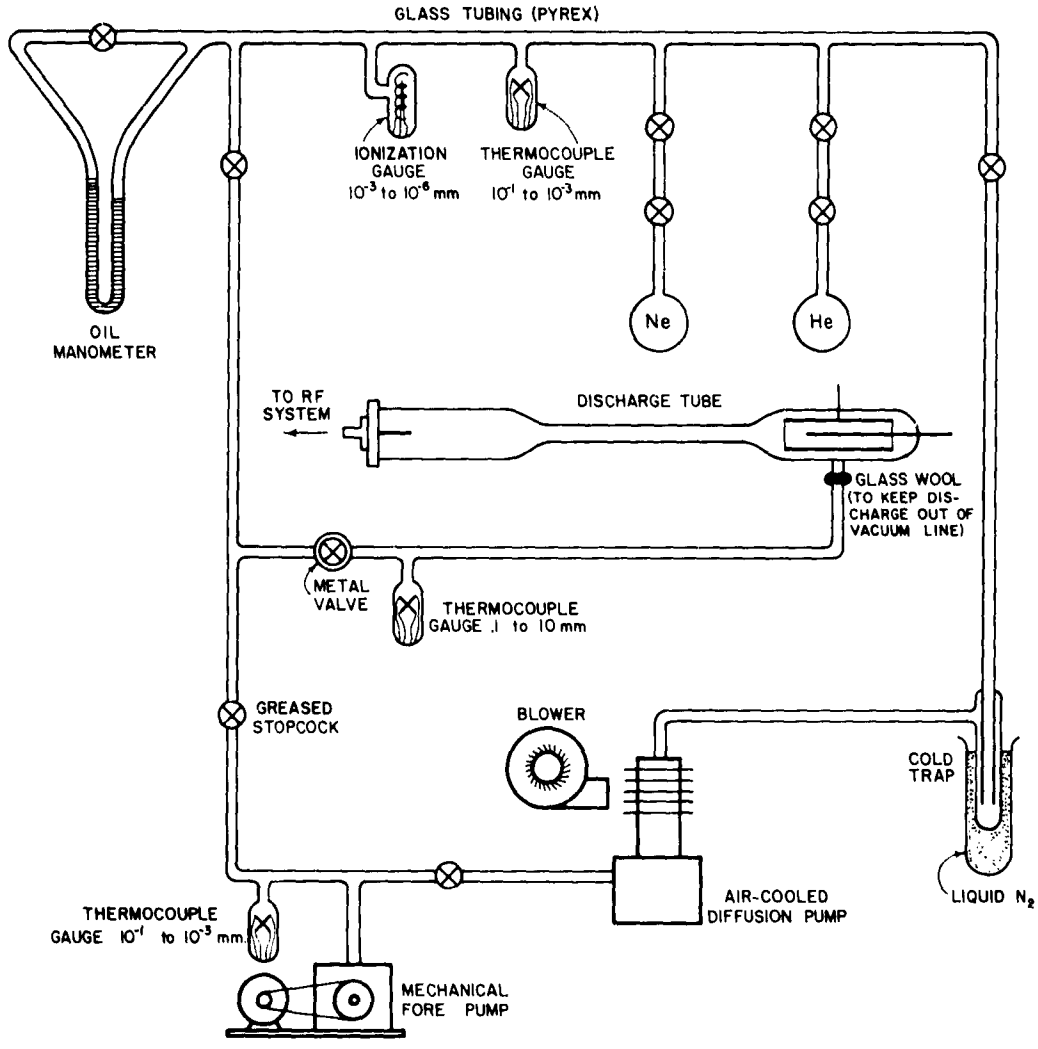

Figure 2.10 The vacuum system

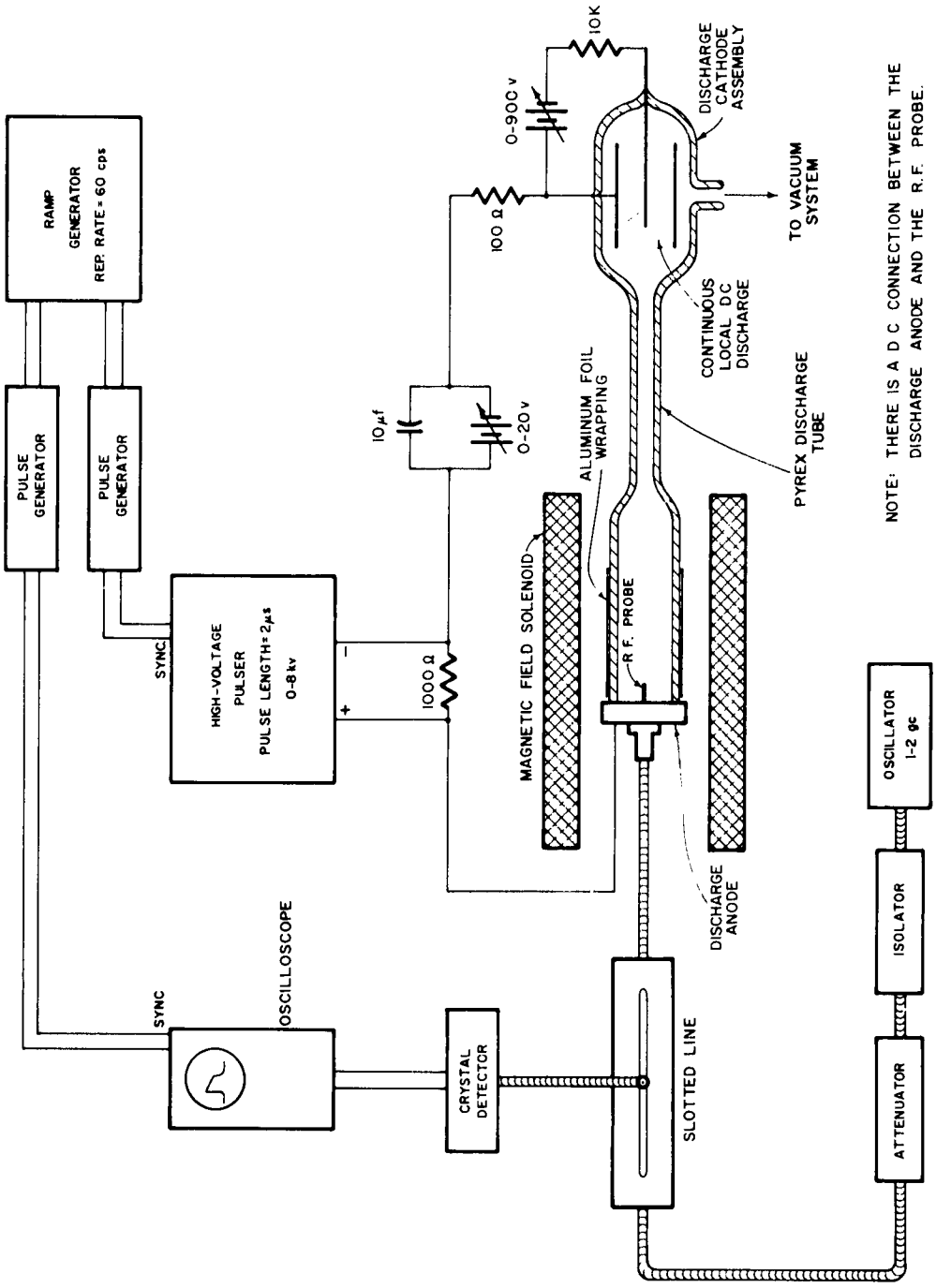

Figure 2.11. The experimental apparatus

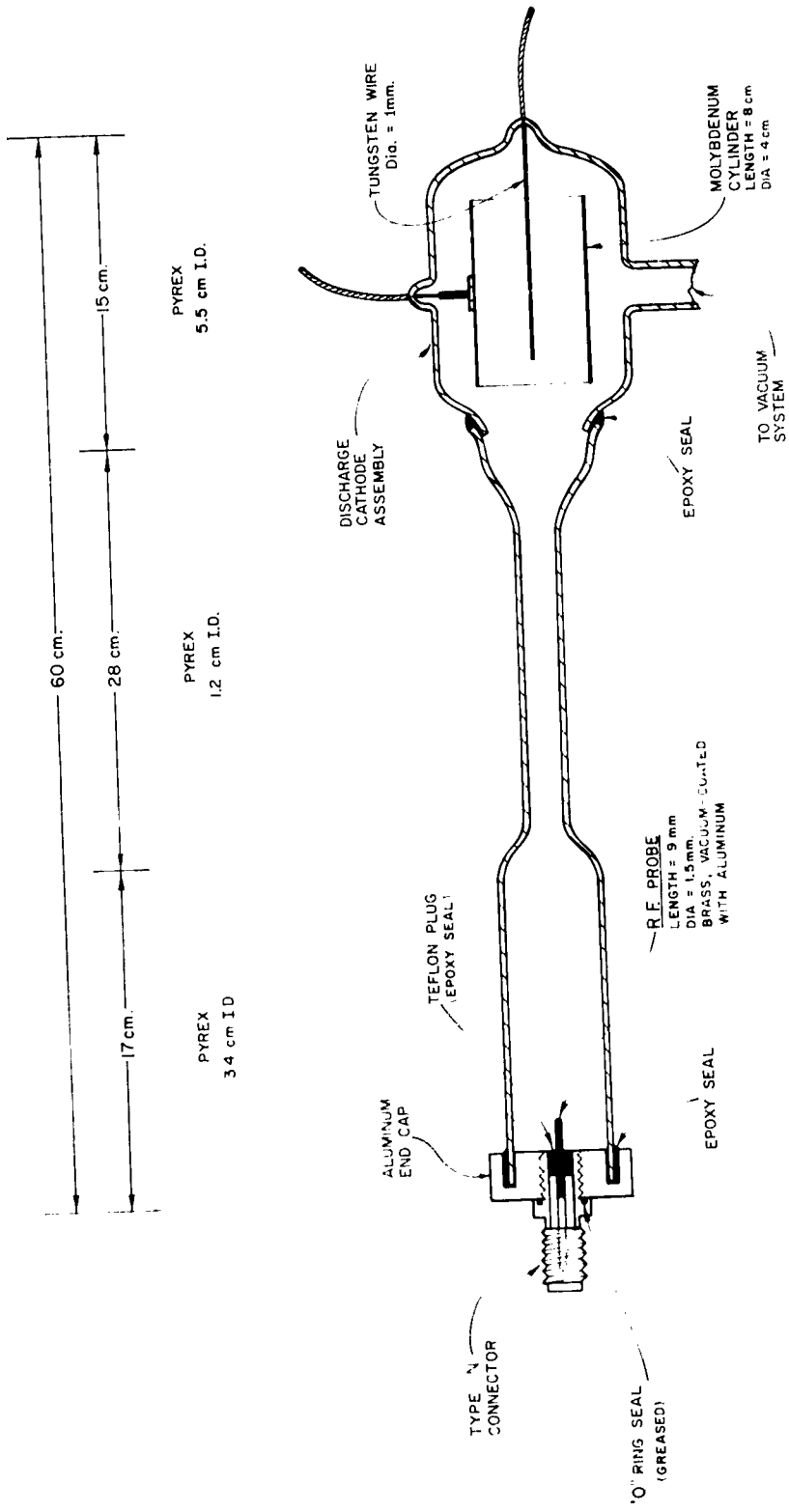

Figure 2.12. The discharge tube and RF probe

must be cleaned off from time to time. It can be seen that the probe dimensions and the discharge tube diameter are small compared to a wavelength. Therefore, this configuration is satisfactory only for testing the quasi-static theory.

2.4.3 The Method of Impedance Measurement

The impedance measurements are made using a slotted line as shown in Figure 2.11; a photograph of the oscillograph trace (probe voltage) is taken at each of four points along the slotted line, the points being spaced 1/8 wavelength. Thus for any desired time in the afterglow, a point on the Smith Chart may be obtained by purely graphical steps as follows.

1. The oscilloscope trace is measured with dividers.
2. This measurement is applied to a parabolic calibration chart which compensates for the crystal detector square-law response and normalizes the resulting voltage for the desired size of Smith Chart.
3. The resulting measurement sets the radius of an arc which is drawn on the Smith Chart. Only three such arcs are really necessary but the extra one is helpful as a check. Thus a point on the chart can be plotted quite accurately.

In general one must try to minimize reflections from either end of the slotted line, since even small reflections can introduce considerable error.

An independent means of electron density determination is not provided in these experiments. It is intended to use the resonance probe method[27,28] for this purpose in later research. It is also intended to provide a Langmuir probe system to measure both electron temperature and density.

2.4.4 The Impedance Results

The impedance results are plotted on Smith Charts (Figures 2.13 to 2.16) by the graphical method described. The Smith Charts are normalized to 50 ohms, the characteristic impedance of the coaxial line. The collision frequency is taken from Figures 2.3a and 2.3b note that neon at 7 mm and helium at 1.2 mm have the same electron-molecule collision frequency. Z varies from about .03 at low electron densities to about 08 at high densities It was assumed in making the calculations that the plasma is in thermal equilibrium at 300° K.

The agreement between theory and experiments is not very good at low magnetic fields and quite good at high magnetic fields By reducing transverse diffusion, the magnetic field probably renders the plasma more uniform. For zero magnetic field the experimental curves appear to suggest high energy loss.

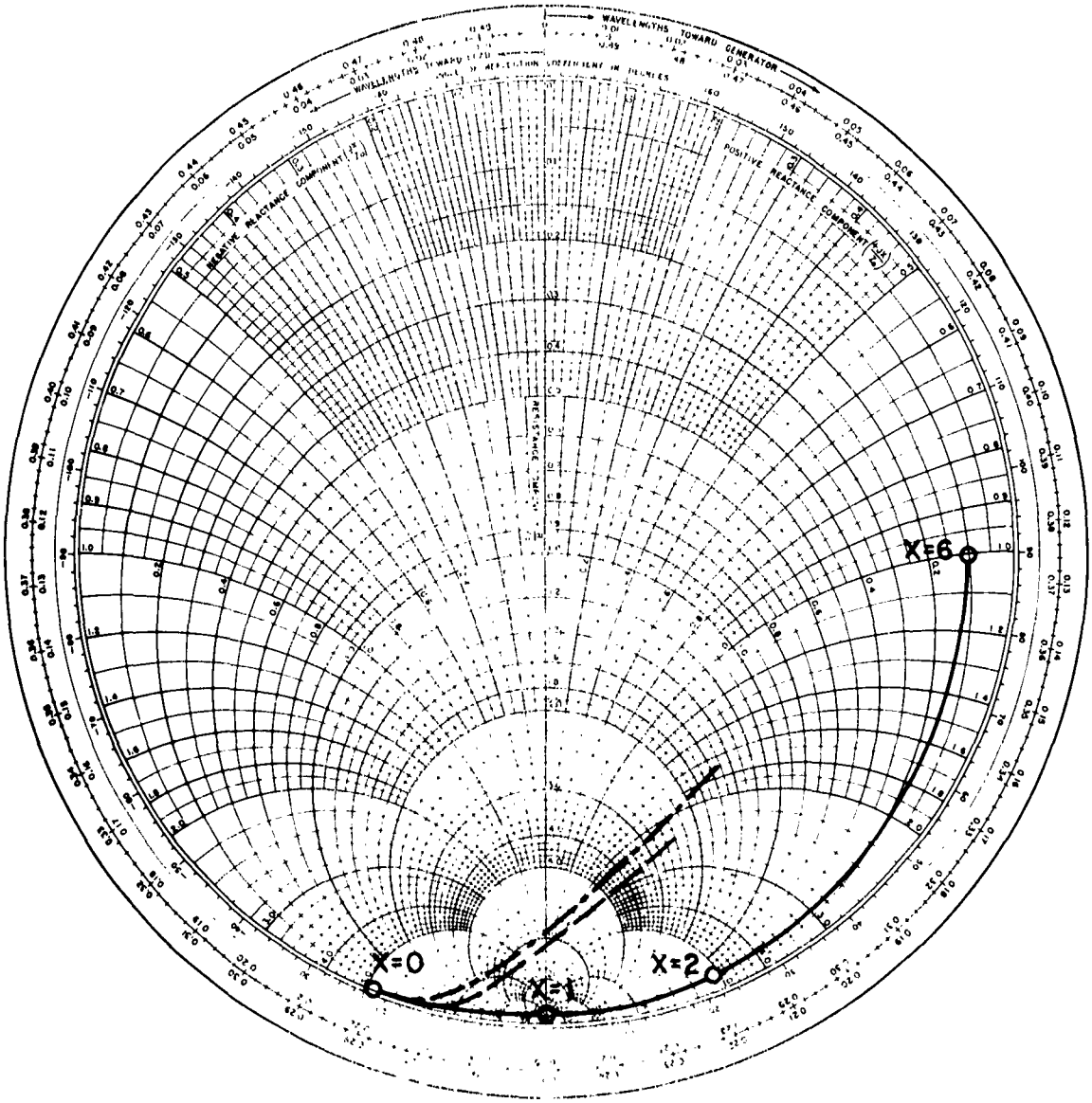

Figure 2.13. Monopole impedance for the case $Y^2 = 0$ as a function of electron density

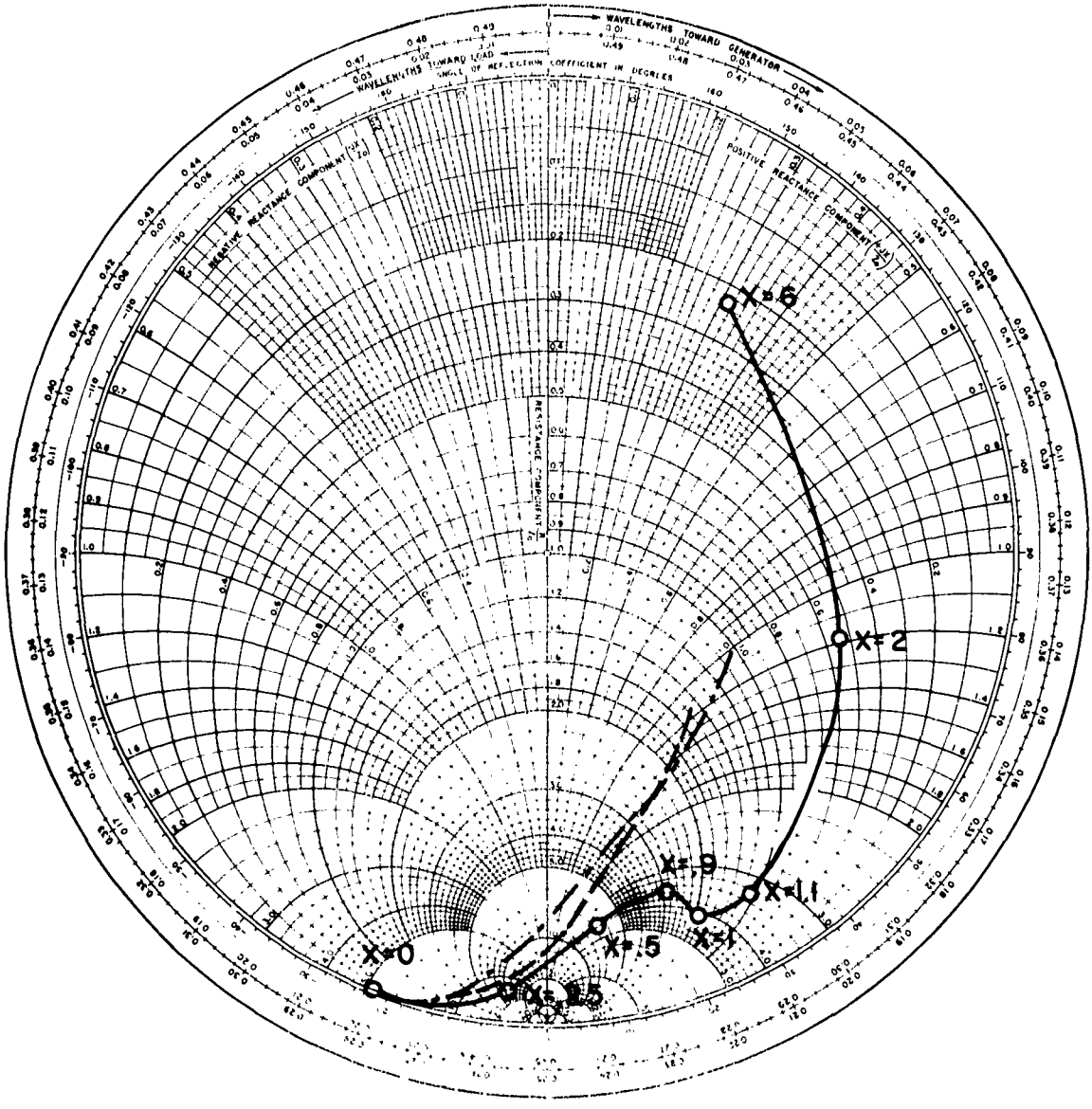

Figure 2.14. Monopole impedance for the case $Y^2 = .75$ as a function of electron density

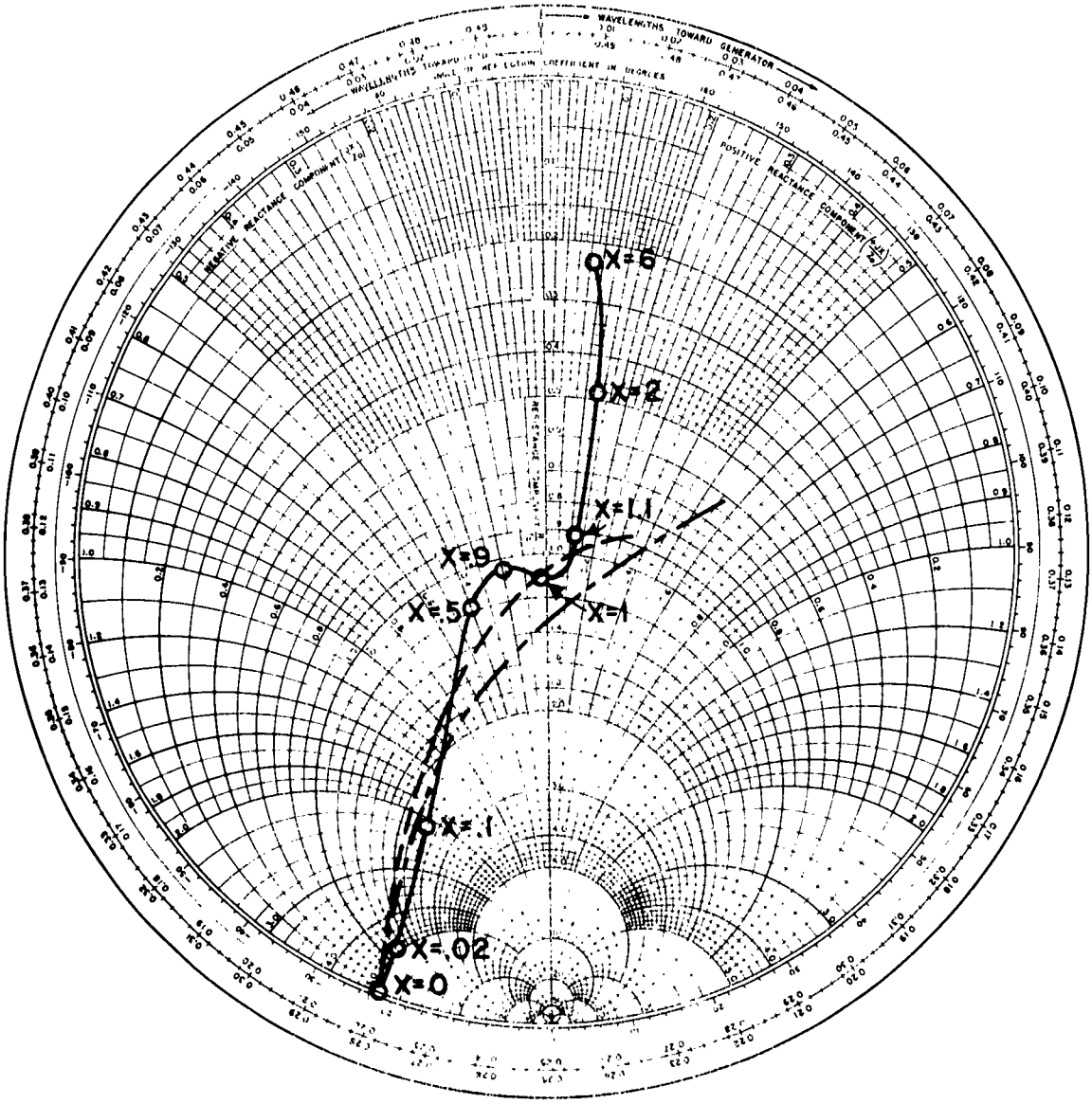

Figure 2.15. Monopole impedance for the case $Y^2 = 1$ as a function of electron density

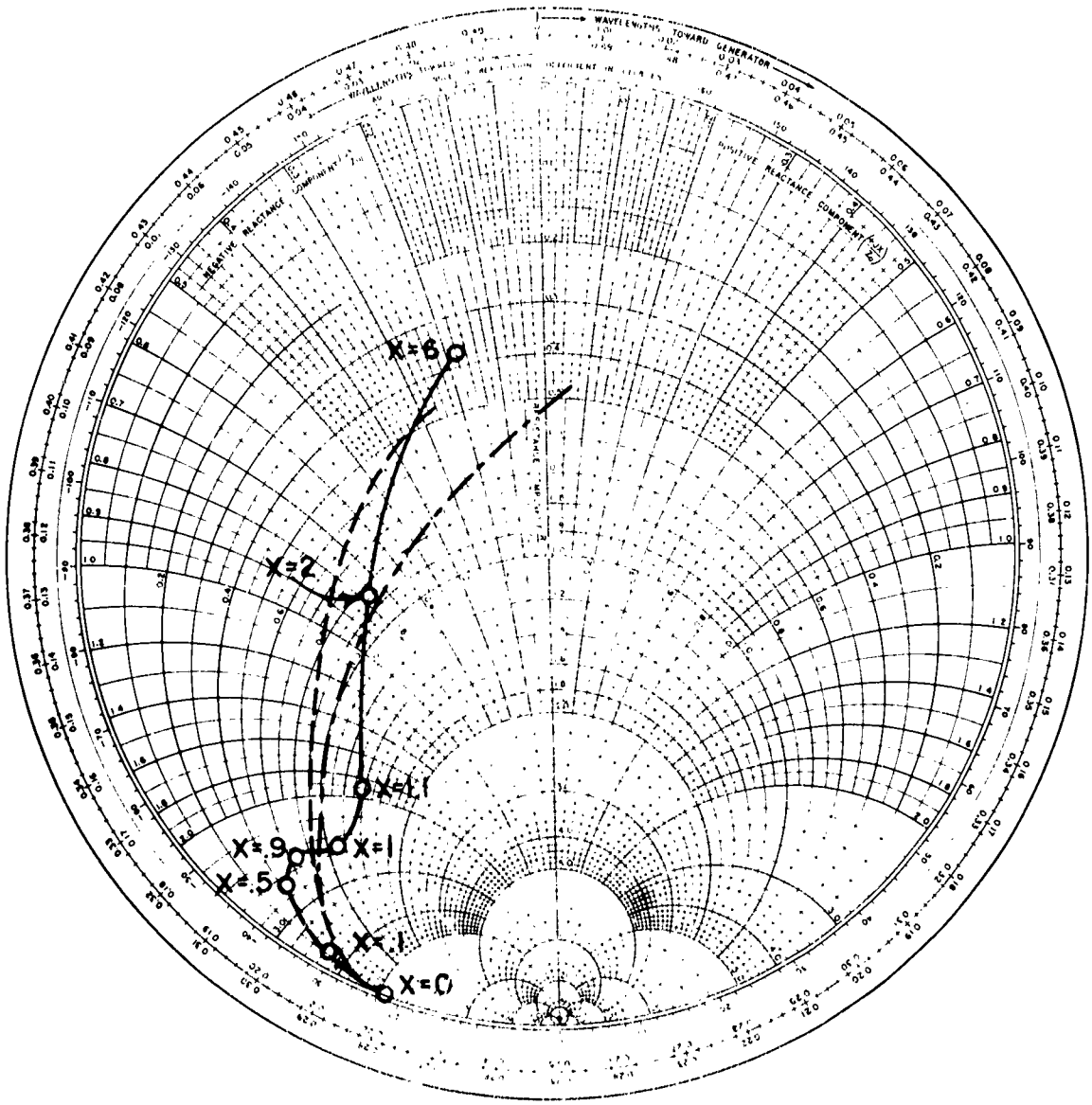

Figure 2.16. Monopole impedance for the case $Y^2 = 1.25$ as a function of electron density

This could be a result of plasma non-uniformity which might increase the apparent resistance of the plasma or permit some form of surface wave to carry energy away from the probe. Another possibility is that the electron temperature decay may have a longer time constant than that given by Dougal and Goldstein[46] (see Section 2.2.4, Equations (2.23) and (2.24)). The theoretical curves exhibit a "kink" in the vicinity of plasma resonance but in the experimental curves this kink is almost indistinguishable. This smoothing effect could be due to non-uniformity in the electron density or to electron temperatures considerably higher than 300° K.

Neon and helium produce similar impedance results but, on the whole, the neon curves are closer to the theoretical curves. This is to be expected since neon has the higher recombination coefficient and therefore should give a more uniform plasma. Also, since the neon is at a higher pressure than the helium, the neon should be less subject to contamination.

To summarize, there is good qualitative agreement between theory and experiment. It is especially interesting that the impedance plot shifts from one side of the Smith Chart to the other as the magnetic field passes through cyclotron resonance. Plasma non-uniformity and elevated temperature are suggested as reasons for the poor quantitative agreement between theory and experiment especially evident at low values of magnetic field The problem of non-uniformity is considered in the following chapter.

2.5 The Effect of Non-Uniform Electron Density

In any decaying plasma, recombination, ambipolar diffusion and ion sheath formation will all be present. Far from the container walls volume recombination should tend to dominate and maintain a uniform plasma density. Closer to the wall, ambipolar diffusion dominates, causing the electron and ion densities to decrease Very close to the wall there is produced an ion sheath in which the electron density drops exponentially. If the wall is a conductor, it may be possible to collapse the sheath using positive bias. From these considerations it is clear that the plasma may be quite non-uniform, especially in the vicinity of a boundary such as an antenna surface

The problem of non-uniformity was considered by Tonks[30] who noted that a parallel-plate 'capacitor' containing a non-uniform plasma would appear to have an unexpectedly high loss if the observer had assumed uniformity

Tonks shows how a broad plasma resonance could result from either a non-uniform plasma or a lossy, uniform plasma. Let us now consider the effect of collisions which were not included in the calculations reported by Tonks. We shall determine the impedance of an isotropic plasma between two parallel plates for four electron density profiles as shown in Figure 2.17.

For the case of unit spacing between plates of unit area, we have

$$Z_{in} = \frac{1}{j\omega\epsilon_0} - \frac{1}{j\omega\epsilon_0}\int_0^1 \frac{1}{K_0}\,dx$$

$$= \frac{1}{j\omega\epsilon_0}\int_0^1 \frac{1}{1 - \frac{X(x)}{1 - jZ}}\,dx$$

For example, consider the linear distribution $X(x) = X_0 x$ as shown in D of Figure 2.17.

$$Z_{in} = \frac{1}{j\omega\epsilon_0}\int_0^1 \frac{1}{1 - \frac{X_0 x}{1 - jZ}}\,dx$$

$$= \frac{1}{j\omega\epsilon_0}\,\frac{1 - jZ}{X_0}\,\ln\left[\frac{1 - jZ}{1 - jZ - X_0}\right]$$

The calculations using this type of formula are shown in Figure 2.17. It is assumed that $Z = \nu/\omega = .1$ and the impedance is normalized to give a free-space impedance of -j5 in order to allow comparison with the experiments.

It is evident from an inspection of Figure 2.17 that a non-uniform plasma with a low collision frequency may be indistinguishable from a uniform plasma with a much higher collision frequency. For instance, an investigator who measured curve B would have concluded (assuming uniform density) that $Z \approx .2$ when the correct value was $Z = 1$. Thus non-uniformity tends to magnify the apparent collision frequency.

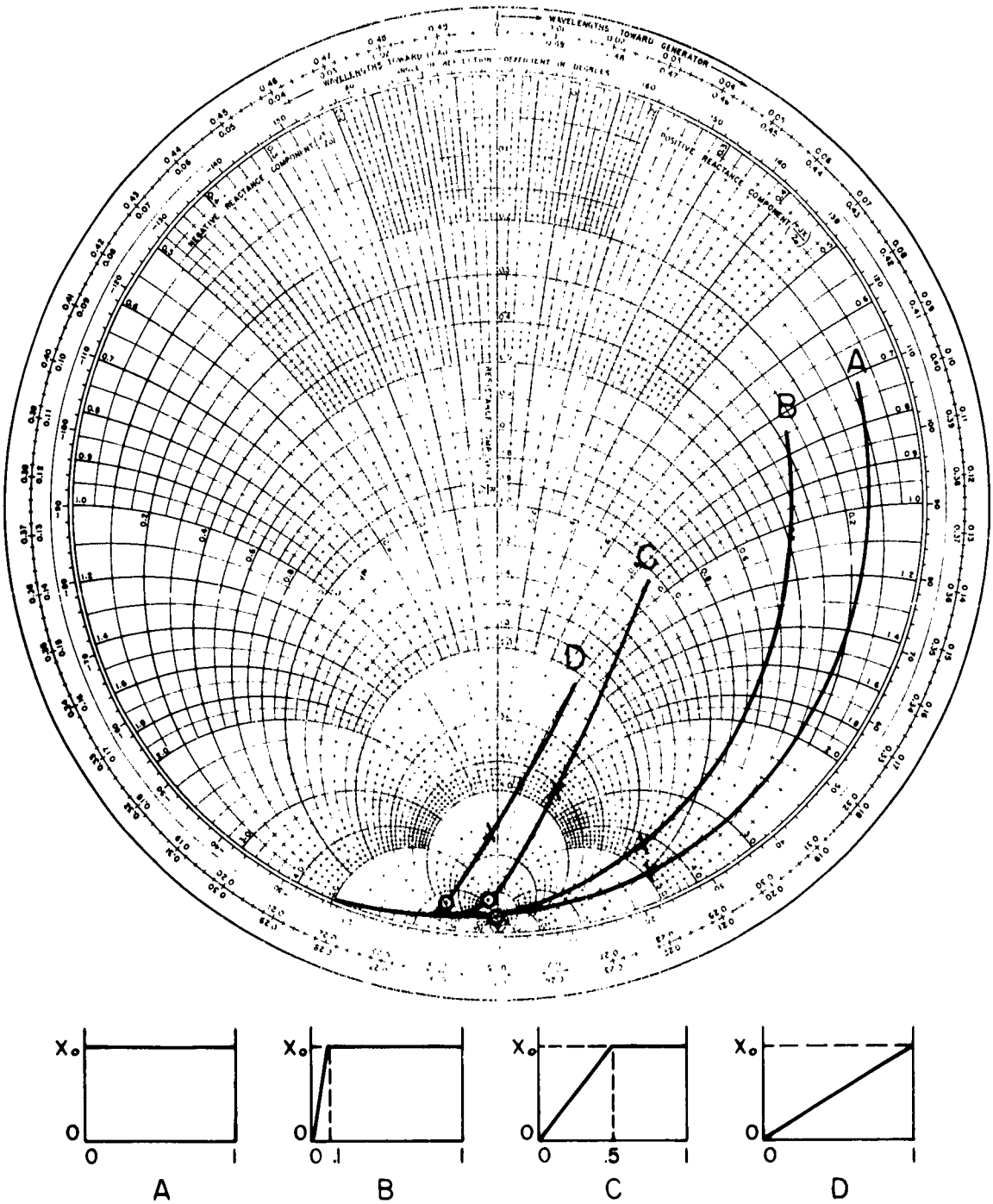

Figure 2.17. The impedance of a non-uniform, isotropic plasma between parallel plates as a function of peak electron density X_0 ($0 \leq X_0 \leq 8$)
Note: ⊙ indicates $X_0 = 1$ and X indicates $X_0 = 2$

If curve D is compared with curve A, it will be observed that the point of zero reactance is a good indicator of the average electron density. To put it another way, the point $X_o = 2$ of curve D is very close to the resistance axis and for this distribution the average normalized electron density is $X_o/2$. This means that the impedance of a short probe can give a good estimate of average electron density, but such measurements should not be used to estimate collision frequency

The curves of Figure 2.17 (especially curve C) are strikingly similar to the experimental curves of Figure 2.13 (zero magnetic field) This suggests that non-uniformity in the plasma is the major reason for the differences between experiment and theory. The magnetic field reduces transverse diffusion, so the theoretical and experimental results are much closer in Figures 2.14, 2.15 and 2.16. Nevertheless, diffusion (especially longitudinal) is not entirely suppressed and the "kinks" at $X \doteq 1$ are not evident in the experiment results

This exceedingly elementary study of non-uniformity suggests that losses will be quite high as long as some portion of an isotropic plasma is in plasma resonance. Thus phenomena such as the ion sheath cannot be represented by a "step" variation in electron density near an RF probe. Instead, a continuous variation in electron density should be considered especially when the RF signal is at a frequency lower than the highest value of plasma frequency.

2.6 Planning for the Gyro-Interaction Experiment

2.6.1 Description of the Experiment

The ionospheric gyro-interaction experiment is designed to investigate the effects of raising the electron temperature in the D' and E' layers by means of a gyro-frequency transmitter carried by a rocket A second signal sent from the ground traverses the heated region and is picked up by a receiver in the rocket so that the received signal amplitude is a measure of the effect of heating Thus there are two rocket antennas, the receiving loop antenna (sensing antenna) which is entirely inside the fiberglass nose cone and the heating dipole antenna which extends outward from the sides of the rocket. In addition there is a small dipole antenna mounted inside the tip of the nose cone this antenna is used to monitor continuously the field of the heating antenna

The quasi-static theory should be useful for predicting the heating antenna impedance and also the field strength at the nose cone monitoring antenna. Both of these are measured in the rocket experiment. In the experiment the earth's magnetic field acts in a direction approximately perpendicular to the heating antenna. Thus the theory for a dipole along the x-axis (magnetic field along the z-axis) should be suitable for approximate calculations

As described in Chapter 1 of this report the rocket experiment has been carried out. Unfortunately the malfunction of the commutator switch caused the impedance experiment to be omitted entirely and made the monitor probe voltage difficult to interpret (since the heating transmitter operated only at its highest preset level). In addition, a bias circuit malfunction in the monitor probe amplifier cut off its output for low levels so that the leading and trailing edges of the monitored heating pulse were not recorded. Thus it is impossible to draw any conclusions about electron density or temperature from the monitor probe output recording. Nevertheless, calculations for the expected heating antenna field and impedance are presented and could be utilized in further experiments.

2.6.2 The Heating Field at the Nose Cone Tip

The E field parallel to the antenna as given in Section 2.3.4 is

$$E_x = \frac{a}{j\omega\ 4\pi\ \epsilon_o\ K'L}\left[\frac{1}{\left(\rho_1^2 + a^2z^2\right)^{1/2}} + \frac{1}{\left(\rho_2^2 + a^2z^2\right)^{1/2}} - 2\,\frac{1}{\left(\rho_o^2 + a^2z^2\right)^{1/2}}\right]$$

For the case of a pickup antenna on the z-axis, $\rho_1 = \rho_2$ and $\rho_o = 0$ so that

$$E_x = \frac{1}{j\omega\ \ 2\pi\ \epsilon_o\ K'L}\left[\frac{1}{\left(\frac{\rho_1^2}{a^2} + z^2\right)^{1/2}} - \frac{1}{z}\right]$$

Also, $\rho_1 = 3\ 05$ m and $z = 1.90$ m

$\rho_1^2 = 9\ 30\ m^2$ and $z^2 = 3\ 60\ m^2$.

If E_x is proportional to some normalized field E, we may define

$$E = \frac{1}{K'}\left[\frac{1}{\left(\frac{9.30}{a^2} + 3.60\right)^{1/2}} - \frac{1}{1.90}\right]$$

In free space $E = E_o$ ($K' = 1$, $a^2 = 1$) Thus the theoretical relative field strength is $|E/E_o|$ and values will be obtained for the appropriate parameters X, Y, and Z. Since for small Z, $1/K' \doteq j2Z/X$ the magnitude of the signal received at the nose cone tip could give a good indication of the collision frequency if the electron density were known Thus the presence of RF heating (with constant electron density) should be readily detectable.

Calculations of the field strength $|E/E_o|$ are shown graphically in Figure 2.18 (based on a noon electron density profile given by Waynick[53] and collision frequencies given by Nicolet[54]). The effect of heating is estimated by performing some of the calculations using a collision frequency increased by a factor of ten. The calculations suggest that the nose cone field measurement should give a good indication of the magnitude of RF heating at altitudes between 90 km and 105 km. In general, this calculation indicates that antenna near field measurements may be more useful than impedance measurements in ionospheric exploration. In particular, the near field of a secondary antenna (mounted at right angles to the heating antenna) should be a good indicator of the average heating effect in the immediate vicinity of the rocket. (See Figure 2-20).

2.6.3 The Impedance of the Heating Antenna

The input impedance of a short dipole perpendicular to the magnetic field (as given in Section 2.3.4) is

$$Z_{in} = \frac{a}{j\omega \pi \epsilon_o K' L}\left[\ln \frac{L}{\rho} - 1 - \ln \frac{a - \frac{1}{2}}{}\right]$$

The measured free-space impedance of the rocket heating antenna is approximately -j 5000 ohms. The computations based on this value of free space impedance are shown graphically in Figure 2 19. These are based on the Waynick and Nicolet models and are normalized with respect to R_o = 1000 ohms The point chosen for matching network design is a compromise it compensates partially for the electron density and collision frequency but is chosen so that the reflection coefficient always decreases with heating between 85 and 95 km.

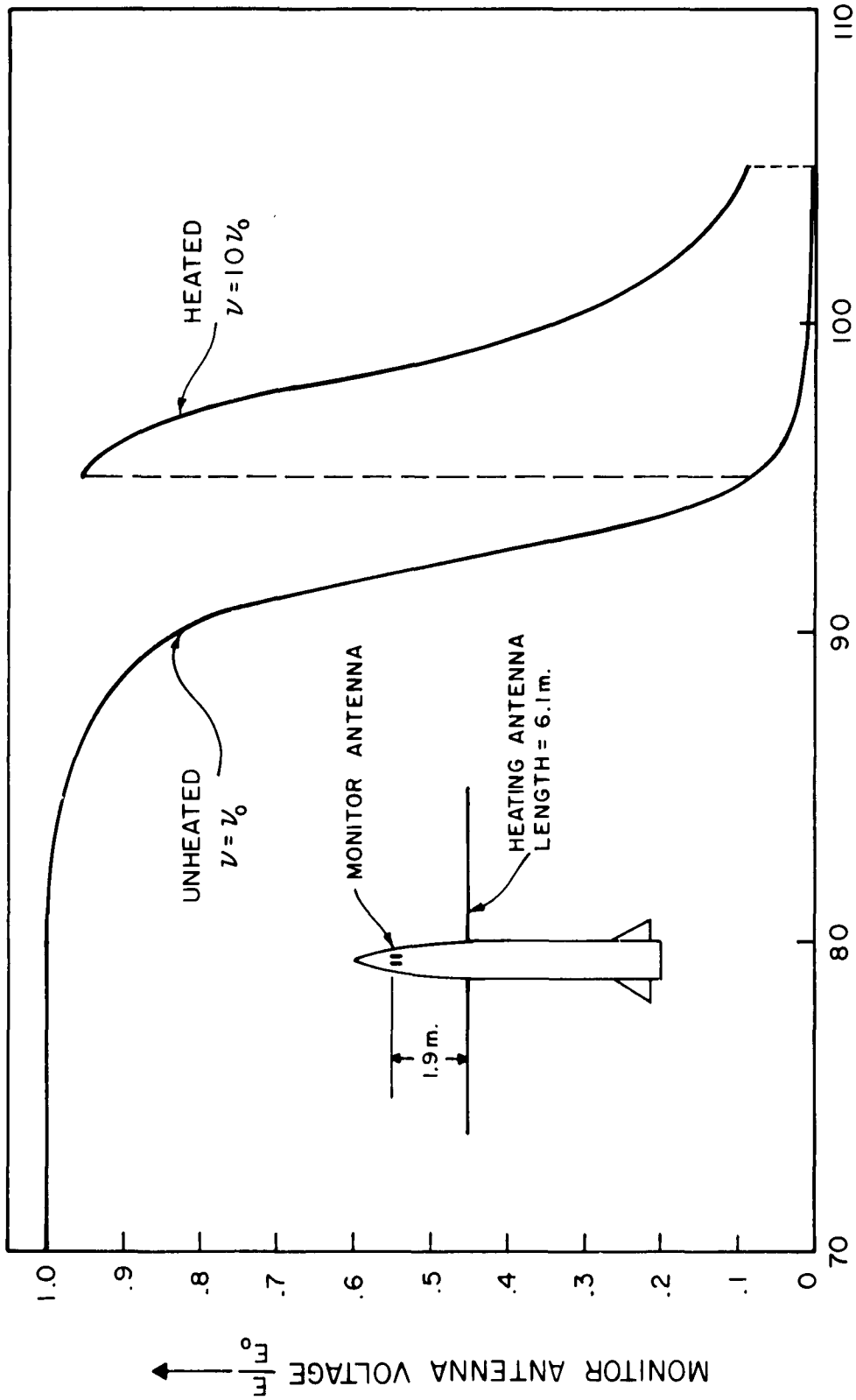

Figure 2.18. Monitor antenna voltage as a function of altitude and heating

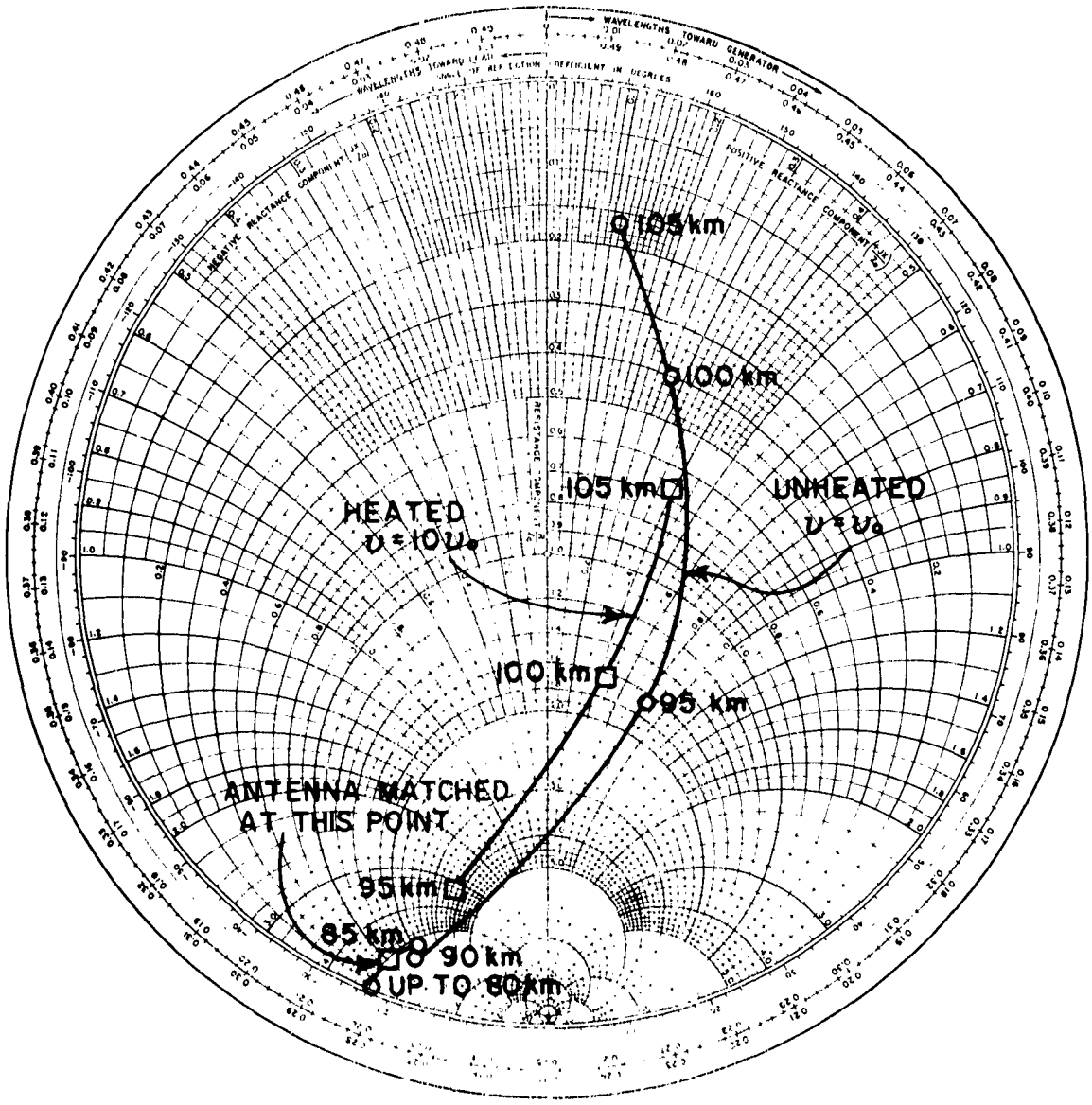

Figure 2.19. The impedance of the rocket heating antenna as a function of altitude and heating

2.7 Recommendations for Future Research

Since the quasi-static theory appears to have some merit, it should be extended. For instance, the impedance calculations might become more accurate if the antenna were taken to be in a close-fitting, free-space hole in the plasma. This would have the effect of reducing the magnitude of the field discontinuities under hyperbolic conditions As another example, the theoretical problem of an antenna inserted in the end of narrow tube might be considered in order to duplicate the experimental conditions more precisely.

The quasi-static theory would also be useful for the calculation of mutual impedances. Such calculations should be relatively simple, especially for the case where both dipoles are parallel to the magnetic field. Mutual impedance measurements should give better results than self-impedance measurements since the former should be less sensitive to ion sheath variations. For this reason it is believed that a "mutual impedance probe" would be useful in ionospheric exploration. In addition it could be tested in the laboratory using the experimental arrangment described in this report.

A further application of the quasi-static theory would be the re-entry sheath problem. The source would be taken to be inside a sphere of anisotropic plasma surrounded by isotropic plasma or free space. Quasi-static theory would be used inside the sphere and full wave theory outside it. Using this approach the effect of a locally strong magnetic field could be estimated

It should be possible to develop a more general impedance theory by utilizing recent research on plasma conductivity[55,56] By this means such effects as Landau damping might be taken into account. Non-linear effects such as the resonance probe method[27,28] also deserve further study, both theoretically and experimentally, and possibly with the inclusion of magnetic field effects.

Another theoretical approach would be to consider the waves which can exist on a long, thin wire in an anisotropic plasma. This could assist in understanding the behavior of antennas with dimensions comparable to a wavelength.

In summary, there are many interesting and possibly fruitful approaches to the problem of antenna impedance in plasma media. In particular, ionospheric and laboratory experiments to measure mutual impedance are strongly recommended. A proposed ionospheric experiment is sketched in Figure 2 20 The cyclotron

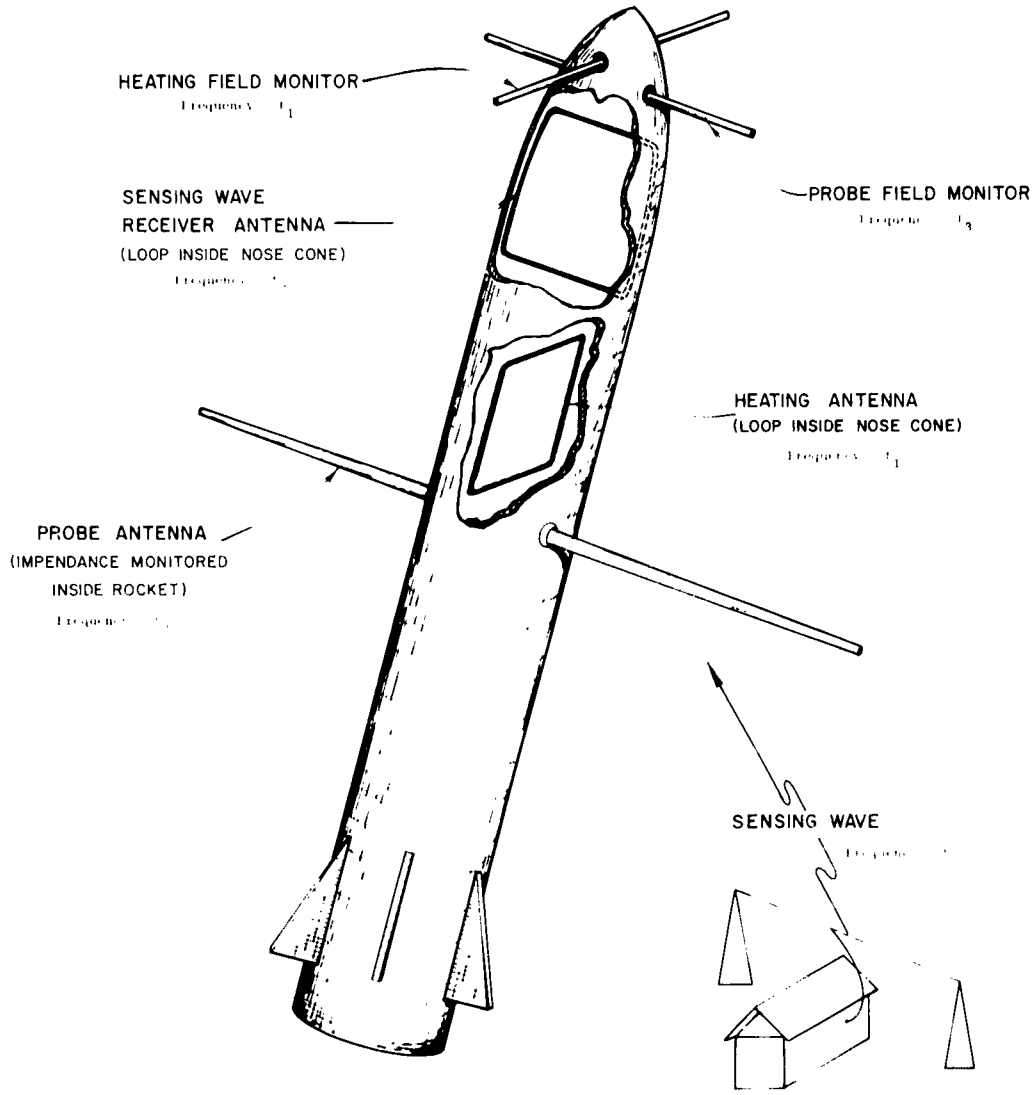

Figure 2.20. A proposed rocket experiment

heating and sensing design is similar to the design already tested, the sensing wave transmission being used to determine the heating effect at points distant from the rocket. The difference is in the addition of an auxiliary probe antenna and its near-field monitor. Measurement of the field and impedance of the probe antenna should permit fairly accurate estimation of electron density and temperature, and especially changes in these parameters.

2.8 Conclusions

A quasi-static theory for the field and impedance of a short dipole has been worked out. Laboratory impedance measurements for a probe in an anisotropic plasma agree fairly well with the theory, especially for the case of a moderate to high magnetic field The theory predicts the excitation of radiating waves by the short dipole but experiments have not yet positively identified this effect

Differences between the theory and the experiments probably are due to non-uniformity in the plasma electron density which causes an apparent increase in the plasma collision frequency. If a short antenna is used as an impedance probe, plasma non-uniformity can seriously affect collision frequency measurements. However, the average electron density can be determined much more accurately (for instance, by observing the frequency at which the reactance vanishes).

The quasi-static theory was used to predict the impedance of the heating antenna used in the gyro-interaction experiments In addition the field of the heating antenna at the nose cone tip was calculated (a small electric field probe was located there) This field magnitude was found to be a good indicator of local plasma heating Unfortunately, a failure in the rocket instrumentation prevented the impedance and field measurements from being carried out.

The formation of the ion sheath has been studied and conditions for its collapse have been obtained (using positive bias) In the laboratory experiments probe bias was found to have a noticeable effect on impedance and thus the sheath was collapsed for the quantitative measurements described in this report. In the experiments the ion sheath introduced additional non-uniformity and thus increased the apparent RF losses in the plasma

Recommendations for future research were made with special attention to the use of short, rocket-mounted antennas to measure electron density and

temperature. Such measurements close to the rocket would help in the interpretation of the sensing wave amplitude, the only recorded parameter related to heating at some distance from the rocket. For future gyro-interaction experiments, measurements of the field and impedance of an auxiliary antenna perpendicular to the heating antenna should give a good estimate of ionospheric properties close to the rocket. Such measurements would be especially useful in studying changes in electron density and temperature (i.e. the transient behavior of the ionosphere).

APPENDIX TO CHAPTER 2

IMPEDANCE OF AN ANTENNA IN A CONDUCTING MEDIUM

Georges A. Deschamps

The dependence of the input impedance of an antenna on the properties of the surrounding medium is particularly simple when the antenna is made of perfect conductors and is fed from a region small in terms of the operating wavelength.

The result can be expressed as follows: the impedance normalized to that of the medium takes the same value at frequency ω in a medium of index n as it does at frequency $n\omega$ in a medium of index 1

This is a known result in the theory of antenna modeling but it is not widely recognized that the relation holds when the medium characteristic constants are complex numbers, as for example in the case of a lossy medium.

The following short proof will convince the reader that this is true. The surrounding medium is assumed homogeneous and characterized by its permittivity and permeability constants ϵ and μ where ϵ and μ may be complex numbers. Consider, at frequency ω_o in the medium (ϵ_o, μ_o) the field $E_o(r)$, $H_o(r)$ which results from applying one ampere current source at the terminals of the antenna. This field is determined by Maxwell's equations and the proper boundary and radiation conditions. When the medium is changed to (ϵ, μ) a field which satisfies the new Maxwell's equations and the same boundary and radiation conditions is obtained by scaling the vector E_o, H_o to $E = E_o(\epsilon_o/\epsilon)^{1/2}$, $H = H_o(\mu_o/\mu)^{1/2}$ and simultaneously changing the operating frequency to $\omega = (\mu_o\epsilon_o/\mu\epsilon)^{1/2}\,\omega_o$. Integrating in the feed region from one conductor to the other (Figure A.1) gives the terminal voltage $V = \int_a^b E.ds$ and integrating along a loop c around the conductors gives the input current $I = \int_c H.ds$ Thus keeping these integration paths fixed when the medium is changed we see that the impedance V/I behaves in the same manner as the ratio E/H at any point. If we denote by $Z(\omega, \epsilon, \mu)$ the impedance of the antenna at frequency ω in the medium (ϵ, μ) we have the relation

$$Z(\omega, \epsilon, \mu) = \left(\frac{\mu}{\epsilon}\right)^{1/2} \left(\frac{\epsilon_o}{\mu_o}\right)^{1/2} Z\left(\omega\left(\frac{\mu\epsilon}{\mu_o\epsilon_o}\right)^{1/2}, \epsilon_o, \mu_o\right) \quad (A.1)$$

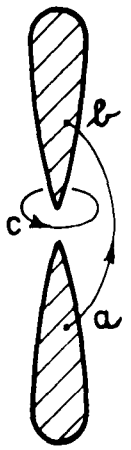

Figure A.1. Two conductor antenna

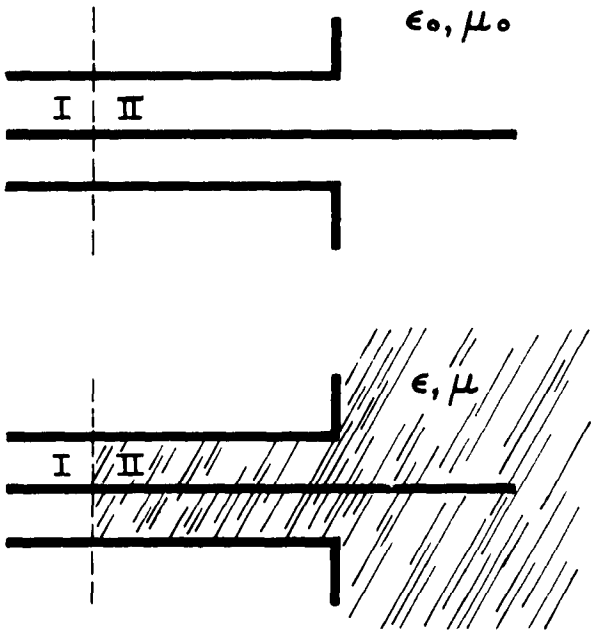

Figure A.2. Antenna with TEM feed waveguide

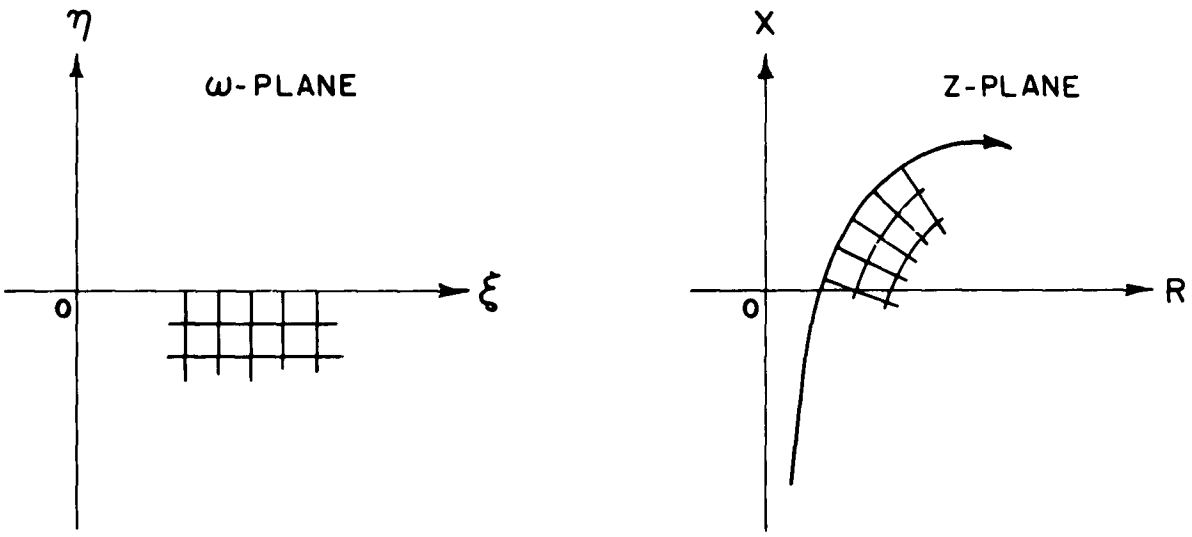

Figure A.3. Sketch of the mapping $\omega \longrightarrow Z$

Introducing the index $n = (\mu\epsilon/\mu_o\epsilon_o)^{1/2}$ and the intrinsic impedances of the medium $\zeta_o = (\mu_o/\epsilon_o)^{1/2}$ and $\zeta = (\mu/\epsilon)^{1/2}$ this becomes

$$\frac{1}{\zeta} Z(\omega, \epsilon, \mu) = \frac{1}{\zeta_o} Z(n\omega, \epsilon_o, \mu_o)$$

which can be expressed by the statement made above.

If only the permittivity is changed from ϵ_o to $\epsilon = n^2\epsilon_o$ the relation simplifies to

$$Z(\omega, \epsilon) = \frac{1}{n} Z(n\omega, \epsilon_o) \qquad (A.2)$$

The proof is obviously valid whether the various characteristic constants are real or complex. The assumption about a perfect conducting antenna is used to assert that, after scaling, the field still satisfies the boundary condition ($E_{tan} = 0$.) [If another value of surface impedance was imposed on the antenna it would have to be changed, together with the medium, so as to keep the same relative value with respect to the surrounding medium.] The condition on the size of the source or feed region is used in identifying the integral of the fields along some paths with the voltage and current inputs. Even with these restrictions, a large number of useful antennas are included: the dipole fed from a small gap, the biconical or discone antenna, log-periodic and log-spiral antennas fed from a point

Strictly speaking the proof does not apply to an aperture antenna because one cannot find integration paths ab and C in the medium such that the integral of E and H represent respectively V and I. The proof can however be extended to an antenna fed by means of a two conductor waveguide supporting a TEM mode provided the change of medium from (ϵ_o, μ_o) to (ϵ, μ) is carried out inside the waveguide all the way to a terminal plane where the field in regions I and II (Figure A.2) can be represented by the principal modes only.

An extreme example of this is a plane wave, normally incident on a slab of material (ϵ, μ) backed by a conducting plane If the thickness of slab is a, the impedance Z = E/H at the interface is

$$Z = -j\,\zeta \tan ka$$

an expression which satisfies Equation (A.1) when the medium characteristics are changed. It is easy to adapt the proof given above to the general TEM waveguide.

When the medium is modified only outside of the actual aperture of the antenna, the field in that aperture usually contains higher order modes and the relation (A.1) may still be applied but only as an approximation.

The relation can be used to find the impedance of an antenna in a lossy medium, i.e., a medium characterized by a complex value of n. This requires a knowledge of $Z(\omega)$ for complex values of ω. The simplest case is when Z is known analytically. Take for example a short antenna, represented by a capacitance C in free space $Z = 1/jC\omega$. Changing the medium to (ϵ, μ) Equation (A.1) reduces to the obvious result, $Z = \epsilon_o/\epsilon \; 1/jC\omega$ If the medium is a plasma with refractive index $n^2 = 1 - \omega_p^2/\omega^2$ relation (A.1), applied to the admittance gives

$$Y(\omega, n) = n\, Y(n\omega, 1) = jC\omega + \frac{1}{jL\omega}$$

with

$$L = \frac{1}{C\omega_p^2}$$

As a next approximation the impedance of a short antenna takes the form $Z = a\,\omega^2 + jb/\omega$ and therefore in a plasma

$$Z = a\,\omega\sqrt{\omega^2 - \omega_p^2} - jb\omega\,(\omega^2 - \omega_p^2)^{-1}$$

When the analytic expression of Z is not known but Z has been measured for real values of ω, its values for complex frequencies (with negative imaginary part) can be deduced by analytic continuation. This can be carried out by graphical methods based on the fact that the mapping $\omega \longrightarrow Z$ must be conformal. An illustration is shown in Figure A 3 Another approach is to note that for negative values of Im ω, Z is an analytic function without singularities, thus the Cauchy formula can be used

$$Z(\omega) = \frac{1}{2\pi j} \int_{-\infty}^{+\infty} \frac{Z(\xi)}{\xi - \omega} d\xi$$

where $Z(\xi)$ is known on the real axis.

Since an experimental knowledge of Z is usually limited in range and accuracy, there will be serious limitations to the validity of this procedure far away from the measured data. Using an analytical form which represents the data over a limited range also permits continuation only in the neighborhood of that range. However, for the case of moderate losses (say for Im n < 10 Re n) even a graphical extrapolation based on a free hand sketch is adequate.

To test the method and illustrate this last point some results obtained recently by R. W. P. King and C. W. Harrison, Jr.[56] were used. These authors consider cylindrical antennas of total length 2h and given diameter-to-length ratio (1/75). The medium is characterized by $\mu = \mu_o$, $\epsilon = \epsilon_o \epsilon_r - j\sigma/\omega$ or $n^2 = \epsilon_r - j\sigma/\omega\epsilon_o$.

For these antennas let us designate the input impedance at frequency ω by $Z(2h, \omega, n)$. Thus letting ω_o be the frequency and λ_o the wavelength corresponding to 6 mc, Table 1 or Figure 4 of the reference gives $Z(\lambda_o/2\sqrt{\epsilon_r}, \omega_o, n)$ for several values of n. Thus only antennas whose length 2h has been adjusted to remain equal to half of a wavelength in the medium are considered

A change in size, the medium being fixed, is equivalent to a change in frequency, thus the expression is also $Z(\lambda_o/2, \omega_o/\sqrt{\epsilon_r}, n)$ and from relation (A.1) this is $1/n\ Z(\lambda_o/2, n/\sqrt{\epsilon_r}\ \omega_o, 1)$ The latter is the impedance of a half-wave antenna in air for the complex frequency $n\omega_o/\sqrt{\epsilon_r}$ (Note that in all these formulas n must be considered as fixed at the value $n(\omega_o)$. For real frequencies we can sketch the locus of Z from the data in the same paper We can then extend this locus to complex values of ω (with negative imaginary part) and deduce from the plot values of $Z(\lambda_o/2\sqrt{\epsilon_r}, \omega_o, n)$ for several $\sigma/\omega\epsilon_o$.

$\frac{\sigma}{\omega\epsilon_o}$	Z (from reference)	Z (from analytic continuation)
0	83 + j 40	83 + j 40
.05	100 + j 36	100 + j 35
.10	116 + j 32	117 + j 31
.15	131 + j 30	132 + j 27
.20	167 + j 28	168 + j 24

The agreement is very good in that range. For larger values of $\sigma/\omega\epsilon_0$ it becomes doubtful and the method of continuation would have to be refined to take into account a larger part of the locus $Z(\omega)$ for ω real.

The total complex plot of $Z(\omega)$ suggests a simple method for interpreting the result of an impedance measurement in terms of the medium characteristics. The accuracy of this plot can be improved by taking a few measurements in a lossy medium. Making use of the analyticity of $\omega \longrightarrow Z$ should help organize the results and reduce appreciably the experimental effort.

This work was done in connection with contract AF19(604)-5565. The computations reported here were carried out by Mr. K. G. Balmain.

3. PLASMA NONLINEARITIES - J. T. Verdeyen

3.1 Introduction

The nonlinear response of plasmas to electromagnetic waves, as evidenced by the generation of power at the second harmonic of the applied frequency, was studied during the period of this contract. The results of the theoretical analysis and the laboratory experimental study have been given in a separate report[58]. This section will deal only with the pertinent features of the nonlinear study which apply to the rocket probe of the ionosphere.

It was found in the experimental study that mixing of two electromagnetic waves of frequencies f_1 and f_2 occurred in a plasma provided the amplitude of one of the waves was sufficiently great. It was found that if this amplitude was great enough to cause an additional degree of ionization (i.e. breakdown) then the conversion efficiency was greatly enhanced over the case without breakdown.

It was estimated that the heating wave in the rocket would cause a local breakdown in the E layer of the ionosphere, and thus could perform the function of a local oscillator in a superheterodyne receiver. One could then attempt to detect one of the products of the mixing of the heating wave and the sensing wave in this localized region of the ionosphere.

The difference frequency was chosen to be the signal to be detected in this rocket probe for two reasons:

1. The lower regions of the ionosphere would provide an effective shield against any spurious signals from other radio stations. Thus, if any signal was detected, one could be sure that it was a product of the nonlinearity in the ionosphere, and not a signal from the various local radio stations.
2. The use of the low frequency signal permits one to use less sophisticated circuitry in the RF section of the receiver. The weight and space requirements of this receiver dictated that transistors be used throughout. The stability of transistor radio receiver is easier to achieve at the lower frequencies. Furthermore the difference between the sensing and the heating frequency (610 kc) was low enough so that a TRF receiver was feasible rather than a heterodyne

scheme. The use of the TRF receiver avoids one source of noise in the heterodyne scheme--the first detector.

It should be emphasized here that this part of the rocket probe was conceived only four months prior to actual firing of the rocket, and thus time limitations and availability of components dictated the choise of the circuitry.

3.2 System Concept of the Difference Frequency Receiver (610 kc)

The operation of difference frequency receiver and its place in the rocket system is best illustrated by the use of the timing diagram in Figure 3.1. The heating wave transmitter in the rocket was pulsed on for 500 μseconds with 13.3 milliseconds between pulses. The power level of the transmitter was to be changed in ratios of 1:10:100, with each power level being held fixed during 45 pulses. This is shown in Figure 3.1a. The sensing wave was broadcast from the ground to the rocket as a CW wave. It is obvious therefore that a 610 kc signal would only be present during the time interval of the heating wave, and thus the receiver for this 610 kc signal need only be on during this time interval. The block diagram for this receiver is shown in Figure 3.2.

The 610 kc signal was to be amplified by the TRF section and then fed into the gated clamp. This clamp is open for a time duration ($\sim$ 1 msec) determined by the monostable multivibrator, which is triggered by the same pulse which triggers the transmitter. During the duration when the clamp is open, the 610 kc passes through to the detector. The output of the detector is amplified, and the energy contained in the pulse is stored on a large capacitor. Thus the voltage on the condensor is proportional to the energy contained in the pulses of 610 kc signal. The peak voltage on the capacitor is limited to 5 volts by a Zener diode across the output.

The voltage on this capacitor was to be sampled three times during each power level of the transmitter. At the end of each power level, the capacitor was shorted to ground by a reset switch. The signal for a reset was derived by a coincidence of two pulses, reset 1 and 2, which were fed into the "and" gate.

3.3 Conclusions

It has already been noted that considerable data was lost when the telemetering switch failed. Unfortunately, the data from this part was among that which was lost. However it is felt that any future probes such as this should be instrumented to observe coherent nonlinearities such as described above

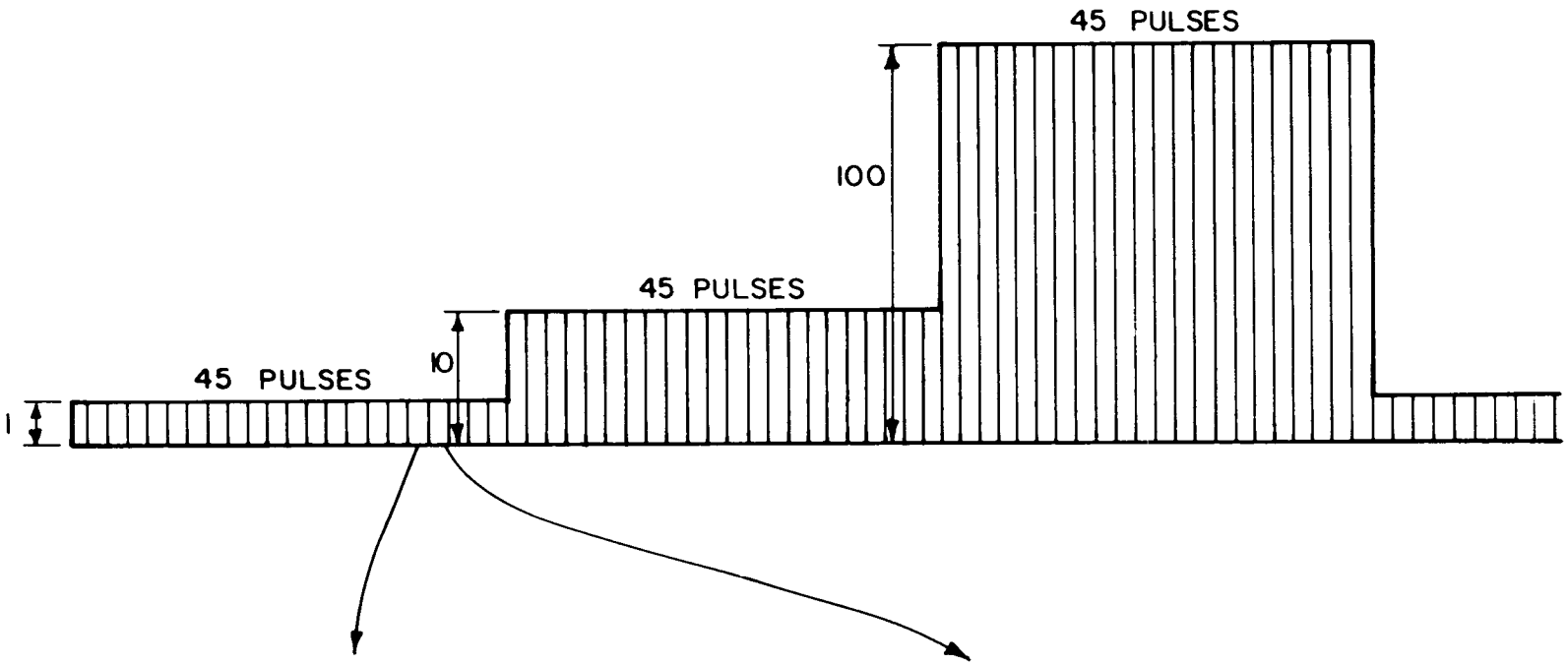

Figure 3.1a. Pulse train of the heating wave

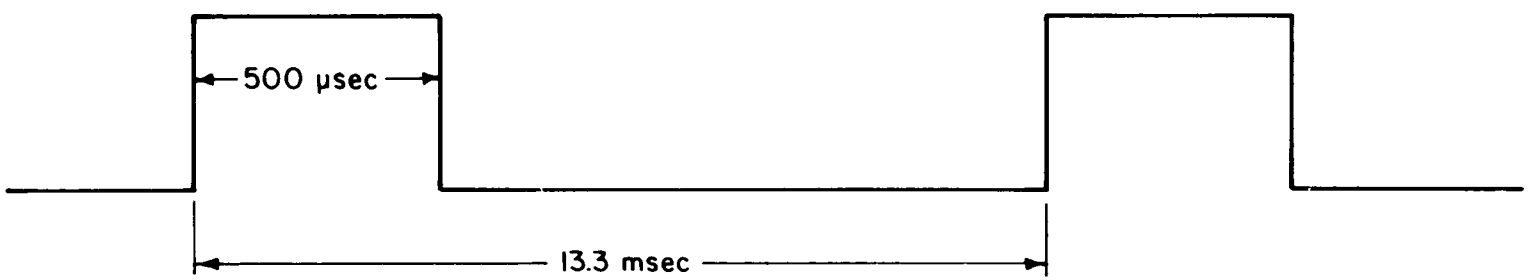

Figure 3.1b. Detail of envelope of the heating wave

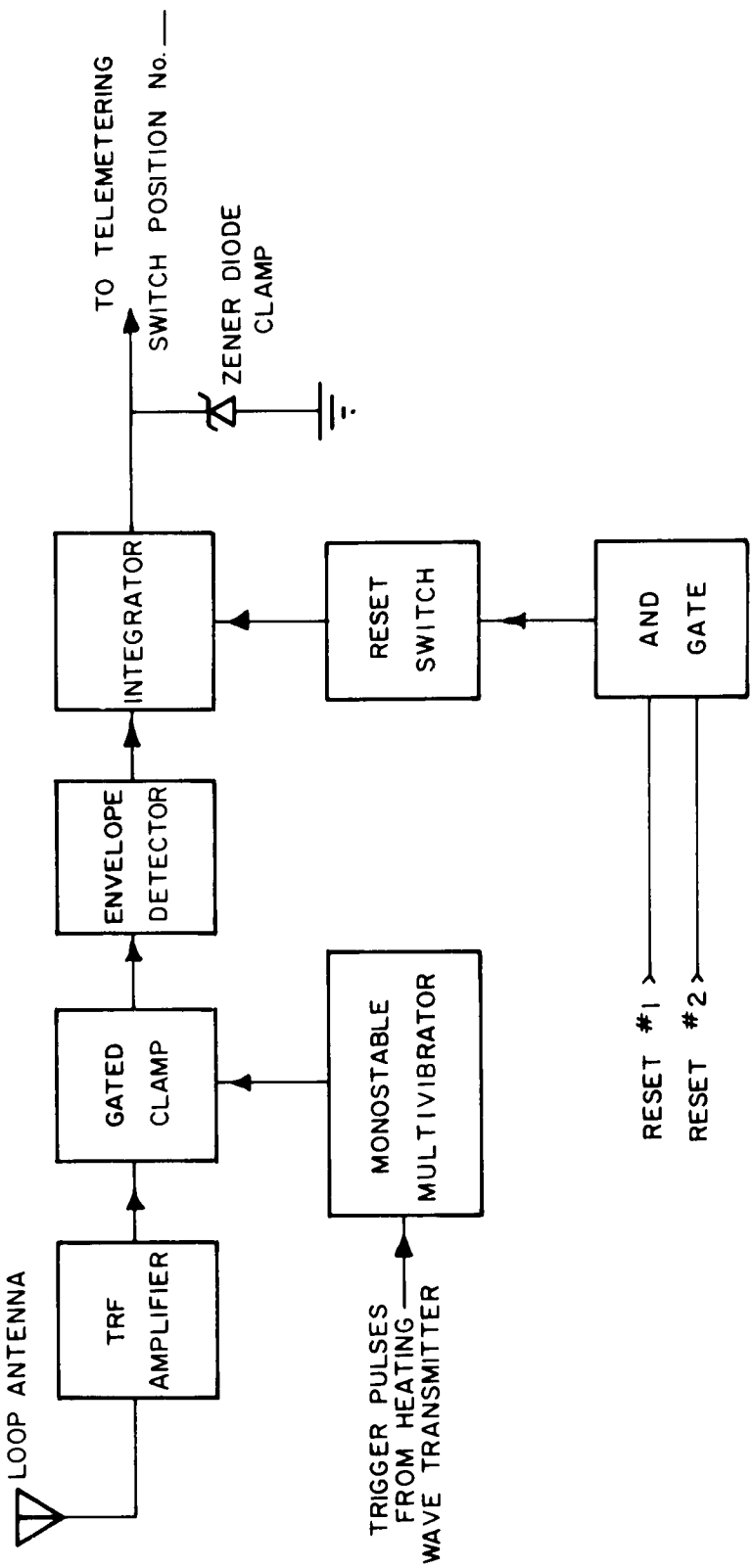

Figure 3.2 Block diagram of difference frequency receiver

REFERENCES

1. G. A. Deschamps and W Weeks, "Use of the Smith Chart and Other Graphical Constructions in the Magneto-Ionic Theory," Scientific Report No. 1, Contract AF19(604)-5565, Antenna Laboratory, Electrical Engineering Research Laboratory, University of Illinois, Urbana, Illinois, 26 April 1960.

2. G. A. Deschamps, "Refractive Index for Plane Wave Propagation in a Lossless Magneto-Ionic Medium," Scientific Report No. 2, Contract AF19(604)-5565, Antenna Laboratory, Electrical Engineering Research Laboratory, University of Illinois, Urbana, Illinois, 15 July 1960.

3. G. A. Deschamps, "Polarization of Characteristic Waves in a Magneto-Ionic Medium," Scientific Report No. 3, Contract AF19(604)-5565, Antenna Laboratory, Electrical Engineering Research Laboratory, University of Illinois, Urbana, Illinois, 15 March 1961.

4. R. Mittra, "Solution of Maxwell's Equations in a Magneto-Ionic Medium with Sources," Scientific Report No. 4, Contract AF19(604)-5565, Antenna Laboratory, Electrical Engineering Research Laboratory, University of Illinois, Urbana, Illinois, 18 January 1962.

5. J. T. Verdeyen and L. Goldstein, "Non-Linear Response of Plasmas to Electromagnetic Waves and Surface Wave Propagation in Magneto-Ionic Plasmas," Scientific Report No. 5, Contract AF19(604)-5565 and Scientific Report No. 4, Contract AF19(604)-3481, Gaseous Electronics Laboratory, Electrical Engineering Research Laboratory, University of Illinois, Urbana, Illinois, 1 May 1962.

6. B. D. H. Tellegen, "Interactions between Radio Waves," Nature, Vol. 131, p. 840 (1933)

7. V. A. Bailey and D. F. Martyn, "The Influence of Electric Waves on the Ionosphere," Phil. Mag., Vol 18, p. 369 (1934)

8. V. A Bailey, "On Some Effects Caused in the Ionosphere by Electric Waves, Part II," Phil. Mag , Vol. 26, p. 425 (1938).

9. M. Cutolo, "Effects of Radio Gyrointeraction and their Interpretation," Nature, Vol. 166, p. 98 (1950).

10. V. A Bailey, R. A Smith, K Landecker, A. J Higgs, and F. H Hibbend, "Resonance in Gyro-Interaction of Radio Waves, Nature, Vol 169, p. 911, 1952

11. A. H. Waynick, "The Present Knowledge concerning the Lower Ionosphere," Technical Report, Ionospheric Research Laboratory, Pennsylvania State University, University Park, Pennsylvania (1956)

12. R. A. Minzner, K W Champion, and H Pond, "The 1959 ARDC Model Atmosphere," Air Force Surveys in Geophysics, No. 115, ARCRC (1959)

REFERENCES (Continued)

13. M. Nicolet, "The Collision Frequency of Electrons in the Ionosphere," J.A.T.P., Vol. 3, p. 200 (1953)

14. V. A. Bailey, "Some Possible Effects Caused by Strong Gyro-Waves in the Ionosphere--I," J.A.T.P., Vol. 14, p. 299 (1959).

15. A. W. Trivelpiece and R. W. Gould, "Space Charge Waves in Cylindrical Plasma Columns," Journ. of Appl. Phys., 30, No. 11, p. 1784, November 1959 (also P.I.B. Symp. on Electronic Waveguides, p. 215-228).

16. A. W. Trivelpiece, A. Ignatius, P. C. Holscher, "Backward Waves in Longitudinally Magnetized Ferrite Rods," Journ. of Appl. Phys., 32, No. 2, p. 259-267, February 1961.

17. R. I. Joseph, E. Schlomann, "Theory of Magnetostatic Modes in Long, Axially Magnetized Cylinders," Journ. of Appl. Phys , 32, No. 6, p. 1001-1005, June 1961.

18. O. C. Haycock and K. D. Baker, "Measuring Antenna Impedance in the Ionosphere," Electronics, January 13, 1961.

19. G. Hok, N W. Spencer, A Reifman, W. G. Dow, "Dynamic Probe Measurements in the Ionosphere," Rpt. No. 3, Upper Air Research Program, U. of Mich., Ann Arbor, (Eng. Res. Inst), August 1951.

20. A. Reifman and W. G. Dow, "Theory and Application of the Variable Voltage Probe for Exploration in the Ionosphere," Phys. Rev ,75, p. 1311A, 1949.

21. A. Reifman and W. G. Dow, "Dynamic Probe Measurements in the Ionosphere," Phys. Rev., 76, p. 987-988, October 1, 1949

22. R. L. Boggess, "Electrostatic Probe Measurements of the Ionosphere," Scientific Report No. GS-1, Space Physics Research Laboratory, University of Michigan, November 1959.

23. J. E. Jackson and J. A. Kane, "Breakdown and Detuning of Transmitting Antennas in the Ionosphere," U. S. Naval Research Lab. Report 5345, August 24, 1959.

24. J. E. Jackson and J A Kane, "Measurement of Ionospheric Electron Density with an RF Probe," Journ Geophys Res , Vol. 64, p 1074, August 1959.

25. J. A. Kane, J E. Jackson, H. A. Whale, "The Simultaneous Measurement of Ionospheric Electron Densities by CW Propagation and RF Impedance Probe Techniques," NASA Technical Note D-1098, 1962

26. W. Pfister, J. C. Ulwick, R P Vancour, "Some Results of Direct Probing in the Ionosphere," Journ. of Geophys. Res , 66, No. 4, p. 1293-1297, April 1961.

REFERENCES (Continued)

27. K. Takayama, H. Ikegami, and S. Miyazaki, "Plasma Resonance in a Radio-Frequency Probe," Phys. Rev. Lett., 5, No. 6, p. 238-240, September 15, 1960.

28. S. Miyazaki, K. Hirao, et al, "Resonance Probe--A new probe method for measuring electron density and electron temperature in the ionosphere," Journ. of the Radio Res. Labs. (Jap), 7, No. 34, November 1960.

29. R. King and C. W. Harrison, "Half-Wave Cylindrical Antenna in a Dissipative Medium: Current and Impedance," J. of Res. NBS (D), 64D, No. 4, p. 365, July-August 1960.

30. R. King, C. W. Harrison, Jr. and D. H. Denton, Jr., "The Electrically Short Antenna as a Probe for Measuring Free Electron Densities and Collision Frequencies in an Ionized Region," J. Res. NBS, 65D, No. 4, p. 371-384, July-August 1961.

31. J. C. Katzin and M. Katzin, "The Impedance of a Cylindrical Dipole in a Homogeneous Anisotropic Ionosphere," Report No. NAS 585-2, Electromagnetic Research Corp., College Park, Md., 26 September 1961.

32. B. P. Kononov, A. A. Rukhadze, G. V. Solodukhov, "Electric Field of a Radiator in a Plasma in an External Magnetic Field," Soviet Physics--Technical Physics, 6, No. 5, p. 405-410, November 1961.

33. R. W. Damon and J. R. Eshbach, "Magnetostatic Modes of a Ferromagnetic Slab," Journ. of Appl. Phys., Supplement to Vol. 31, No. 5, p. 104S-105S, May 1960.

34. L. B. Loeb, "Basic Processes of Gaseous Electronics," U. of Calif (Berkely) Press, 1955.

35. E. O. Johnson and L. Malter, "A Floating Double Probe Method for Measurements in Gas Discharges," Phys. Rev., 80, No. 1, p. 58-68, October 1, 1950.

36. L. Malter and W. M. Webster, "Rapid Determination of Gas Discharge Constants from Probe Data," RCA Review, p. 191-210, June 1951.

37. T. Okuda and K. Yamamoto, "Asymmetrical Triple Probe Method for determining Energy Distribution of Electron in Plasma," Journ. of Appl. Phys., Vol. 31, No. 1, p. 158, January 1960.

38. J. B. Bernstein and J. N. Rabinowitz, "Theory of Electrostatic Probes in Low-Density Plasma," Phys. of Fluids (U.S.A.), 2, No. 2, p. 112-121, March, April, 1959.

39. B. Bertotti, "Theory of an Electrostatic Probe in a Plasma in a Strong Magnetic Field," Phys. of Fluids (U.S.A.), 4, No. 8, p. 1047-52, August 1961.

40. Kun-Mu Chen, J. Meixner, D. Sengupta, R. E. Kleinman, O. G. Ruehr, "Studies in Non-Linear Modeling--III On the Interaction of EM Fields with Plasmas," Report 4134-2-F, U. of Mich Electrical Engineering Radiation Lab., AFCRL 746.

REFERENCES (Continued)

41. R. Jastrow and G. A. Pearse, "Atmosphere Drag on a Satellite," J. Geophys. Res., 62, p. 413, 1957

42. G. Schulz and S. C. Brown, "Microwave Study of Positive Ion Collection by Probes," Phys. Rev. 98, p. 1642, June 15, 1955.

43. J. D. Cobine, Gaseous Conductors, Dover Publications, 1958.

44. K. R. Spangenberg, Vacuum Tubes, McGraw-Hill Book Co., 1948.

45. W. W. Zachary, "The Distribution of Particles around Vehicles moving through the Ionosphere," Report No. NAS 585-3, Electromagnetic Research Corp., College Park, Md., 15 December 1961.

46. A. A. Dougal and L. Goldstein, "Energy Exchange Processes through Coulomb Collisions in Gaseous Discharge Plasma Studied by Microwave Interaction Techniques," University of Illinois Gaseous Electronics Laboratory, Urbana, Illinois, Scientific Report No 1, Contract AF19(604)-2152.

47. L. Goldstein, "Electrical Discharge in Gases and Modern Electronics," Advances in Electronics and Electron Physics, Vol. VII, Academic Press, 1955.

48. S. C. Brown, "Basic Data of Plasma Physics," Technology Press & Wiley, 1959.

49. W. Pfister, "Studies of the Refractive Index in the Ionosphere. The Effect of the Collision Frequency and of Ions," The Physics of the Ionosphere--Report of the 1954 Cambridge Conference, p. 394-401

50. L. Tonks, "The High Frequency Behaviour of a Plasma," Phys. Rev. 37, p. 1458-1483, June 1, 1931.

51. I. N. Sneddon, Elements of Partial Differential Equations, McGraw-Hill Book Co., 1957.

52. R. Mittra, "Solution of Maxwell's Equations in a Magneto-Ionic Medium with Sources," Antenna Laboratory, Electrical Engineering Research Laboratory, University of Illinois, Urbana, Illinois, Scientific Report No. 4, Contract AF19(604)-5565, 18 January 1962

53. A. H. Waynick, "The Present State of Knowledge concerning the Lower Ionosphere," Technical Report, Pennsylvania State University, 1956.

54. M. Nicolet, "The Collision Frequency of Electrons in the Ionosphere," J.A.T.P. 3, No. 4, p 200-211, May 1953.

55. J. E. Drummond, R A. Gerwin, and B G. Springer, "The Concept of Conductivity," J Nuc'l Energy, Part C: Plasma Physics 2, p 98-108, 1961

REFERENCES (Continued)

56. D. L. Sengupta, "The Electrical Conductivity of a Partially Ionized Gas," Proc. I.R.E. 49, No. 12, p. 1872-1876, December 1961.

57. "Half-Wave Cylindrical Antenna in a Dissipative Medium; Current and Impedance," J. Research of N.B.S., 640, p. 365-380, 1960.

58. J. T. Verdeyen and L. Goldstein, "Non-Linear Response of Plasmas to Electromagnetic Waves and Surface Wave Propagation in Magneto Plasmas," Scientific Report No. 5, Contract AF19(604)-5565 and No. 4, Contract AF19(604)-3481, Gaseous Electronics Laboratory, University of Illinois, Urbana, Illinois, 1 May 1962.

SUPPLEMENTAL DISTRIBUTION LIST
Contract AF19(604)-5565

AFCRL, OAR(CRZI)
L G. Hanscom Field
Bedford, Mass. (2)

AFCRL, OAR(CRRCPG)
L G. Hanscom Field
Bedford, Mass

AFCRL, OAR(CRRK)
L.G Hanscom Field
Bedford, Mass

Hq , AFSW(SWRP)
Kirtland AFB
Albuquerque, New Mexico

Director
Naval Electronics Laboratory
San Diego 52, California

Commanding Officer
U.S. Army Signal R&D Lab.
Attn. Mr. Irving Reingold
SIGRA/SL-PRM
Ft Monmouth, New Jersey

Library
John Hopkins University
Baltimore, Maryland

Stanford Electronics Laboratory
Document Library
Stanford University
Stanford, California

Department of Mathematics
Research Group
New York University
45 Astor Place
New York, New York

Professor K.M Siegel
Radiation Laboratory
University of Michigan
912 Main Street
Ann Arbor, Michigan

The Engineering Department
Princeton University
Princeton, New Jersey

Mr. Dwight Isbell
963 13th Avenue East
Seattle 2, Washington

Electrical Engineering Res. Lab.
University of Illinois
Urbana, Illinois (10)

Professor W. E. Miller
University of Illinois
Urbana, Illinois

Mr. Martin Katzin, President
Electromagnetic Research Corporation
5001 College Avenue
College Park, Maryland

Director, Geophysics Observatory
University of Alaska
College, Alaska

Professor A.H. Waynick, Director
Ionosphere Research Laboratory
The Pennsylvania State University (2)
University Park, Pennsylvania

Professor Obed Haycock
408 Engineering Hall
University of Utah
Salt Lake City, Utah

Professor Rene Marcou
Department of Mathematics
Boston College
Chestnut Hill 67, Mass.

Dr. B. Chatterjee
Indian Institute of Technology
Communication Engineering Department
Kharagpur (S.E. Rly.)
Indiz

Dr. E. C. Jordan
University of Illinois
Urbana, Illinois

Professor Ronald W P. King
Cruft Laboratory
Harvard University
Cambridge, Mass.

Science Advisor
Department of State
Washington 25, D.C.

Institute of Technology Library
MCLI-LIB, Bldg. 125, Area B
Wright-Patterson Air Force Base, Ohio

Hq. USAF (AFCSA, Secretary)
Washington 25, D.C.

Hq. USAF (AFRDR)
Washington 25, D.C.

AFCRL, OAR(CRIPA) Stop 39
L. G. Hanscom Field (20)
Bedford, Mass.

ESD(ESRDG)
L.G. Hanscom Field
Bedford, Mass.

Boston Office
Patents & Royalties Div.(Hq AFLC)
Bldg. 133, 424 Trapelo Rd.
Waltham 54, Mass.

ASD (ASAPRD-Dist)
Wright-Patterson AFB, Ohio

ACIC (ACDEL-7)
2d & Arsenal
St. Louis 18, Mo.

NAFEC LIBRARY BRANCH, Bldg. 3
Atlantic City, New Jersey
Attn: RD-702

AFCRL, OAR(CRT, Dr. A.M. Gerlach)
L. G. Hanscom Field
Bedford, Mass.

NASA
Attn. Library, Code AFET-LA
Stop 85
Washington 25, D.C.

Librarian
Boulder Laboratories
National Bureau of Standards
Boulder, Colorado

Library
National Bureau of Standards
Washington 25, D.C.

Director of Meteorological Research
U.S. Weather Bureau
Washington 25, D.C.

Library
U.S. Weather Bureau
Suitland, Maryland

Director, USAF Project RAND
The Rand Corporation
1700 Main Street
Santa Monica, California
Thru A.F. Liaison Office

Dr. William W. Kellogg
Rand Corporation
1700 Main Street
Santa Monica, California

Mr. Malcolm Rigby
American Meteorological Society
P.O. Box 1736
Washington 13, D.C.

Institute of Aerospace Sciences, Inc.
2 East 64th Street
New York 21, New York

Library
Geophysical Institute
University of Alaska
P.O. Box 938
College, Alaska

Dr. Joseph Kaplan
Dept. of Physics
University of California
Los Angeles, California

Professor Fred L. Whipple
Harvard College Observatory
60 Garden Street
Cambridge 38, Massachusetts

Dr. David Fultz
Dept. of Meteorology
University of Chicago
Chicago, Illinois

Office of Secretary of Defense
(DDR & E, Tech. Library)
Washington 25, D.C.

AFOSR(SRGL)
Washington 25, D.C.

AWS (AWSSS/TIPD)
Scott AFB, Ill.

A.U. (Library)
Maxwell AFB, Ala.

Dept. of the Army (SIGRD-8-B-5)
Washington 25, D.C.

Technical Documents Center
Evans Signal Labs.
Belmar, New Jersey

Technical Reports Librarian
U.S. Naval Postgraduate School
Monterey, California

Director
U.S. Naval Research Laboratory
Code 2027
Washington 25, D.C.

ONR(Geophysics Code N-416)
Office of Naval Research
Washington 25, D.C.

Documents Expediting Project (UNIT X)
Library of Congress
Washington 25, D.C.

Superintendent of Documents
Government Printing Office
Washington 25, D.C.

ASTIA (TIPAA)
Arlington Hall Station (10)
Arlington 12, Virginia

National Research Council
2101 Constitution Avenue
Washington 25, D.C.

Dr. A. M. Peterson
Stanford University
Stanford, California

Professor Clarence Palmer
Institute of Geophysics
University of California
Los Angeles 24, California

Technical Information Office
European Office, Aerospace Research
Shell Building, 47 Cantersteen
Brussels, Belgium